Temporal lobe epilepsy: a combined study with high field (7T) Magnetic Resonance Imaging and optical and ultrastructural histopathology

Dr. Gloria Milesi
matricola 025568

Tutor Dr. G. Finocchiaro
Co-tutor Dr. R. Garbelli

TABLE OF CONTENTS

Chapter 1

1.1 INTRODUCTION TO EPILEPSY

Epilepsy is a chronic neurological condition characterized by recurrent and spontaneous seizures due to alterations in the central nervous system that leads to an excessive and synchronous activation (hyperexcitability) of clusters of neurons.

Epilepsies are divided into two main groups: generalized epilepsies with seizures that begin simultaneously in both hemispheres with no apparent focal origin and the partial epilepsies whose seizures have focal origin.

Approximately 60% of patients with epilepsy (0.4% of the population of industrialized countries) is suffering from focal epileptic syndromes, among them about 30% is affected by drug-resistance and about the 30% could be candidabile to **epilepsy surgery**.

The aim of epilepsy surgery is to achieve seizures control by removing the brain region from which they originate, so accurate diagnostic procedures are necessary in order to select the patients that could benefit from it. The diagnostic work-up must provide:

- the definition of the **epileptogenic zone** (EZ, defined as the brain region involved in the origin and primary organization of the critical activity), that represent the minimum amount of cortex that must be resected to achieve seizure freedom;
- the search of a possible structural lesion and definition of its patho-physiological and anatomical relationships with the EZ;
- – the planning of the surgical treatment on the base of prognostic expectations and the risks for the patient.

1.2 TEMPORAL LOBE EPILEPSY

The focal epilepsies are classified according to the cerebral lobe which is supposed to be involved in the seizure generation, so the **temporal lobe epilepsy** (TLE) term has been introduced.

TLE is the most common form of focal epilepsy and it represents 60-70% of cases of surgical series. It is not an uniform pathology, in fact elettroclinical, neuroimaging and neuropathological data show an anatomical substrate more widespread with involvement of the mesial temporal structures and temporal neocortex (Bernasconi et al. 2005; Chassoux et al. 2004; Concha et al. 2009). From a clinical point of view, TLE is distinguished into temporal epilepsy at hippocampal or mesial origin (MTLE) and lateral neocortical temporal epilepsy.

1.2.1 DIAGNOSTIC APPROACHES IN TLE

In the diagnostic process there is a need to find relationships between the clinical manifestations, the electrical manifestations and the possible anatomical alterations. Precise anatomo-electro-clinical correlations are crucial to establish a priori if a patient could have seizure control by surgery.
The principal pre-surgical investigations are:

ELECTRO ENCEPHALOGRAFIC ANALYSIS (EEG)
The video-EEG monitoring (V-EEG) constitutes a fundamental method to get electroclinical correlations (between seizures semeiology and the EEG activity), in fact thanks to the synchronization of the EEG with video images it allows to obtain more precise data than the surface EEG recording.

INTRACRANIC EEG

The presurgical diagnostic work-up in patients with drug-resistant focal epilepsy can requires an invasive method that allows the acquisition of EEG signals directly from the brain, increasing the topographical definition of the affected areas and providing functional information to better define the extent of surgical resection. The intracerebral recording is important when it is not adequately defined the EZ, for example in the absence of congruity between clinical and instrumental data (RM, EEG surface), in the absence of focal cerebral alterations or in the presence of a double pathology when it is assumed that the anatomical limits of the alterations are not easily definable.

DIAGNOSTIC IMAGING

Approximately 2/3 of patients with temporal lobe epilepsy have structural alterations of the temporal lobe such as tumours, vascular malformations, abnormalities of cortical development and hippocampal sclerosis (HS). Different neuroradiological diagnostic methods for study these abnormalities, though to be potentially epileptogenic lesions, are employed. In the context of TLE, the main radiological examination is magnetic resonance imaging (MRI).

MAGNETIC RESONANCE IMAGING (MRI)

It represents the main morphologic investigation to study the anatomy and the epileptic lesions in temporal lobe and to select patients candidable to surgery. In fact it is an useful non-invasive method in the pre-surgical planning to identify the area to be removed but also in post-surgical phase to verify the extent of resection and the possible presence of remaining lesion.

FUNCTIONAL IMAGING

The radiological investigations with isotopes (PET and SPEC) are also used in evaluation of focal epilepsies. Although the spatial resolution is low, these methods allow assessing local cerebral metabolism (consumption of glucose and oxygen, blood flow) and so contributing to the delimitation of the epileptogenic region.

NEUROPSYCOLOGICAL EVALUATION

Neuropsychological tests are performed to assess cognitive functions, memory and language in the pre-surgical phase both as diagnosis and prognostic aspect because surgery may compromise these functions.

1.2.2 SURGERY

Following the identification of the EZ and its relationship with the surrounding brain areas, the surgical treatment can be planned. It is important to remember that, to achieve seizure freedom is necessary to completely remove the EZ.

The most frequent surgical approach employed in the epilepsy surgery consists in the resection of about 4-6 cm of the anterior temporal lobe; in the mesial region the resection includes the amygdala and from 1 to 3 cm (often also 4 cm) of the anterior portion of the hippocampus (Wiebe et al 2001).

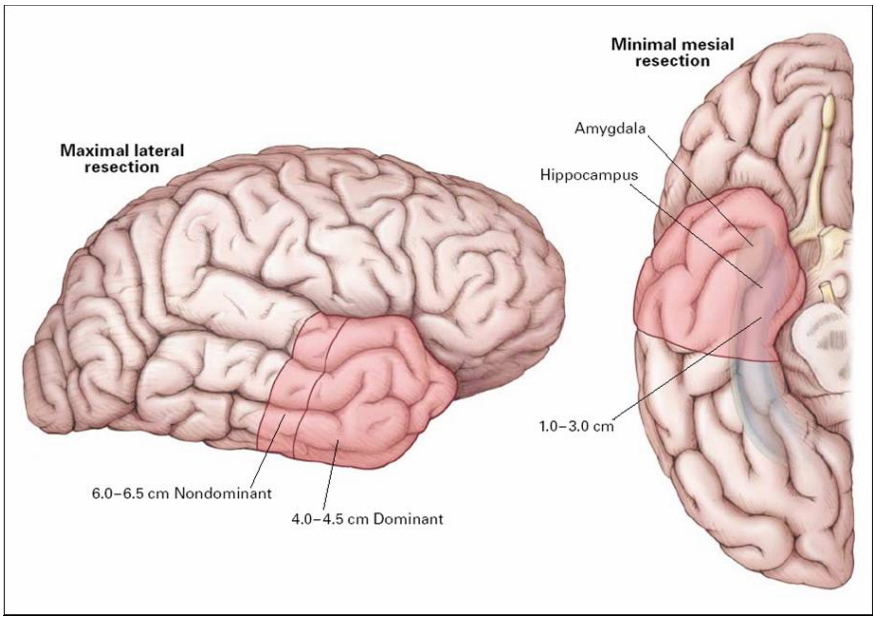

1.2.3 NEUROPATHOLOGY IN TLE

The most frequent neuropathological finding, in approximately two thirds of patients with TLE, is the pattern of **hippocampal sclerosis** (HS). The histopathological hallmark of HS is segmental pyramidal cell loss, which can variably affect all sectors of the Ammon's horn. Neuronal cell loss is always associated with cellular and more often fibrillar astrogliosis. This pathogenic response to any neuronal degeneration has established the original term of "Ammon's horn sclerosis" (Sommer 1880).

However, pathological studies show that lesions correlated with TLE may be found well beyond the hippocampal formation. In fact, in approximately one third of pharmacoresistant patients, TLE is associated with focal lesions located in the temporal lobe such as: slow-growing **tumours** (gangliogliomas, astrocytomas, and dysembryoplastic neuroepitelial tumours-DNET), **arterovenous malformations** and more frequently malformations of cortical

development (in particular the **focal cortical dysplasia**, FCD). These lesions can coexist with the HS in about in 5-30 % of cases constituting a condition defined as "**dual pathology**" (Blumcke et al. 2002; Tassi et al. 2009). This data suggest that TLE may depend on either a more widespread temporal lobe disturbance or is the result of so-called dual pathology, (i.e. HS plus alterations in neocortical temporal structures). Since an optimal outcome is obtained when both the lesions are removed it seems evident that both contribute to seizure genesis.

HIPPOCAMPAL SCLEROSIS

Hippocampal sclerosis is characterized by gliosis and neuronal loss, most prominently in the CA1 field of the hippocampus, followed by CA4 and CA3 fields. Neurons in the dentate granular cell layer and in the CA2 field are relatively unaffected. In addition, there is often a dispersion of the dentate granular cell layer, and/or ectopic neurons being found in the molecular layer. Neuronal loss is accompanied by axonal reorganization involving both excitatory and inhibitory neurons. Moreover, there are particular synaptic reorganization that involves the axons of the cells of the dentate gyrus (mossy fibers) that normally innervate pyramidal neurons in CA3 and mossy cells in CA4. In the presence of hippocampal sclerosis, these axons have no more their natural target (due to marked cell loss), so they create an aberrant sprouting to the dentate gyrus cells in the inner portion of the molecular layer, as result a reverberate excitatory circuit establish itself on DG and is thought to be involved in generating of the epileptic discharges (theory of the mossy cells sprouting; Sutula et al., 1989). The particular vulnerability of the CA1, CA3 and CA4 is due to their high content of a particular type of glutamate receptors: NMDA for the CA1 region and the receptors for the kainate for CA4, the dentate gyrus and CA3 region. These receptors, when strongly activated by glutamate or aspartate as occurs during a crisis, cause an

excessive flow of calcium ions inside the pyramidal cells which, therefore, may be damaged because an excessive amount of it activates citotoxic events. On the contrary the cells of the CA2 region and those of the granules of the dentate gyrus contain calbindin and chromogranin A, calcium-binding proteins that protect them from excitotoxicity. Even the GABAergic neurons, containing calbindin or parvalbumin, are protected from the damage induced by calcium, while the subiculum is preserved for its low content of NMDA receptors. These calcium binding proteins are absent in the CA3 and CA4 regions and only present in small quantities in the CA1 region so they are very vulnerable to epileptic discharges.

Recently the ILAE commission has proposed a classification in which three HS subtypes was identified (Blumcke et al., 2013).
HS ILAE Type 1 refers always to severe neuronal cell loss and gliosis predominantly in CA1 and CA4 regions, compared to CA1 predominant neuronal cell loss and gliosis (**HS ILAE Type 2**), or CA4 predominant neuronal cell loss and gliosis (**HS ILAE Type 3**). HS ILAE Type 1 is more often associated with a history of initial precipitating injuries before age five years, with early seizure onset and **favourable post-surgical** seizure control. CA1 predominant HS ILAE Type 2 and CA4 predominant HS ILAE Type 3 have been studied less systematically so far, but some reports point to **less favourable outcome**, and to differences regarding epilepsy history, including age of seizure onset. The proposed international consensus classification will aid in the characterization of specific clinico-pathological syndromes, explore variability in imaging and electrophysiology findings, and post-surgical seizure control.

HS Type 1 HS Type 2

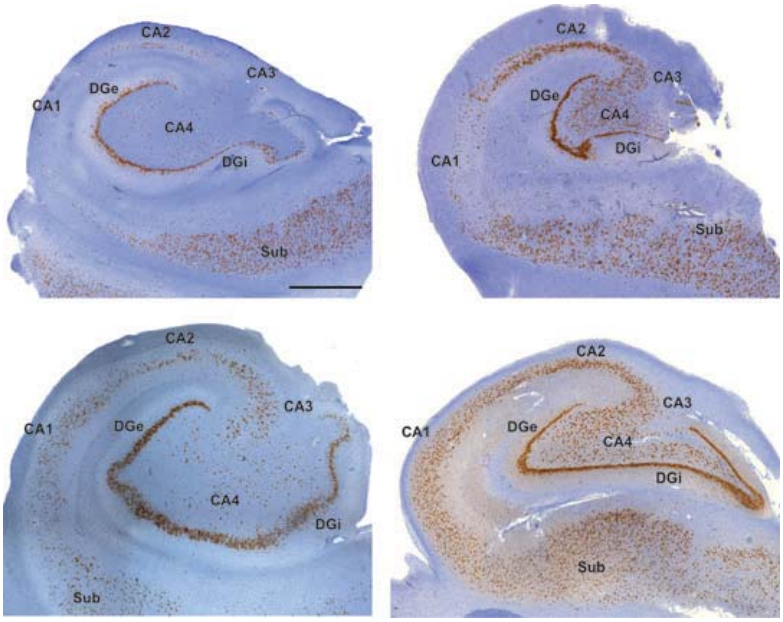

HS Type 3 No HS

FOCAL CORTICAL DYSPLASIA

Focal Cortical Dysplasias (FCD) are highly epileptogenic brain lesions and a frequent cause for drug-resistant focal epilepsies in humans. FCD are characterized by a disruption of the normal lamination of the cortex that can vary in severity, ranging from a mild disruption of lamination with normal-apparing neurons to a profound laminar disorganization, frequently accompanied by the appearance of dysmorphic an misoriented neurons, neuronal clustering, giant neurons, and balloon cells.

Pathomechanisms compromising neuroblast proliferation, migration or differentiation are likely to play a role in the aetiology of FCD variants. FCDs were subsumed, therefore, into the broad spectrum of Malformations of Cortical Development.

Detailed neuropathologic studies of FCD suggest that distinct histologic subtypes exist. According to a widely applied comprehensive classification (Blumcke et al., 2011), cortical dysplasia may be categorized as following:

FCD type I *(Isolated architectural abnormalities)*
These are cortical lesions characterized by dyslamination and columnar disorganization without any cytological alteration. These lesions represent the mildest form of the histopathologic spectrum of FCD

FCD type II *(Cyto-architectural abnormalities)*
It is a malformation presenting disrupted cortical lamination associated to specific cytologic abnormalities, which differentiates FCD Type IIa (dysmorphic neurons) from FCD Type IIb (dysmorphic neurons and balloon cells). It is the most severe form of FCD.

FCD type III *(Architectural abnormalities associated with a second pathology)*
It refers to cortical lamination abnormalities associated with a principal lesion, usually adjacent to or affecting the same cortical area/lobe. Four variants should be distinguished:
-FCD Type IIIa associated with hippocampal sclerosis;
-FCD Type IIIb associated with tumors;
-FCD Type IIIc associated with vascular malformations
and FCD Type IIId associated with any other principal lesion acquired during early life (e.g., trauma, ischemic injury, encephalitis).
In patients with TLE, FCD type IIIa is the most second frequent alteration observed in association with HS.
This form of dysplasia, although istopatologically similal to FCD Type I, has been considered separately on the basis that the isolated forms

may evolve during cortical development, whereas the others may be acquired as a result of the main epileptogenic lesion (i.e., AHS).

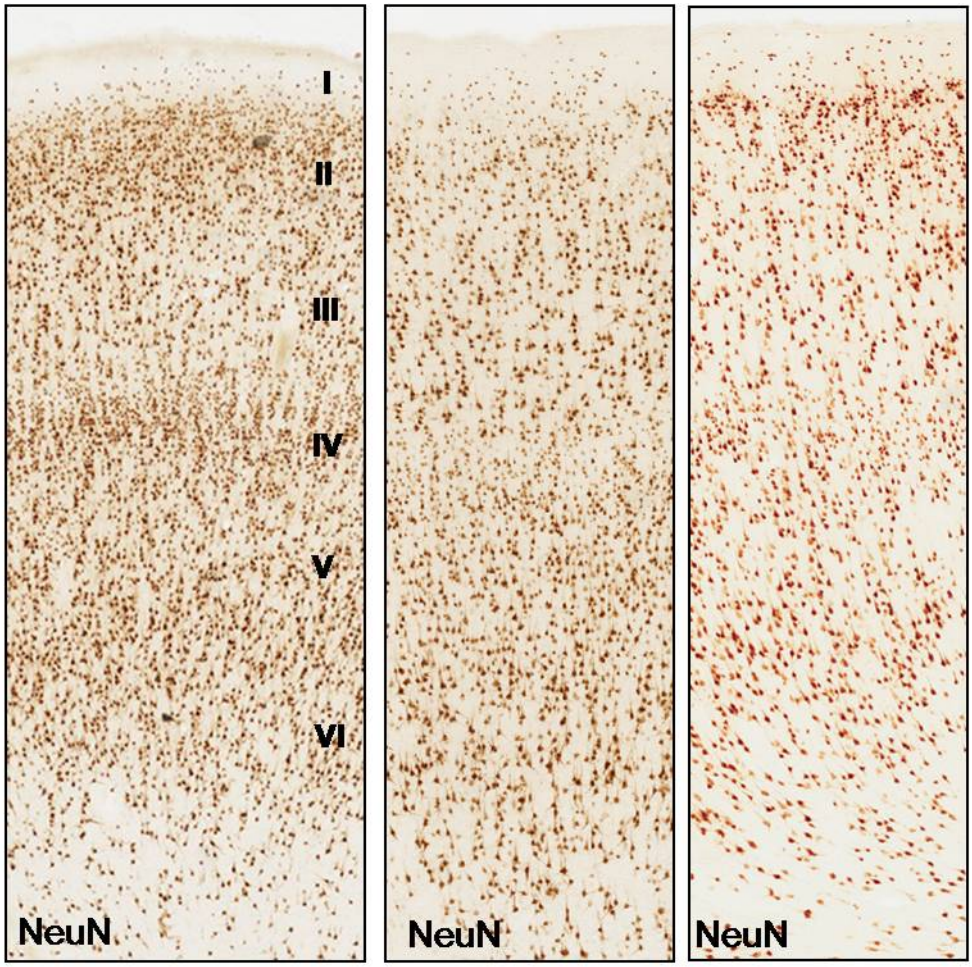

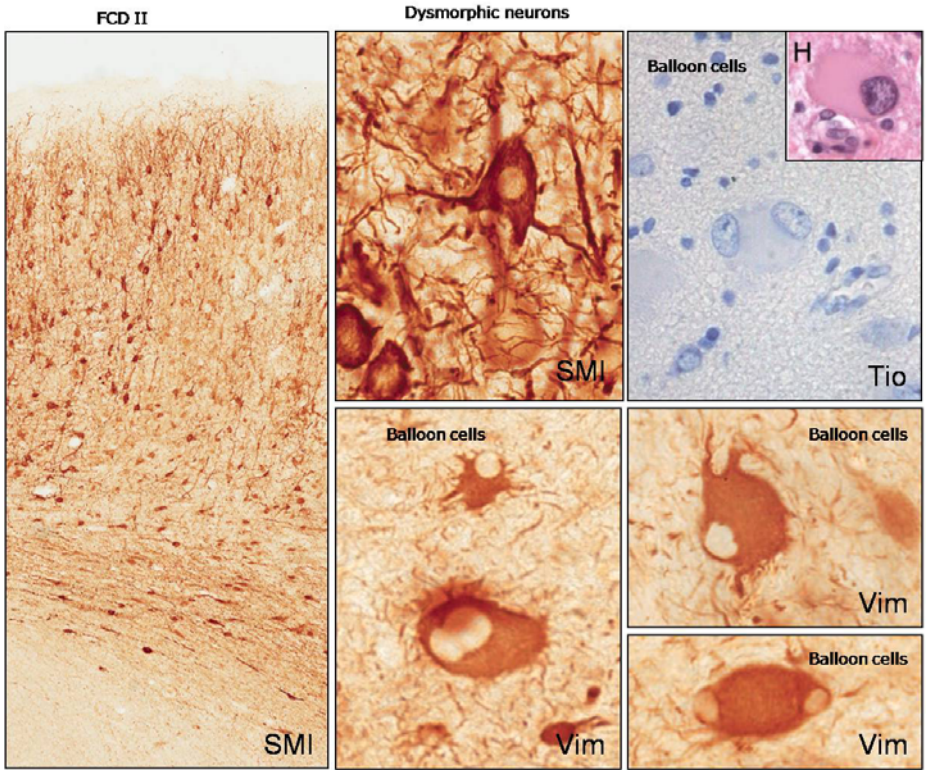
FCD II
Dysmorphic neurons
SMI
SMI
Balloon cells
H
Tio
Balloon cells
Vim
Balloon cells
Vim
Balloon cells
Vim

FCD are characterized by intrinsic epileptogenicity due to an impaired imbalance between excitatory and inhibitory systems involving modifications of neurotransmitters and receptors. In fact it seems that the glutamate, the major excitatory neurotransmitter in the central nervous system, and also the expression of some subunits of NMDA receptor are increased in dysplastic tissue, in particular in dysplastic neurons. The hyperexcitability in dysplastic tissue may be also a consequence of an impairement in GABAergic function, the amino-butyric acid (GABA) is the major inhibitory neurotransmitter in cortical areas released by various types on interneurons. This alteration could be attributed to either a reduction in the number of inhibitory neurons, synapses or in GABA receptor subunits (Thom et al., 2003; Garbelli et al., 2006 Najm et al., 2007; Crino et al., 2001).

1.2.4 OUTCOME IN TLE

The aim of epileptic surgery is seizure control with consequent improvement in the quality of life, in the absence of psychiatric and neurological deficits. Currently, the classification system of post-surgical outcome is the Engel scale (Engel et al. 1993).This classification correlates the frequency of seizures after surgery and the benefit, or not, obtained from the patient with regard to the quality of life. Factors that may affect the surgical outcome are the brain region, the nature of the pathology, and the extension of the resection.

Recent data suggest that surgical resection offers postoperative seizure freedom at two years in 60-80% of patients with drug-resistant TLE. Longer-term follow-up studies present less favourable results, supporting the notion that TLE is a heterogeneous condition in terms of network properties and prognostic features. (Blumcke et al. 2013)

1.2.5 PATHOGENESIS OF TEMPORAL LOBE EPILEPSY

In drug-resistant TLE, the hippocampal sclerosis (HS) is the most frequent neuropathological finding and patients affected frequently had a history of febrile seizures in the early childhood. In fact, it is thought that between 6 months and 5 years the hippocampus is particularly susceptible to damage. This suggests that the development of the TLE pathology is a long and complex process that begins much earlier that seizures appear. In fact, in many patients an initial precipitating event injury such as a status epilepticus or a head trauma, or febrile seizures, occur in the early life which conduces to a cascade of neurobiological events corresponding to the **epileptogenesis process**.

The epileptogenesis occurs in a silent period, before refractory chronic epilepsy develops, and consists in neuronal loss, neurogenesis, glial proliferation and glial proprieties alterations, synaptic plasticity and inflammation. All these changes during the latent period, contribute to the occurrence of spontaneous seizures

On the basis of these observations, the following pathogenetic model for TLE has been proposed.

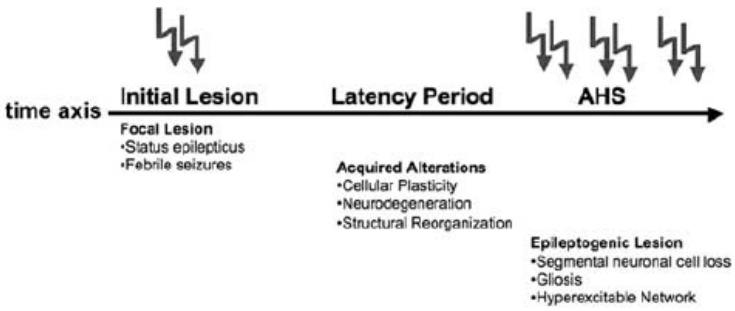

1.2.6 NEURORADIOLOGICAL ASPECT OF HS AND FCD IN TLE PATIENTS

MRI investigation of the HS allows to assess the atrophy of the hippocampus by volumetric measurements and the degree of integrity of this structure by observing changes in the signal intensity. Unfortunately it is still possible to clearly identify the affected subregions of the hippocampus and the degree of sclerosis which it could constitute an index of surgical outcome in TLE patients.
Except for a possible reduction in the temporal pole volume, actually FCDs are poorly defined by MRI and this can affect the success of the surgical treatment by to an incomplete resection and, consequently, with the inability to achieve the seizures freedom for patient.

1.3 ADVANCES IN NEUROIMAGING

Magnetic Resonance Imaging (MRI)

This technique allows obtaining morphological and functional images of soft tissues of the human body with high definition. It is a non-invasive method because it uses no ionizing radiation but magnetic fields and it is based on the principle of Nuclear Magnetic Resonance (NMR) that uses the physical properties of the hydrogen atom subjected to magnetic fields and radio-frequency pulses.
Currently in clinical practice 1.5-3 Tesla (T) scanners are used, however in recent years ultra-high field (more than 3 T) MRI instruments have been introduced in the preclinical studies. The latter provide greater spatial resolution of structures whose images with a better anatomical detail are elaborated by dedicated software. Moreover, new neuroimaging techniques based on MRI have been developed for the study of the brain. An important development is given by the dMRI (Diffusion-weighted Magnetic Resonance Imaging).

This technique is sensitive to water diffusion, that is the random motion of water molecules in the tissue, driven by their internal kinetic energy. Studying diffusion in the biological and medical field may allow to make inferences about the environment where diffusion takes place. Indeed, although free diffusion (i.e. diffusion in an unlimited space without obstacles) is determined only by the properties of the molecule and the fluid in which it diffuses, this is rarely the case in biological tissues. Here, diffusion is always hindered by the presence of obstacles (macro-molecules, cells, …) or restricted by impermeable barriers. Thus the diffusion parameters estimated by dMRI are indirect indices of the microstructure of the tissue, at a scale well below the resolution of structural MRI. The most popular dMRI method is diffusion tensor imaging (DTI) that allows the three-dimensional characterization of water diffusion in anisotropic conditions, in which the diffusive motions of water molecules depend on the spatial direction considered, because of the presence of ordered structures with one predominant direction. For example, in the white matter of the brain water molecules diffuse preferentially along the axis of the nerve fibers. Comparing the acquisitions obtained with diffusion weighting along at least 6 different directions, the diffusion tensor can be estimated. The principal diffusion direction (corresponding to the fiber direction in white matter) and information about different characteristics of diffusion can be inferred from the diffusion tensor; among the many proposed parameters, the most commonly used ones are the Mean Diffusivity (MD), describing the degree of water mobility averaged over all the directions and the Fractional Anisotropy (FA), describing the preponderance of the principal diffusion direction over the others. The DTI data may also be used for three-dimensional mapping of the fibers of the white substance (tractography) for in vivo exploration of the anatomical connectivity of the human brain. The main fiber bundles, in particular in cerebral white matter, are shown in a three-dimensional reconstruction and with different colours,

corresponding to different directional vectors using a special software. An important application of DTI is the analysis of the integrity of cerebral white matter, particularly in the case of demyelinating disorders (multiple sclerosis), degenerative diseases (Alzheimer's disease) and brain tumors that infiltrate the fiber bundles or for example associated to "blurring".

In conclusion the fields of application of MRI can be many, in general for the study of the brain structures in both physiological and pathological conditions. Moreover it represents an useful support in the diagnostic phase, in the planning of a treatment or a surgical resection and in a follow-up process.

1.4 SCOPE OF THE THESIS

Aim of the present project is to better characterize the most frequent abnormalities that occur in TLE patients, such as the **focal cortical dysplasia** (FCD Type IIIa) and **hippocampal sclerosis**, in surgical samples from TLE patients both at the radiological and neuropathological level.

Specific aims:

1) To correlate high-field *ex-vivo* MR imaging and histopathological features in normal and dysplastic cortex in order to improve the diagnostic criteria of this form of dysplasia that is poor defined both at the neuropathologic and radiologic level.

2) To assess the neuropathological substrate and the possible clinical significance of the radiological temporo-polar gray-white matter abnormality (usually called "blurring") that is frequently reported in TLE patients in order to investigate the possible long lasting effect of epilepsy.

3) To investigate the hippocampal structure and to correlate high-field *ex-vivo* MR imaging with histopathological features:
a) in sclerotic hippocampi from TLE patients; in this case, we aimed to identify specific patterns of HS subtypes on the basis of their proposed value to predict post-surgical seizure outcome;
b) in healty hippocampi at different stages of development.

1.5 REFERENCES

Bernasconi N, Natsume J, Bernasconi A. Progression in temporal lobe epilepsy: Differential atrophy in mesial temporal structures. Neurology 2005; 65: 223-8.

Blumcke I, Thom M, Wiestler OD. Ammon's horn sclerosis: A maldevelopmental disorder associated with temporal lobe epilepsy. Brain Pathol 2002;12:199-211.

Blumcke I, Thom M, Aronica E, Armstrong DD, Vinters HV, Palmini A, et al. The clinicopathologic spectrum of focal cortical dysplasias: A consensus classification proposed by an ad hoc task force of the ILAE diagnostic methods commission. Epilepsia 2011; 52: 158-74.

Blümcke I, Thom M, Aronica E, Armstrong DD, Bartolomei F, Bernasconi A, Bernasconi N, Bien CG, Cendes F, Coras R, Cross JH, Jacques TS, Kahane P, Mathern GW, Miyata H, Moshé SL, Oz B, Ozkara C, Perucca E, Sisodiya S, Wiebe S, Spreafico R. International consensus classification of hippocampal sclerosis in temporal lobe epilepsy: A Task Force report from the ILAE Commission on Diagnostic Methods. Epilepsia 2013 54:1315:1329

Chassoux F, Semah F, Bouilleret V, Landre E, Devaux B, Turak B, et al. Metabolic changes and electro-clinical patterns in mesio-temporal lobe epilepsy: A correlative study. Brain 2004; 127: 164-74.

Concha L, Beaulieu C, Collins DL, Gross DW. White-matter diffusion abnormalities in temporal-lobe epilepsy with and without mesial temporal sclerosis. J Neurol Neurosurg Psychiatry 2009; 80: 312-9.

Crino PB, Duhaime AC, Baltuch G, White R. (2001). "Differential expression of glutamate and GABA-A receptor subunit mRNA in cortical dysplasia". Neurology 56(7):906-13.

Engel J Jr, Van Ness PC, Rasmussen TB, Ojemann LM. Outcome with respect to epileptic seizures. In Engel J Jr (ed). Surgical Treatment of the Epilepsies, 2nd edn,1993; pp 609-621. New York: Raven Press

Garbelli R, Meroni A, Magnaghi G, Beolchi MS, Ferrario A, Tassi L, Bramerio M, Spreafico R. (2006). "Architectural (Type IA) focal cortical dysplasia and parvalbumin immunostaining in temporal lobe epilepsy". Epilepsia 47(6):1074-8.

Najm IM, Tilelli CQ, Oghlakian R. (2007). "Pathophysiological mechanisms of focal cortical dysplasia: a critical review of human tissue studies and animal models". Epilepsia 48 Suppl 2:21-32. Review.

Sommer W. (1880) Erkrankung des Ammonshorns als aetiologischesMoment der Epilepsie. Arch Psychiatr 10:631–675

Tassi L, Meroni A, Deleo F, et al. Temporal lobe epilepsy: Neuropathological and clinical correlations in 243 surgically treated patients. Epileptic Disord 2009;11:281-292.

Thom M, Harding BN, Lin WR, Martinian L, Cross H, Sisodiya SM. (2003). "Cajal-Retzius cells, inhibitory interneuronal populations and neuropeptide Y expression in focal cortical dysplasia and microdysgenesis". Acta Neuropathol 105(6):561-9.

Wiebe S, Blume WT, Girvin JP, Eliasziw M. A randomized, controlled trial of surgery for temporal lobe epilepsy. N Engl J Med 2001; 345: 311-318

Chapter 2

Combined 7 T-MRI and histopathological study of normal and dysplastic samples from TLE patients

Neurology 2011;76(13):1177-85

Rita Garbelli[1], PhD, Ileana Zucca[4], PhD, **Gloria Milesi**[1], MSc, Alfonso Mastropietro[4,7], MSc, Ludovico D'Incerti[2], MD, Laura Tassi[5], MD, Nadia Colombo[6], MD, Carlo Marras[3], MD, Flavio Villani[1], MD, Ludovico Minati[4], MSc, and Roberto Spreafico[1], MD, PhD

[1]Clinical Epileptology and Experimental Neurophysiology Unit, [2]Neuroradiology Unit, [3]Department of Neurosurgery and [4]Scientific Department, "Fondazione IRCCS Istituto Neurologico "C. Besta", Milano, Italy

[5] "C. Munari" Epilepsy Surgery Centre and [6]Departments of Neuroradiology, Niguarda Hospital, Milano, Italy

[7] Politecnico di Milano, Department of Bioengineering, Italy

ABSTRACT

Objectives: The purpose of the study was to investigate the abnormalities of cortical lamination observed in temporal lobe specimens obtained during surgery for intractable TLE with hippocampal sclerosis. Specifically, we aimed 1) to correlate high-field ex-vivo MR imaging with histopathological analysis and 2) to evaluate the effect of tissue fixation on image contrast.

Methods: A cohort of thirteen specimens was considered. T2-weighted imaging and relaxometry were performed during and after fixation using a 7 T experimental scanner. After imaging, the specimens were studied with histopathological (Black Gold myelin fiber staining) and immunohistochemical (NeuN neuronal staining) methods in order to explore the correspondence between MRI and histopathological features.

Results: The principal findings of this study are 1) that superior MRI contrast is obtained among the cortical layers using completely fixed specimens as opposed to recently-excised tissue, 2) that the intensity of the T2-weighted MRI signal is lowest (hypointensity) at the site of highest fibre concentration and cellular density, and highest (hyperintensity) when the density of fibres and cells is lowest, and 3) that the MRI signal is altered in presence of abnormal cortical lamination (FCD Type IA).

Conclusions: High resolution ex-vivo MRI enables the study of intracortical organization in normal and pathological areas. Comparisons between MRI, NeuN and Black Gold indicate that the differences apparent in T2-weighted images are mainly related to fiber concentration, although neuronal density might also play a role.

INTRODUCTION

A central issue for the clinical interpretation of structural magnetic resonance imaging (MRI) findings is the relationship between image contrast and cyto- and myeloarchitectonic patterns. Although several high-resolution post-mortem studies have been performed and have established, for example, the importance of the density of myelin, cellular density and iron concentration (1-6), the exact anatomical-pathological correlates of observed MRI abnormalities remain unclear for many disorders.

Hippocampal sclerosis (HS), the prevalent cause of temporal lobe epilepsy (TLE), is frequently associated with Focal Cortical Dysplasia (FCD) Type IA within the temporo-polar region (7-9). The characteristic finding in this form of cortical dysplasia is dyslamination of the cortical architecture, but the diagnostic criteria remain ill-defined, both at the neuropathological (8) and at the radiological level (10).

Here, we present a case series in which ex-vivo high-resolution 7 T MRI and histopathological studies were jointly performed on surgical specimens from TLE patients. We aimed at obtaining information useful to improve the detection and specification of FCD type IA, and to contribute in the characterization of the correspondence between MRI contrast and histopathological features. Towards this purpose, we included in the study both surgical samples containing Type IA FCDs and samples of normal-appearing cortex. Prior to investigating the correspondence between MRI and histopathology, we performed preliminary experiments to verify the effect of tissue fixation on MRI contrast in these samples.

METHODS

Patients and clinical data

Surgical specimens were obtained from 13 patients who had undergone surgery for refractory TLE with HS either at the "C. Munari" Epilepsy Surgery Center of the Niguarda Hospital or at the "C. Besta" Neurological Institute (Milano, IT). All resections were performed for strictly therapeutic reasons after informed consent.

Pre-surgical evaluation included taking a detailed family and epileptologic history, neurological examination, complete neuropsychological study, high-resolution 1.5 T MRI performed according to a standard protocol (10), and comprehensive EEG or video-EEG.

The anterior temporal lobe and the hippocampus were always resected. Postoperative histopathological evaluation confirmed the presence of HS in all patients. FCD Type IA was detected in nine cases, whereas in the remaining four cases the temporal cortex appeared normal (see Table 1). The diagnosis of FCD Type IA was established, according to the current classification scheme (11), in presence of cortical dyslamination, whereas HS was diagnosed in presence of diffuse gliosis associated with pyramidal cell loss in the CA1, CA3 and CA4 (hilus) sectors of Ammon's horn (12).

Standard protocol approvals, registration, and patient consents

The local ethics committee formally approved the study, and all patients gave written informed consent to use cerebral specimens for research purposes.

Experimental protocol

In a subgroup of six patients (no. 4-7 and 11-12 in Table 1), the effect of fixation on MRI contrast was evaluated. Towards this purpose, MR imaging (see below) was performed twice, according to the following

procedure. First, the whole resected specimen was placed in fixative solution (4% paraformaldehyde) immediately after surgery and submitted for imaging (5 hours on average, ± 1 hour). Then, the specimen was divided in 4 coronal slabs and post-fixed in the same solution for 4-5 days at 4°C. Subsequently, alternate slabs cut through the antero-posterior extent of the temporal lobe were embedded in 6% agarose and imaged again. The adjacent slabs were embedded in paraffin and processed for routine neuropathology.

In the remaining patients (no. 1-3, 8-10 and 13 in Table 1), MRI was performed only once, on selected slabs embedded in agarose after an appropriate fixation time (4-5 days at 4°C). Embedding the samples in agarose has the advantage of attenuating potential artefacts related to motion and flow of the fixative solution, and reduces susceptibility differences.

Because of this experimental protocol, in four cases out of the nine affected by FCD, the slab submitted for MRI and subsequently considered for the correlative neuropathological investigation did not contain the dysplastic lesion (Table 1, n. 5-8).

The hippocampi were kept separately and not considered for this study.

Histopathological study

After MR imaging, each fixed slab was cut into 50 µm-thick serial coronal sections by means of a vibratome (VT1000S, Leica, Heidelberg, Germany), attempting to maintain the same orientation for MRI and histology. Alternate sections were processed for i) NeuN immunocytochemistry (1:3000, Chemicon, Tamecula, CA, USA) according to the standard immunoperoxidase protocol (13) in order to detect neuronal distribution, ii) thionin (0.1% in distilled water) for cytoarchitectonic analysis, and iii) Black-Gold II (0.3% dissolved in 0.9% saline, Histo-Chem) for myelin staining.

MR image acquisition and analysis

Imaging was performed on a 7 Tesla horizontal-bore scanner (BioSpec 70/30 USR, Bruker, Ettlingen, Germany) equipped with 200 mT/m gradients and a 35 mm transceiver quadrature coil. An automated water cooling system maintained the bore temperature below 20°C.

High resolution T2-weighted images were acquired with TE=50 ms, TR=4.3 s, NA=36, slice thickness=0.7 mm, field-of-view=32×32 mm^2, data matrix=256×256; this yielded a 73×73 $\square m^2$ in-plane resolution. Further, in the samples that were imaged during and after fixation, T2 relaxometry was performed applying a mono-exponential model and using TE=13, 26, 39, 52 … 208 ms, TR=5 s, slice thickness=0.7 mm, NA=4, field-of-view=44×44 mm^2, data matrix=256×256.

Preliminary observations indicated that penetration of the fixative agent diffusing inwards from the cortical surface resulted in signal intensity inhomogeneities visible on the T2-weighted images. In order to assess this feature when comparing the images acquired during and after fixation, we performed automated segmentation using a K-means algorithm (14) implemented in MATLAB (MathWorks Inc., Natick MA, USA).

To further examine the effect of fixation and highlight the differences between FCD and normal-appearing samples, the signal intensity of the supra- and infra-granular layers was compared using both histograms and non-parametric Wilcoxon tests.

Additionally, we generated signal intensity profiles for both MR and histopathological images, utilizing the ImageJ software (http://rsbweb.nih.gov/ij/, National Institute of Health, USA; (4, 5, 15, 16) to extract values along a vector oriented perpendicular to the pial surface.

RESULTS

Effect of fixation on MR image contrast

Visual analysis of the T2-weighted images acquired after complete fixation revealed a clear signal intensity difference between the upper and lower parts of the cortical ribbon, which were separated by a thin band of low signal intensity. By contrast (Fig. 1A vs. Fig. 1B), images acquired with incomplete fixation were characterized by very uneven grey matter signal intensity throughout the whole anteroposterior extent of the specimen. These qualitative findings are confirmed by automated segmentation, which successfully separated the supra- and infra-granular layers of the cortex on images acquired after complete fixation, but failed even in reliably identifying grey and white matter on images acquired with incomplete fixation (Fig. 1C vs. Fig. 1D).

Analysis of the voxel values in two regions-of-interest (ROIs) drawn manually on the infra- and supra-granular layers revealed a different level of overlap between the two histograms (Fig. 1E vs. Fig. 1F); in fact, the average signal difference was 11±3% in incompletely fixed vs. 22±3% in fixed tissue (Fig. 1G, $p=0.03$).

The T2 relaxometry maps obtained from the same specimen during and after fixation are shown in Fig. 1H and Fig. 1I. A change in relaxation rates is evident, and was confirmed averaging the values obtained from the other six specimens, which gave 20±5 ms (during fixation) vs. 60±8 ms (after fixation) for grey matter close to the pial surface, 40±8 ms vs. 50±8 ms vs. for grey matter in deeper sub-granular layers, and 30±5 ms vs. 30±8 ms for white matter.

Considering the improved contrast obtained after fixation, the imaging-histopathology correlation was only performed on images acquired on completely fixed tissue.

Comparison of MR and histopathological images in samples with normal cortical layering

As expected, a clear boundary between grey and white matter was observed on both MR (Fig. 2A) and histopathological (Fig. 2B and Fig. 2C) images. As described above, on the MR images the supra-granular layers appeared hyperintense with respect to the infra-granular layers (Fig. 2A and Fig. 2D). This feature closely parallels the myelin-stained sections, in which higher density of fibres was observed in the deeper part of grey matter (Fig. 2C and Fig. 2F).

Moreover, in MR images a hypointense band running longitudinally to the pial surface was consistently observed (Fig. 2A and Fig. 2D). This corresponds to layer IV, as demonstrated by the presence of densely packed NeuN-positive neurons (Fig. 2B and Fig. 2E) and by high concentration of myelinated fibres (Fig. 2C and Fig. 2F).

Line profiles (Fig. 2G, Fig. 2H and Fig. 2I) confirmed that layer IV is visible as a signal intensity dip on MR images and histological sections.

Comparison of MR and histopathological images in samples with FCD

The MR images obtained from specimens no. 9 and 10 did not show any appreciable difference in signal intensity between the supra- and infra-granular layers (Fig. 3A and Fig. 3D vs. Fig. 2A and Fig. 2D). Furthermore, the hypointense band corresponding to layer IV was absent, while a thin hyperintense longitudinal band, located just beneath layer I, was apparent. In these specimens, NeuN immunocytochemistry demonstrated that individual cortical layers were not clearly distinguishable, with blurred borders between layers III-IV and IV-V (Fig. 3B and Fig. 3E). Furthermore, we observed a peculiar abnormality in the superficial cortex, characterized by partial depletion of neurons in layers II and III, putatively corresponding to the hyperintense line seen on the MR images, and by a band of apparently elevated cellular concentration at the outer border of layer

II (Fig. 3A, Fig. 3D and e-Fig. 1A). In these cases, we also observed reduced density of myelinated fibres, particularly in the infra-granular layers (Fig. 3C and Fig. 3F). The line profiles appeared markedly different with respect to those obtained in control specimens (Fig. 3G, Fig. 3H and Fig. 3I vs. Fig. 2G, Fig. 2H and Fig. 2I); namely, the dip corresponding to layer IV was absent and no difference between supra/infra-granular layers could be seen.

In case no. 11, while the signal intensity difference between the supra- and the infra-granular layers was absent, the hypointense band corresponding to layer IV was present (Fig. 4A). NeuN immunohistochemistry revealed a blurred boundary between layers II-III, with relative preservation of the other layers (Fig. 4B). Further, the myelin-stained sections indicated reduced fibre density in the infra-granular layers (Fig. 4C). In agreement with these findings, the line profiles highlighted the absence of an intensity difference between the supra- and infra-granular layers, whereas the dip corresponding to layer IV was visible (Fig. 4D, Fig. 4E and Fig. 4F).

The qualitative observation that MRI images obtained from some FCD samples did not reveal difference between the infra- and supra-granular layers, were quantified by analysis of the voxel values in these two regions-of-interest (ROIs). A higher level of overlap was obtained in dysplastic cases in comparison to control cases (Fig. e-1B vs. Fig. 1F), and the average signal difference was 6.7±4% in dysplastic vs. 22±3% in control tissue (Fig. e-1C, $p=0.03$).

In specimens from cases no. 12 and 13, the MR images appeared normal, but NeuN immunohistochemistry revealed mild neuronal clustering in cortical layer II, limited to one gyrus, without any appreciable alteration in myelin staining (not shown).

DISCUSSION

The principal findings of this study are 1) that better MRI results are obtained using completely fixed specimens as opposed to recently-excised tissue, 2) that the MRI signal is related to both myelin and cellular density, and 3) that the MRI signal is altered in presence of abnormal cortical lamination (FCD Type IA).

Previous work correlating ex-vivo MRI with histopathology has already highlighted the possibility of artefacts related to the fixation process. During fixation, there is a competition between multiple factors. Ongoing decomposition is characterized by increasing water content and progressive destruction of the cell matrix. This process is slowed and eventually stopped by the action of the fixative agent, which diffuses inwards from the tissue surface and promotes protein cross-linking and immobilization of tissue water. The primary effects of decomposition and fixation are paralleled by those related to washing the sample in buffer solution and embedding it in agar, which increase the water content. The competition between these processes leads to complex dynamic changes in tissue properties, complicating the choice of acquisition parameters and potentially confounding the interpretation of imaging findings. Importantly, the relaxation times stabilize after fixation is complete, on levels which depend on the relative contribution of each factor (17-20). Our findings show that, for these samples, it is advantageous to wait until the fixation process is complete prior to performing MR imaging, as this leads not only to reduced fixation-related inhomogeneities, but also to generally superior T2 contrast among cortical layers.

Our results indicate that the MRI signal intensity on T2-weigthed images is strongly related to the density of myelinated fibres as revealed in both normal and pathological specimens. In normal samples, we observed that the higher density of myelinated fibres found in the deep part of the cortex corresponded to reduced MRI

signal intensity in the infra-granular layers. In the FCDs in which fibre density was reduced, the T2-weighted signal intensity difference normally observed between supra- and infra-granular layers was lost, as confirmed by the results from automated segmentation. This relation between MRI signal and myelin density had already been described in a number of studies, mainly performed on the human visual cortex, both in-vivo and ex-vivo. In particular, the lowest signal intensity has been reported for the stripe of Gennari, which is composed by heavily myelinated fibres (1, 3-5, 21, 22). Our results nevertheless contribute to the existing literature by confirming that this relation extends beyond the visual cortex, and is indeed highly relevant to the study of temporal lobe specimens. Further, the present study is, to our knowledge, the first demonstrating that ex-vivo MRI can differentiate the contrast of supra- and infra-granular layers of the cortex.

Our histological data suggest that the marked hypointensity observed in layer IV is likely due to the combined effects of increased fibre density, due to the horizontal plexus, and increased cellular density. This hypothesis is supported by the line profile results and, importantly, by our findings on FCD samples: whenever cellular density or myelin density were altered, a corresponding abnormality was detected on the MR images.

Previous studies have demonstrated that high cellular density, even when coupled with low myelin content, such as found in the granule cell layer of the dentate gyrus, results in low MR signal intensity; this leads to the hypothesis that regional and pathological variations in MRI contrast may at least partly reflect neuronal density (4). This finding has been replicated in several correlative studies performed in neocortex (2, 16).

One needs to consider that also the concentration of iron strongly modulates MR signal intensity, especially on T2- and T2*-weighted images. Unfortunately, despite the fact that much is known about iron

in neurodegenerative and vascular disorders, only limited information is available regarding its role in determining the contrast observed between cortical layers. In a recent paper, Fukunaga and colleagues (23) have demonstrated that iron is distributed over the cortical layers in a pattern closely following regional myeloarchitecture. This leads to the hypothesis that the observed correspondence between myelin density and MR signal intensity could be mediated by iron concentration differences; in turn, this opens the possibility that some of the observed MRI contrast abnormalities could be directly caused by primary iron concentration changes. We cannot exclude this outright on the basis of our data alone, however we note that, at present, there is no evidence for abnormal iron concentration in FCD.

FCD Type IA are as-yet poorly defined in histopathological terms, and standard structural MRI is often unrevealing. Recent attempts to utilize voxel-based morphometry to identify these subtle abnormalities have been unsuccessful (24). By contrast, our results, obtained at high field intensity, clearly demonstrate that abnormal cortical layering, such as blurred demarcation of the layer IV and clustered neurons in the outer part of the supragranular layers, can be detected by MR imaging. Therefore, these results are potentially relevant from a clinical diagnostic perspective, because the close matching that we have observed between MR imaging features and histopathology provides the ultimate demonstration that, if sufficient resolution could be attained in-vivo, structural MRI could detect the minute intra-cortical abnormalities which characterize FCD Type IA. Indeed, the demonstration of cortical laminae has been achieved several times using ex-vivo MRI, and in some cases also in in-vivo MRI studies.

The last decade has been characterized by a steady shift from 1.5 T to 3 T scanners at the majority of epilepsy surgery centres worldwide, and 4 T and 7 T systems are already rapidly diffusing. It appears reasonable to speculate that increasing field strength, coupled with the development of new coils, pulse sequences and software, may

make it possible to replicate our findings in-vivo in the near future in a setup transferable to clinical practice. The possibility of utilizing high-resolution MRI in selected cases to detect currently inaccessible features such as the absence or thinning of layer IV or the alteration of contrast between supra- and infra-granular layers would completely revolutionize the diagnostic protocols for epilepsy. Our results, although limited in the number of cases, provide a strong motivation for such technical efforts by demonstrating that MRI can in principle detect the subtle alterations found in this poorly characterized FCD type. Indeed, even though our observations were made on fixated samples, the existing literature demonstrates that the cortical layers are potentially visible to MR under normal *in-vivo* conditions (3,5,21). Here, the effect of fixation becomes particularly important under *ex-vivo* conditions, but fixation is not a fundamental pre-requisite for layer visibility. While brain pulsatility may pose specific challenges, cardiac-gating and movement-correction techniques enable to attenuate its effects (25,26).

Acknowledgements

The authors thank Dr. A. Cattalini (Clinical Epileptology and Experimental Neurophysiology Unit, Fondazione I.R.C.C.S., Istituto Neurologico "C. Besta", Milano, Italy) for his skilful technical support.

Table MRI and neuropathologic features in the considered specimens

Patients	Age, y/sex	Preoperative MRI 1.5 T: Temporal lobe atrophy	Patient diagnosis: Histopathologic analysis	MRI features of the slabs submitted to experimental 7-T MRI		Neuropathologic characteristic of the slabs submitted to experimental MRI		
				Different intensity between supragranular and infragranular L	Hypointensity in L IV	FCD	NeuN immunohistochemistry	Myelin staining
1	10/M	No	HS	Yes	Yes	No	Normal cortical layering	Normal
2	48/F	No	HS	Yes	Yes	No	Normal cortical layering	Normal
3	9/M	No	HS	No	+/−	No	Normal cortical layering	Reduced in L IV
4	36/M	No	HS	Yes	Yes	No	Normal cortical layering	Normal
5	37/F	No	FCDIA + HS	Yes	Yes	No	Normal cortical layering	Normal
6	53/F	No	FCDIA + HS	Yes	Yes	No	Normal cortical layering	Normal
7	51/F	No	FCDIA + HS	Yes	Yes	No	Normal cortical layering	Normal
8	32/M	No	FCDIA + HS	Yes	Yes	No	Normal cortical layering	Normal
9	47/M	Yes	FCDIA + HS	No	No	IA	Abnormalities in L II and IV	Reduced in L IV, V, VI
10	44/M	No	FCDIA + HS	No	No	IA	Abnormalities in L II and IV	Reduced in L V, VI
11	58/M	Yes	FCDIA + HS	No	No	IA	Abnormality in L II	reduced in L IV, V, VI
12	40/F	Yes	FCDIA + HS	Yes	Yes	IA	Abnormality in L II	Normal
13	46/F	No	FCDIA + HS	Yes	Yes	IA	Abnormality in L II	Normal

Abbreviations: FCD = focal cortical dysplasia; HS = hippocampal sclerosis; L = cortical layer.

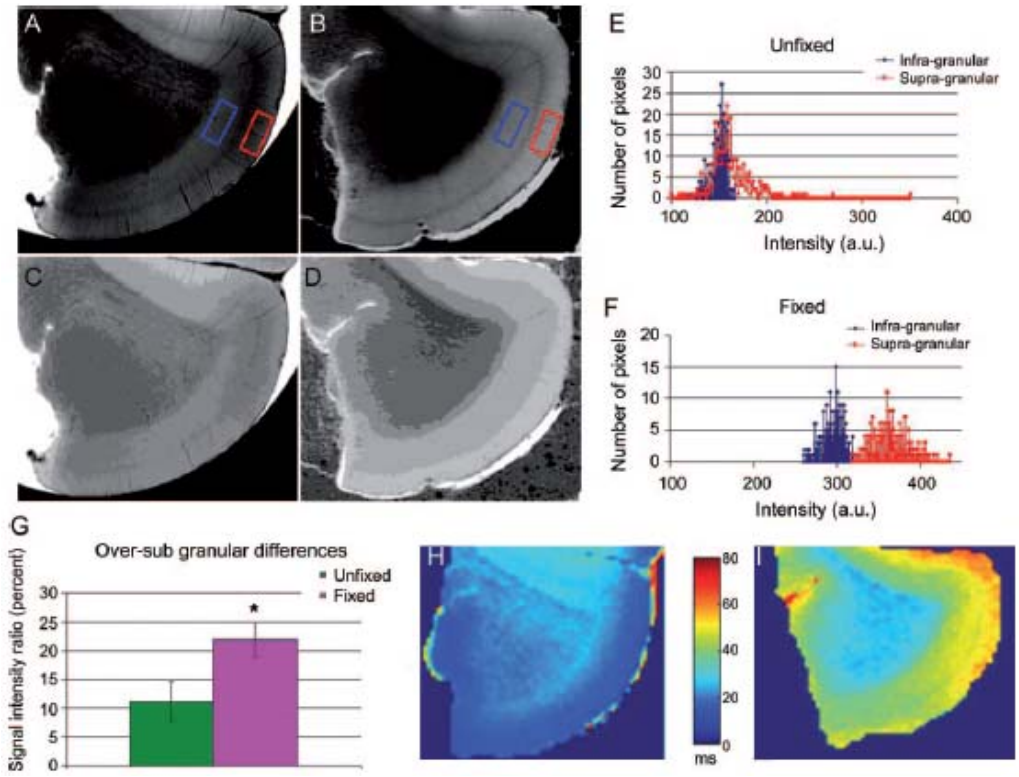

Fig. 1

Effect of fixation on MR image contrast in a sample with normal cortical layering

Example T2-weighted images from case no. 4 obtained during (A) and after complete fixation (B), and corresponding results from K-means segmentation (C and D) confirming improved contrast following fixation. Histograms of signal intensity during (E) and after fixation (F) show clear differentiation between the supra- (red) and infra-granular (blue) layers only after complete fixation. Bar-chart (G) of the signal intensity ratio between the supra- and infra-granular layers during (green) and after (purple) fixation. T2 relaxometry maps obtained during (H) and after complete fixation (I), indicating a diffuse increase in relaxation times.

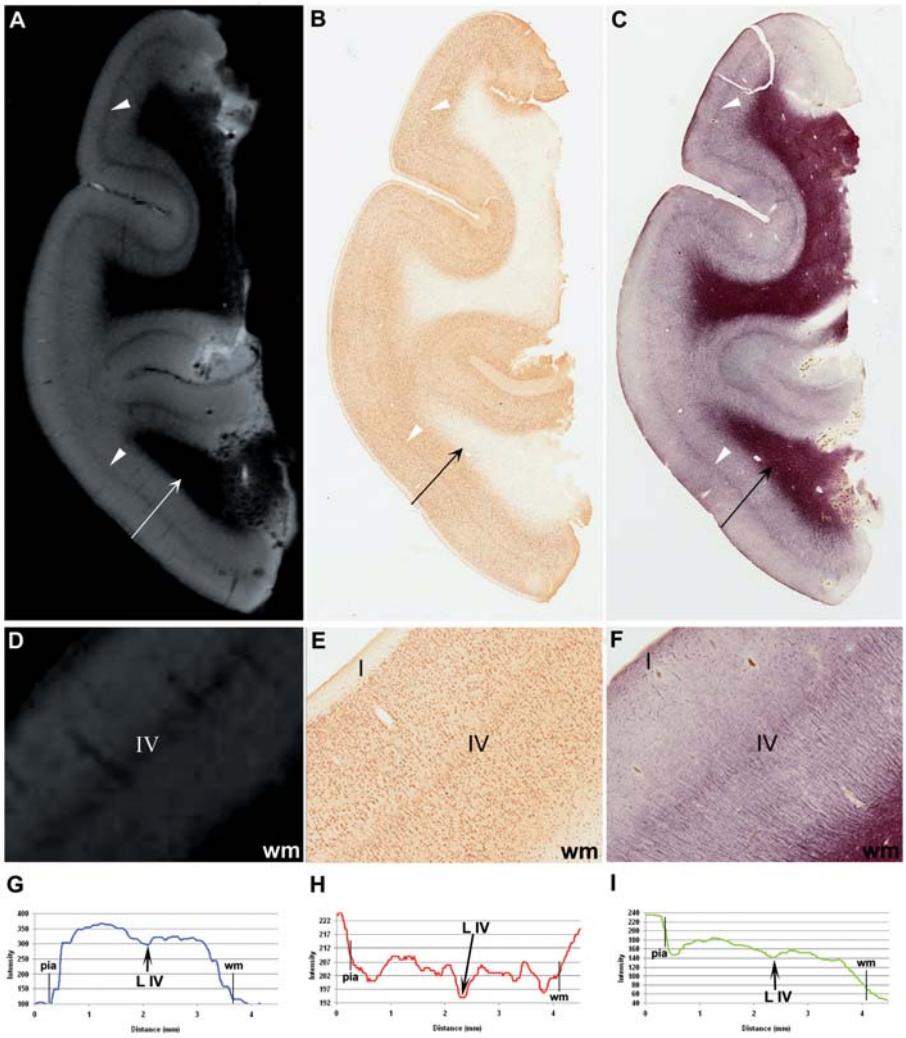

Fig. 2

Comparison of MR and histopathological images in a sample with normal cortical layering

Comparison of T2-weighted MR images (A), NeuN immunohistochemistry (B) and myelin staining (C) for case no. 2. The areas indicated by the arrows are shown at higher magnification in panels D, E and F. Note the hypointense band running along the middle of the cortex on the MR images (A and D, arrowheads) and corresponding to layer IV as confirmed by NeuN (B and E) and myelin-stained sections (C and F). Moreover, note the different signal intensity between the supra- and infra-granular layers (A and D), closely following myelin distribution (C and F). The line profiles, calculated as shown by the arrows, exhibit a dip corresponding to layer IV on the MR images (G) and stained sections (H and I).

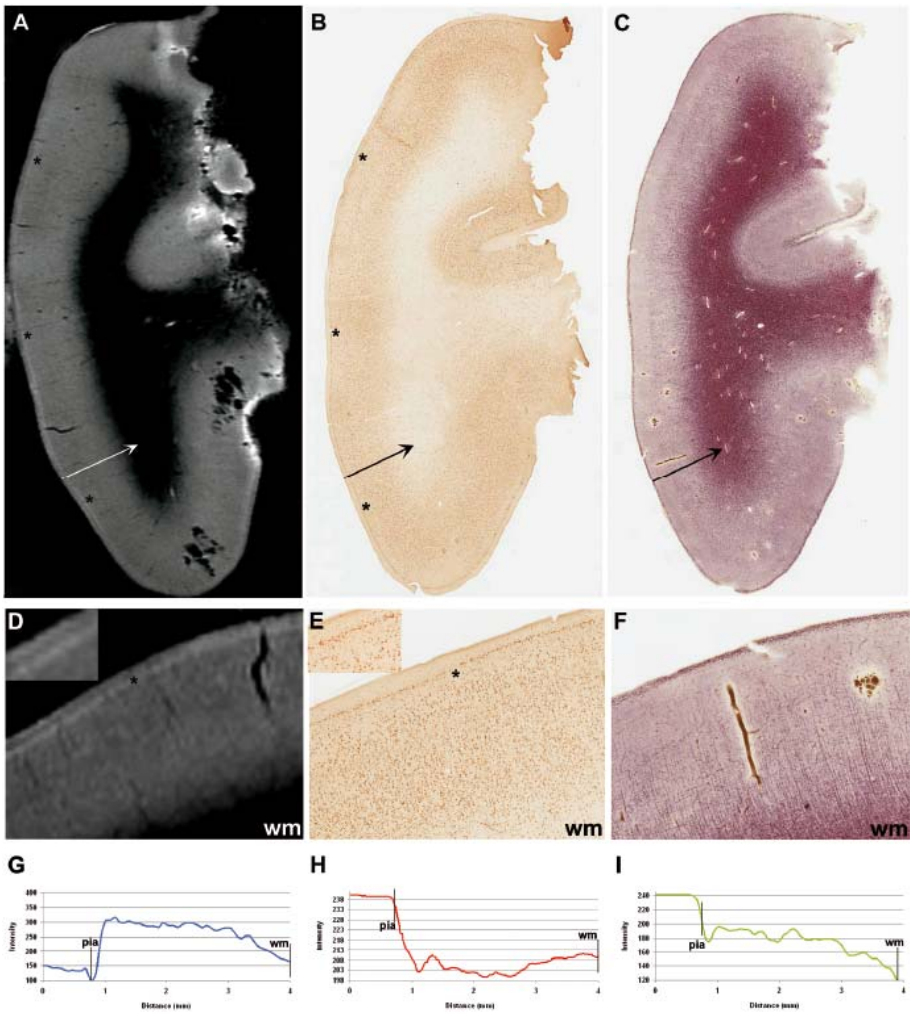

Fig. 3

Comparison of MR and histopathological images in a sample with FCD, case no. 9

Comparison of T2-weighted MR images (A), NeuN immunohistochemistry (B) and myelin staining (C) for case no. 9 (higher magnification in D, E and F). Note the absence of the hypointense band on the MR images (A and D), corresponding to the lack of a clear layer IV on the NeuN (B and E) and myelin-stained sections (C and F). Further, note that the MRI images (A and D) do not show a signal intensity difference between the supra- and infra-granular layers; this parallels reduced fibre density visible in the myelin-stained sections (C and F). A peculiar hyperintense signal is observed in the superficial part of the cortex (marked by asterisks on A and D), corresponding to abnormal cellular density observed across

layers II and III (B and E, asterisks). The line profiles confirm the absence of a dip corresponding to layer IV on the MR image (G) and histological sections (H and I).

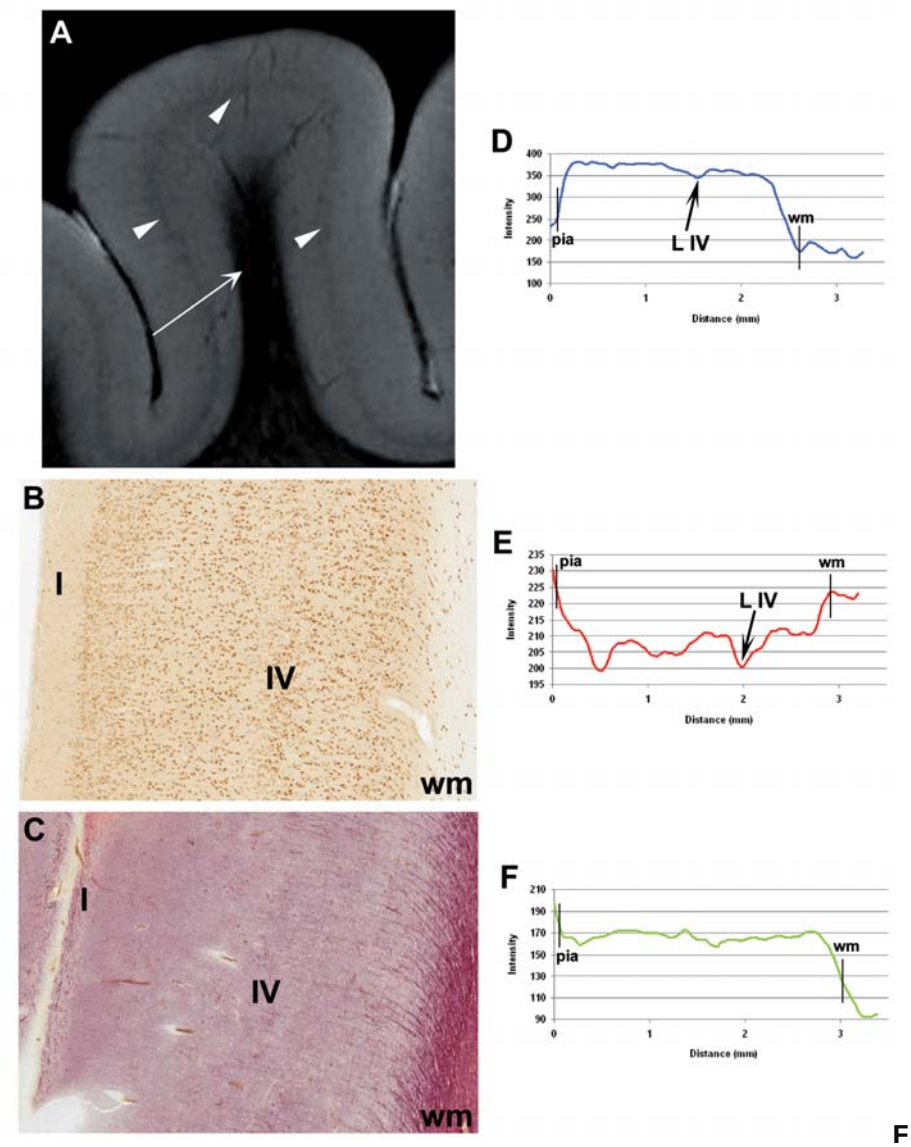

Fig. 4

Comparison of MR and histopathological images in a sample with FCD, case no. 11

T2-weighted MR image (A) from case n. 11, highlighting a hypointense band corresponding to layer IV (arrowheads) in absence of a marked signal intensity difference between the supra- and infra-granular

layers. These features correspond to the presence of a well organized layer IV, as revealed by NeuN immunohistochemistry (B), combined with reduced fibre concentration in the deeper part of the cortex as shown by the myelin-stained sections (C). The line profiles (D, E and F) confirm these observations.

References

1. Clark VP, Courchesne E, Grafe M. In vivo myeloarchitectonic analysis of human striate and extrastriate cortex using magnetic resonance imaging. Cereb Cortex 1992;2:417-424.

2. Yoshiura T, Higano S, Rubio A, et al. Heschl and superior temporal gyri: Low signal intensity of the cortex on T2-weighted MR images of the normal brain. Radiology 2000;214:217-221.

3. Barbier EL, Marrett S, Danek A, et al. Imaging cortical anatomy by high-resolution MR at 3.0T: Detection of the stripe of gennari in visual area 17. Magn Reson Med 2002;48:735-738.

4. Fatterpekar GM, Naidich TP, Delman BN, et al. Cytoarchitecture of the human cerebral cortex: MR microscopy of excised specimens at 9.4 tesla. AJNR Am J Neuroradiol 2002;23:1313-1321.

5. Walters NB, Egan GF, Kril JJ, et al. In vivo identification of human cortical areas using high-resolution MRI: An approach to cerebral structure-function correlation. Proc Natl Acad Sci U S A 2003;100:2981-2986.

6. Fischl B, Wald LL. Phase maps reveal cortical architecture. Proc Natl Acad Sci U S A 2007;104:11513-11514.

7. Fauser S, Schulze-Bonhage A, Honegger J, et al. Focal cortical dysplasias: Surgical outcome in 67 patients in relation to histological subtypes and dual pathology. Brain 2004;127:2406-2418.

8. Blumcke I, Vinters HV, Armstrong D, Aronica E, Thom M, Spreafico R. Malformations of cortical development and epilepsies: Neuropathological findings with emphasis on focal cortical dysplasia. Epileptic Disord 2009;11:181-193.

9. Tassi L, Meroni A, Deleo F, et al. Temporal lobe epilepsy: Neuropathological and clinical correlations in 243 surgically treated patients. Epileptic Disord 2009;11:281-292.

10. Colombo N, Salamon N, Raybaud C, Ozkara C, Barkovich AJ. Imaging of malformations of cortical development. Epileptic Disord 2009;11:194-205.

11. Palmini A, Najm I, Avanzini G, et al. Terminology and classification of the cortical dysplasias. Neurology 2004;62:S2-8.

12. Blumcke I, Thom M, Wiestler OD. Ammon's horn sclerosis: A maldevelopmental disorder associated with temporal lobe epilepsy. Brain Pathol 2002;12:199-211.

13. Garbelli R, Munari C, De Biasi S, et al. Taylor's cortical dysplasia: A confocal and ultrastructural immunohistochemical study. Brain Pathol 1999;9:445-461.

14. Sharma N, Aggarwal LM. Automated medical image segmentation techniques. J Med Phys 2010;35:3-14.

15. Annese J, Pitiot A, Dinov ID, Toga AW. A myelo-architectonic method for the structural classification of cortical areas. Neuroimage 2004;21:15-26.

16. Eickhoff S, Walters NB, Schleicher A, et al. High-resolution MRI reflects myeloarchitecture and cytoarchitecture of human cerebral cortex. Hum Brain Mapp 2005;24:206-215.

17. Shepherd TM, Flint JJ, Thelwall PE, et al. Postmortem interval alters the water relaxation and diffusion properties of rat nervous tissue--implications for MRI studies of human autopsy samples. Neuroimage 2009;44:820-826.

18. Shepherd TM, Thelwall PE, Stanisz GJ, Blackband SJ. Aldehyde fixative solutions alter the water relaxation and diffusion properties of nervous tissue. Magn Reson Med 2009;62:26-34.

19. Fishbein KW, Gluzband YA, Kaku M, et al. Effects of formalin fixation and collagen cross-linking on T2 and magnetization transfer in bovine nasal cartilage. Magn Reson Med 2007;57:1000-1011.

20. Dawe RJ, Bennett DA, Schneider JA, Vasireddi SK, Arfanakis K. Postmortem MRI of human brain hemispheres: T2 relaxation times during formaldehyde fixation. Magn Reson Med 2009;61:810-818.

21. Bridge H, Clare S. High-resolution MRI: In vivo histology? Philos Trans R Soc Lond B Biol Sci 2006;361:137-146.

22. Hinds O, Polimeni JR, Rajendran N, et al. The intrinsic shape of human and macaque primary visual cortex. Cereb Cortex 2008;18:2586-2595.

23. Fukunaga M, Li TQ, van Gelderen P, et al. Layer-specific variation of iron content in cerebral cortex as a source of MRI contrast. Proc Natl Acad Sci U S A 2010;107:3834-3839.

24. Eriksson SH, Thom M, Symms MR, et al. Cortical neuronal loss and hippocampal sclerosis are not detected by voxel-based morphometry in individual epilepsy surgery patients. Hum Brain Mapp 2009;30:3351-3360.

25. Skare S, Andersson JL. On the effects of gating in diffusion imaging of the brain using single shot EPI. Magn Reson Imaging. 2001;19:1125-1128.

26. Nieman BJ, Szulc KU, Turnbull DH. Three-dimensional, in vivo MRI with self-gating and image coregistration in the mouse. Magn Reson Med. 2009;61:1148-1157.

Chapter 3

Blurring in temporal lobe epilepsy patients: clinical, high-field imaging and ultrastructural study

Brain 2012, 135(P8):2337-49

Rita Garbelli,[1] **Gloria Milesi**,[1] Valentina Medici,[1] Flavio Villani,[1] Giuseppe Didato,[1] Francesco Deleo,[1] Ludovico D'Incerti,[2] Michela Morbin,[3] Giulia Mazzoleni,[3] Anna Rita Giovagnoli,[4] Annalisa Parente,[4] Ileana Zucca,[4] Alfonso Mastropietro,[4,5] and Roberto Spreafico[1]

[1]Clinical Epileptology and Experimental Neurophysiology Unit, [2]Neuroradiological Unit, [3]Neuropathology Unit, [4]Scientific Department, Fondazione IRCCS, Istituto Neurologico "C. Besta", Milan, Italy; [5]Department of Bioengineering, Politecnico di Milano, Milan, Italy

Key words: Temporal lobe epilepsy; neuropathology; electron microscopy; high-field MRI, epilepsy surgery

SUMMARY

Magnetic Resonance Imaging (MRI)-positive temporal lobe atrophy with temporo-polar grey/white matter abnormalities (usually called "blurring") has been frequently reported in patients with temporal lobe epilepsy associated with hippocampal sclerosis. The poor distinction of grey and white matter has been attributed to various causes, including developmental cortical abnormalities, gliosis, myelin alterations, a non-specific increase in temporal lobe water content, and metabolic/perfusion alterations. However, there is still no consensus regarding the genesis of these abnormalities, and no histopatologic

prove for a structural nature of MRI changes. The aim of this study was to investigate the pathological substrate of temporo-polar blurring using different methodological approaches and evaluate the possible clinical significance of the abnormalities. The study involved 32 consecutive patients with medically intractable temporal lobe epilepsy and hippocampal sclerosis who underwent surgery after a comprehensive electroclinical and imaging evaluation. They were divided into two groups on the basis of the presence/absence of temporo-polar blurring. Surgical specimens were examined neuropathologically and selected samples from both groups underwent high-field 7T MRI and ultrastructural studies. At clinical level, the two groups were significantly different in terms of age at epilepsy onset (earlier in the patients with blurring) and epilepsy duration (longer in the patients with blurring). Blurring was also associated with lower neuropsychological test scores, with a significant relationship to abstract reasoning. Upon 7T MRI examination, the borders between the grey and white matter were clear in all of the samples, but only those with blurring showed a dishomogeneous signal in the white matter, with patchy areas of hyperintensity mainly in the depth of the white matter. Sections from the patients with blurring that were processed for myelin staining revealed dishomogeneous staining of the white matter, which was confirmed by analyses of the corresponding semi-thin sections. Ultrastructural examinations revealed the presence of axonal degeneration and a significant reduction in the number of axons in the patients with blurring; there were no vascular alterations in either group. These data obtained using different methodological approaches provide robust evidence that temporo-polar blurring is caused by the degeneration of fibre bundles, and suggest slowly evolving chronic degeneration with the redistribution of the remaining fibres. The paper also discusses the correlations between the morphological findings and clinical data.

Abbreviations: EM**:** electron microscopy; FCD: focal cortical dysplasia; GWM: grey/white matter; GM: grey matter; WM: white matter

INTRODUCTION

The findings of studies by Falconer *et al.* (1964) and Margerison and Corsellis (1966), reinforced by those of recent magnetic resonance imaging (MRI) studies (Bernasconi *et al*., 2000), suggest that hippocampal sclerosis (HS) plays a leading role in the genesis of seizures in patients with temporal lobe epilepsy (TLE). Recent reports indicate that HS is frequently associated with other pathologies (Blumcke *et al*., 2002; Tassi *et al*., 2009), but a number of studies have shown that, even in the absence of a second and independent principal lesion, the abnormalities found in TLE patients go beyond the hippocampus, thus suggesting a more widespread substrate for the generation or persistence of seizures. MRI has revealed ipsilateral temporal atrophy with temporo-polar grey/white matter (GWM) abnormalities in 32-68% of TLE patients with associated HS, which have been described as a loss of GWM demarcation together with increased signal intensity in T2-weighted images (Adachi *et al*., 2006; Choi, *et al*., 1999; Coste *et al*., 2002; Meiners *et al*., 1999; Mitchell *et al*., 1999; Mitchell *et al*., 2003). This type of abnormality (commonly called "GWM blurring") is described in many papers as one of the most sensitive radiological markers of focal cortical dysplasia (FCD), but some authors suggest that it may reflect the presence of densely heterotopic neurons in the subcortical white matter (WM) or myelin alterations (Choi *et al*., 1999; Hardiman *et al*., 1988; Meiners *et al*., 1999; Thom *et al*., 2001).

Recent imaging techniques have confirmed that the loss of GWM demarcation in the temporal pole of TLE patients with HS is not due to

imaging artefacts, thus corroborating the hypothesis that epilepsy may depend on a more widespread temporal lobe disturbance (Bernasconi *et al*., 2005; Concha *et al*., 2009; Kahane *et al*., 2002; Meiners *et al*., 1994; Meiners *et al*., 1999; Mitchell *et al*., 1999; Moran *et al*., 2001; Sankar *et al*., 2008). The suggestion that extra-hippocampal structures (particularly the temporal pole) may play an important role in TLE patients with HS is supported by electroclinical and perfusion data (Chabardes *et al*., 2005; Chassoux *et al*., 2004; Mitchell *et al*., 1999; Moran *et al*., 2001; Ryvlin *et al*., 1998; Ryvlin *et al*., 2002; Weder *et al*., 2006).

As TLE is the most frequent form of drug-resistant focal epilepsy, surgery is an important and safe option allowing patients to gain seizure freedom (Wiebe *et al*., 2001) and the increasing number of operated subjects with a good postoperative follow-up have also provided specimens for precise neuropathological studies and the investigation of anatomo-clinical correlations. However, there is still no consensus regarding the genesis of these abnormalities, and no definite correlation has yet been found between histopathological findings and MRI-revealed structural abnormalities, with gliosis (Falconer *et al*., 1964), developmental cortical abnormalities (Hardiman *et al*., 1988; Thom *et al*., 2001), myelin loss (Meiners *et al*., 1999), and a non-specific increase in temporal lobe water content (Concha *et al*., 2009; Mitchell *et al*., 1999) all being suggested as possible causes. Furthermore, the question as to whether the GWM abnormalities revealed by MRI are epileptogenic has not been answered, although studies by Coste *et al*. (2002) and Adachi *et al*. (2006) argue in favour of an epileptogenic zone involving the side of the abnormalities. There are also conflicting data concerning surgical outcomes: Mitchell *et al*. (1999) found that the proportion of seizure-free patients was the same in those with and without GWM abnormalities, whereas Choi *et al.* (1999) found a significantly higher success rate in the patients with abnormalities, although Mitchell's

findings are supported by those of a recent study by Schijns *et al.* (2011) that examined the impact of temporal lobe GWM abnormalities on postoperative seizure outcome in patients with TLE and HS undergoing selective amygdalohippocampectomy or anterior temporal lobectomy. All of these studies were carried out using traditional methods that are routinely available in clinical practice, and the results did not reveal with certainty the etiology of the temporo-polar abnormalities found in a variable proportion of TLE patients.

The aim of this study was to investigate the pathological substrate of the temporo-polar blurring revealed by means of routine clinical 1.5 T MRI using the non-traditional approaches of high-field (7 T) MRI combined with light and electron microscopy (EM) of surgical specimens taken from drug-refractory TLE patients with HS. The clinical correlations of the abnormalities were also investigated.

MATERIALS AND METHODS

Subjects

The study involved 32 consecutive patients (11 males and 21 females; mean age 40 ± 9 years, range 24–60) with medically intractable TLE and radiological evidence of HS who underwent surgery at the Carlo Besta Neurological Institute in Milan, Italy. Patients with evidence of HS associated with other principal lesions (tumours, vascular malformations, scars, etc.) were excluded.

The patients underwent surgery after a comprehensive electroclinical and MRI evaluation; none of them required the invasive pre-surgical identification of the epileptogenic zone to be removed.

On the basis of the findings of the presurgical 1.5 T MRI evaluation, the patients were divided into two groups: 18 with HS plus ipsilateral temporo-polar abnormalities (group 1), and 14 with HS but normal ipsilateral GWM definition in the temporal pole (group 2). In order to

assess the presence or absence of these abnormalities, all of the MR images were independently reviewed by two experienced observers (LD, FV) blinded to the neuropathological findings, who used the criteria proposed by Colombo *et al.* (2009) and issued a consensus report.

Preoperative 1.5 T MRI

All of the MRI studies were performed using the same 1.5 T instrument (Siemens Avanto). The MRI protocol included transverse spin-echo (SE) double-echo images of the entire brain (repetition time, TR: 2,000-2,500 msec, echo time, TE: 20-90 msec), number of average, NA: 1, matrix 128 x 256, field of view (FOV) 230 mm, slice thickness 5 mm; coronal fast spin-echo T2-weighted images (wi) (TR: 2300 msec TE: 100 msec), NA: 4, matrix 256 x 256, FOV 230 mm, thickness 3 mm; coronal TSE fluid- attenuated inversion-recovery (FLAIR) images (TR:8,000 msec, TE: 100 msec, inversion time, TI: 2,000 msec), NA: 3, matrix 238 x 256, FOV 230 mm, thickness 3 mm; and coronal FSE inversion-recovery (IR), T1-wi images (TR: 3,000 msec, TE: 20msec, TI: 400 msec), NA: 3, matrix 256 x 256, FOV 230 mm, thickness 3 mm. The transversal and coronal sections were respectively acquired parallel and perpendicular to the axis of the hippocampal formation.

No contrast medium was used, and all of the T1- and T2-wi were qualitatively evaluated by means of careful visual inspection in terms of morphology, the thickness and signal intensity of the cortex of the cerebral hemispheres, and the distribution and signal intensity of the WM. The MRI features of malformed cortical development, atrophic changes and signal abnormalities in the cortex and WM were recorded. HS was qualitatively demonstrated by means of the comparative visual detection of atrophy and loss of definition of the internal structures of the hippocampal formation, and increased signal intensity in the T2-wi. Associated abnormalities of mammillary bodies,

the fornix and the fimbria were also evaluated. Particular attention was given to the interface between the cortex and the underlying WM, with the definition of the inner margin of cortical ribbon and even mild signal abnormalities from the subcortical WM being carefully investigated. The morphology and signal intensity of the grey matter (GM) and WM of the temporal poles were evaluated on the coronal sections throughout the antero-posterior extent of the temporal lobe.

Neuropsycological testing

All of the patients underwent a neuropsychological assessment before surgery, and six months afterwards. Abstract reasoning, immediate and long-term memory, and verbal fluency were evaluated using Raven's Coloured Progressive Matrices, Short Story, Rey's Complex Figure, Selective Reminding, Corsi Blocks Supraspan, and Word Fluency tests (Giovagnoli *et al*., 2011). The controls were 32 healthy subjects matched in terms of chronological age (mean age 38.18 ± 11.00), years of schooling (mean age 12.12 ± 3.38), and gender (21 males, 11 females).

Surgery and follow-up

All of the resections were performed for strictly therapeutic reasons after the patients had given their informed consent. None of the patients underwent selective amygdalohippocampectomy. The resections were limited to the temporal lobe in all cases, and their extent was planned pre-operatively on the basis of the location of the epileptogenic zone (as shown by electroclinical data) and the risk of post-surgical deficits. Seizure freedom was monitored periodically, and determined using Engel's classification (Engel Jr J., 1987); only patients with a minimum follow-up of 12 months were considered.

Histology

Immediately after surgery, the resected temporal lobes and hippocampi were fixed in 4% paraformaldehyde buffered solution. After 24 h, the temporal lobe specimens were cut into 4-6 coronal slabs (5 mm thick) throughout its antero-posterior extent, and post-fixed in the same solution for 4-5 days. Alternate slabs were embedded in paraffin or in 6% agarose to be cut by a vibratome (VT1000S, Leica, Heidelberg, Germany). For routine neuropathology, 7 μm thick sections were cut and stained with thionin (0.1%), hematoxylin and eosin, and Kluver-Barrera. Additional serial sections were processed for immunohistochemistry (IHC) using antibodies against glial fibrillary acidic protein (GFAP;1:1,000 Millipore, Tamecula, CA), non-phosphorylated neurofilaments (SMI 311;1:250, Sternberger Monoclonals Incorporated, Lutherville, MD), neuron-specific nuclear protein (NeuN;1:1,000; Chemicon International, Temecula, CA), CD68 (1:1,000, Dako, Denmark), and fibrinogen (1:600, Dako). Agarose-embedded slabs were cut into 50 μm thick serial sections, counterstained with thionin, and processed using the primary antibodies and an immunoperoxidase procedure described elsewhere (Garbelli *et al*., 1999).

Quantification of the degree of gliosis and possible inflammatory changes in the WM of all the samples was performed. Images of sections reacted with the corresponding antibodies, GFAP and CD68 respectively, were captured with a digital camera in randomly placed visual fields using Image ProPlus 6.3 software (Media Cybernetics, Silver Spring, MD). Gliosis was evaluated considering the intensity of the colour immunostaining (saturation) in 0.56 mm^2 for each case whereas CD68-positive cells density was calculated in 0.56 mm^2 using two-dimensional cell counting technique. The WM neuronal density was estimated counting NeuN-positive neurons in the depth of the WM, at least 500 μm from the GWM boundary (Blumcke *et al*., 2011), by means two different approaches: a two-dimensional cell counting

technique performed on all samples on representative 2.2 mm^2 and, according to the Optical Fractionator technique (West et al., 1991), with use of the StereoInvestigator software (Micro-BrightField, Williston, VT, USA) in the subgroup of the patients submitted to ulstrastructural study (see below). The Optical Fractionator is a stereological method for estimating the total number of neurons in a region; the technique combines use of the Optical Disector (a three-dimensional probe for counting neuronal nuclei) and the Fractionator (a systematic random sampling). We considered an upper and lower guard zones, corresponding to the surfaces where the tissue is most affected by sectioning, of 3 μm and the square counting frame in the x-y plane was 150x150 μm. The number of frames ranged from 25-36. NeuN-positive nuclei that came into focus either fully inside the counting box or touching the inclusion lines were counted.

Finally, to evaluate abnormalities in blood vessel and blood-brain barrier function, fibrinogen immunoreactivity in all specimens was performed.

The hippocampi were kept separate and processed for neuropathological diagnosis in order to confirm the presence of HS (the grading is not considered in this report). The slides were independently reviewed by two neuropathologists, one of whom was unaware of the initial diagnoses and clinical data. Any disagreements were discussed until an agreed diagnosis had been reached. The presence of FCD was diagnosed on the basis of the new ILAE classification system (Blumcke *et al*., 2011), and classified as type IIIa because of the confirmed neuropathological presence of HS.

Correlative 7 T MRI and ultrastructural study

A subgroup of nine patients (four from group 1 and five from group 2) underwent a combined high- field MRI and morphological/ultrastructural study. To this end, one slab from each specimen (corresponding to the anterior part of the temporal lobe and

embedded in 6% agarose) was examined by means of experimental MRI using a 7 Tesla horizontal-bore scanner (BioSpec 70/30 USR, Bruker, Ettlingen, Germany) equipped with 200 mT/m gradients and a 35 mm transceiver quadrature coil. High-resolution T2-wi were acquired using a TE of 50 ms, a TR of 4.3 s, a NA of 36, a slice thickness of 0.7 mm, a FOV of 32×32 mm^2, and a data matrix of 256×256, which yielded a 73×73 $\square m^2$ in-plane resolution. The diffusion tensor imaging (DTI) acquisitions were carried out using a Spin-Echo sequence (TE 40 ms, TR 5 s, NA 1, slice thickness 0.7 mm, FOV 32×32 mm^2, data matrix 128×128) that yielded a 250×250 $\square m^2$ in-plane resolution. The diffusion times were Δ = 22 ms and ∂ = 12 ms, and there were 5 b0 images, 6 directions, and 7 b-values (800,1500, 2000, 2500, 3000, 3300 and 3500 s/mm^2). Mean diffusivity (MD) and fractional anisotropy (FA) maps were estimated from the raw data images. FSL software (www.fmrib.ox.ac.uk/fsl) was used for the tensorial fitting and for calculating the eigenvalues and eigenvectors.

After MRI, the slabs were cut into 50 μm thick serial coronal sections and processed for: i) staining with 0.1% thionin for structural control, and Black-Gold II (0.3% dissolved in 0.9% saline, Histo-Chem, Jefferson, Arkansas, USA) for myelin visualisation; ii) IHC as previously described; and iii) EM.

One section from each case (chosen from those stained with thionin and Black-Gold II) was processed for EM using a protocol described elsewhere (Garbelli *et al*., 1999). The osmicated sections of group 1 revealed uneven staining, and so two areas of interest in the deep WM were excised: one corresponding to a lightly stained (light) zone, and one corresponding to an intensely and apparently homogeneously stained (dark) zone. The osmicated sections of group 2 showed intense and homogeneous WM staining throughout, and so only one area was excised. From each area, 0.5 μm semi-thin sections were cut by means of an ultramicrotome (Reichert-Jung ULTRACUT E - Buffalo,

NY), mounted on glass slides, and counterstained with Toluidine blue for light microscopy examination. To estimate the number of myelinated fibres in the WM, semi-thin sections were observed using an oil objective lens (100x, NA 1.32) and two area of interest from the upper left and two from under right corners were captured, corresponding to a final surface of 18,544 μm2 for each sample. Afterwards, ultra-thin sections (500 Å) representative of the selected areas were placed on 200-mesh copper grids (EMS, Fort Washington, PA), counterstained with lead citrate and uranyl acetate, and examined using an EM109 electron microscope (Zeiss, Oberkochen, Germany). All of the microphotographs were qualitatively evaluated by two independent and experienced observers (MM e GM) using a non-descriptive numerical code. A modified version of the protocol of Tang *et al.* (2004) was used for the morphometric analyses. Briefly, very thin sections were cut to avoid overlapping bias and, starting from a random mesh of the grid, the two opposite corners of ten consecutive fields of each section were photographed at a magnification of 4400x. Empty or damaged fields were discarded. A total of 20 digital images were taken of each area of interest, and were analysed by three independent observers (GMi, VM and GMa) using a semi-automatic program (NIS-Elements BR 3.1 Software, Nikon, Melville, NY). The area of each counting frame was 379.21 μm^2, and the total examined area was 7584.2 μm^2. The myelinated fibres, on both semi- and ultra-thin sections, were counted when they were completely inside the counting frame or partially inside and only touching the counting lines; they were not counted if they touched the exclusion lines. The glial and microglial cells, present in some microphotographs, were not counted and their presence did not preclude analysis of a microscopy field. As most of the axons had non-circular profiles, it was not possible to estimate myelin thickness accurately; in these cases, the diameter was measured on the shortest axis of the axonal profile, thus introducing an uncontrolled

bias. The evaluated parameters were the mean number of axons, axonal density, circularity, elongation, the circumference and the extra-axonal area. The average parameters of all of the microphotographs of each patient were used for the statistical analysis.

Statistical analysis

Mean age at epilepsy onset, the duration of epilepsy, age at surgery and seizure frequency were compared between the two subgroups using a two-tailed t-test following Levene's test for equality of variances. The remaining electroclinical features and the presence of blurring were analysed using a contingency table and Fisher's exact test (p values of <0.05 were considered significant).

The neuropsychological test scores of the patient and control group were compared using the Mann-Whitney test. The significance limit for seven pair-wise comparisons was set at $p<0.007$ (Bonferroni's correction). Separate Wilcoxon tests were used to compare the preoperative and 6-month follow-up test scores, and regression analyses to explore the role played by blurring in determining neuropsychological performance.

Differences in mean values of gliosis, neuronal density, and CD68-positive cells were evaluated between the two subgroups by two-tailed t-test, whereas differences in the morphometric parameters were assessed by means of one-way ANOVA, followed by individual *post hoc* comparisons using Sheffé's test. A p value of <0.05 was considered significant. The Shapiro-Wilk test was used to prove normal data distribution. Statistical analyses were performed using SPSS v. 17.

RESULTS

Clinical data and follow-up

The main characteristics of the cohort as a whole are shown in Table 1. The patients' mean age at surgery was 40 years (range 24-60; SD 9.3) and the mean duration of epilepsy was 29 years (range 5-54; SD 14.3). Their mean age at epilepsy onset was 12.2 years (range 2-35; SD 8.4) and mean seizure frequency at the time of surgery was 8.1 per month (range 1-30; SD 8.2). After 12 months of follow-up (range 12-60), 29 patients were in Engel's class I, and the remaining three in class II. The cohort was divided into two groups on the basis of the presence of blurring in the preoperative MR images (18 patients, 56%) or its absence (14 patients, 44%).

There were no significant between-group differences in terms of mean age at surgery (p=0.31), mean seizure frequency (p=0.14), the presence of febrile seizures (p=0.93), or post-operative outcomes (p=0.11), whereas the patients in group 1 had a significantly younger mean age at epilepsy onset (p=0.004) and significantly longer mean duration of epilepsy (p=0.004).

A review of the seizure semiology and the video-EEG data showed that the only significant difference between the two groups was the presence of contralateral dystonia during seizures, which was observed 89% of the patients of the group 1 and 36% of those in group 2 (p=0.028) (Table 1).

Preoperative MRI

The FLAIR and T2-wi of all of the patients in group 1 (9 left, 9 right) showed hyperintensity in the WM of the temporal pole ipsilateral to the HS. The intensity of the WM signal was similar to that of the GM, with a blurred GWM junction in the temporal pole and ipsilateral hypoplasia of the temporal pole in 13 subjects (72%) (Fig. 1A-G; 2A). In group 2 (7 left, 7 right), normal and homogenous signal intensity

was observed throughout the temporal lobe WM, and the GWM interface was clearly defined (Fig. 2D); only two cases (1.5%) showed ipsilateral hypoplasia of the temporal pole. No signal abnormalities and no ipsilateral atrophy of the fornix, fimbria or mammillary bodies were detected in any of the 32 patients.

Of the nine cases selected for correlative imaging and EM study, atrophy of the temporal pole ipsilateral to the HS was observed in two group 1 and two group 2 patients.

Neuropsychology

With respect to the controls, blurring patients were significantly impaired at all of the neuropsychological tests, while non-blurring patients were significantly impaired in Short Story and Word Fluency on phonemic and semantic cues. Blurring patients also showed lower Raven Colored Progressive Matrices scores than non-blurring patients. The presence of blurring predicted the preoperative score on Raven's Coloured Progressive Matrices (r^2=0.16, F=5.16, p=0.03) (Table 2). There were no significant postoperative changes and no differences related to the side of the epileptic region in either group.

Histology

The diagnosis of HS was confirmed in all 32 patients. Architectural abnormalities in the temporal cortex, characterised by the blurred demarcation of the layers (type IIIa FCD) was diagnosed in 15 of the 18 patients in group 1 (83%), and 13 of the 14 patients in group 2 (93%). Moreover, five group 1 and three group 2 patients showed the Temporal Lobe Sclerosis (Thom *et al*., 2009), a variant of type IIIa FCD, which is characterised by an atypical band of clustered neurons in the outer part of layer 2 and neuronal depletion in layers 2-3 (Supplementary Fig. 1A, B). In all cases, regardless of the presence/absence of blurring, a variable degree of gliosis of the WM was evident on GFAP immunostaining, and CD68-positive cells were

encountered in all the surgical samples diffusely distributed in the WM and sometime located around vessels. According to these observations, quantitative analysis of the GFAP staining intensity and CD68-positive cell density in the WM revealed no differences between the two groups (p=0.30 for GFAP and p=0.19 for CD68, Supplementary Fig. 1C, D). The presence of an excess of single WM neurons was frequently observed in all samples and their density was estimated in both groups. We found a wide range of WM neuronal density using both two-dimensional (30-94 neurons/mm^2 in group 1 and 21-59 neurons/mm^2 in group 2) and three-dimensional cell counting technique (1777-3504 neurons/mm^3 in group 1 and 1636-4243 neurons/mm^3 in group 2) but no significant differences in the average density between the two groups was observed (p=0.22 and p=0.54, Supplementary Fig. 1E, F). Blood vessels and, when present, perivascular spaces were intensely stained by Fibrinogen immunoreactivity in all samples from both groups (Supplementary Fig. 1G, H).

Correlative 7T MRI and ultrastructural study

Unlike the *in vivo* T2-wi (Fig. 2A and D), there was a clear border between the GW and WM in all of the samples (Figs. 2B and E, 3A and I, and 4A). However, signal intensity in the WM was dishomogeneous in the group 1 samples, with patchy areas of hyperintensity mainly in the depth (Figs. 2B, and 3A and I), whereas visual analysis of the group 2 images showed a homogeneous hypointense signal throughout the WM (Figs. 2E and 4A). The FA maps obtained from the same specimens showed similar GM values in both groups, whereas the WM FA values were lower in group 1 (Fig. 2C *vs* 2F). The MD values did not reveal any clear between-group differences in either the WM or the GM (data not shown).

After the imaging study, the specimens underwent morphological/ultrastructural study. The group 1 sections processed

for Black Gold II revealed dishomogeneous staining in the WM, whereas the same staining was homogeneous in the group 2 sections (Figs. 3B, C, E, J, K and M *vs* 4B and C). Analysis of the adjacent semi-thin sections counterstained with Toluidine blue confirmed this difference (Figs. 3D, F, L and N *vs* 4D). The qualitative ultrastructural examination showed that the samples from group 1 (particularly those from the light zone) had more extra-axonal space, fewer myelinated and unmyelinated axons, which also varied considerably in size and morphology in comparison with the group 2 samples (Figs. 3G, H, O and P *vs* 4E and F). Glial cells, glial processes and vacuoles of different size were also observed in the neuropil. On the contrary, the specimens of both groups showed no alterations in myelin sheath thickness in relation to axonal diameter and no alterations in the vessels walls. In particular, there were no desmosome alterations in the capillary endothelial cells, and no alterations in the elastic and muscular tunica of the arteriolar walls. Quantitative analyses confirmed that the number of axons and axonal density in the WM were significantly reduced in both the light and dark zones of the group 1 samples, with no differences between the zones (Table 3). Moreover, the myelinated axons were less circular and more elongated than those in the group 2 samples, thus indicating a tendency towards tilted axons, and their circumference was larger. The cumulative area occupied by axons represented a smaller fraction of the entire area of the group 1 samples (particularly in the light zone), thus leading to a larger extra-axonal area (86% and 83% in the light and dark zones of the group 1 samples *vs* 79% of the group 2 samples).

DISCUSSION

The MRI features of the anterior temporal signal abnormalities commonly called "blurring" consist of a less marked definition of the

GWM border, frequently coupled with the apparent shrinkage of the WM core of the temporal pole. They have long been described in a subgroup of TLE patients, and the prevalence of ipsilateral anterior temporal abnormalities in patients with intractable TLE and HS has been estimated as being 32-66% (Choi *et al*., 1999; Meiners *et al*., 1999; Mitchell *et al*., 1999) in adults, and 57% in children (Mitchell *et al*., 2003). Over the last ten years, numerous attempts have been made to assess the etiopathogenesis of temporo-polar blurring but none of the various hypotheses has been confirmed, which means that, although the MRI appearance may reflect a change in the water content of the temporal lobe, the pathological substrate of the change is still unknown. We used different methodological approaches to collect robust evidence that the blurring is caused by fibre bundle degeneration, and will here discuss the morphological data and its possible clinical implications separately.

Temporo-polar blurring and WM fibre degeneration

It has been suggested that temporo-polar blurring is due to vasculo-metabolic disturbances in the temporal lobe that are presumably secondary mechanisms of repetitive seizures (Ryvlin *et al*., 1998; Weder *et al*., 2006), and Chassoux *et al.* (2004) found that temporal hypometabolism was more extended in patients with temporo-polar signal changes. We therefore assumed that, if the blurring is due to functional vasculo-metabolic mechanisms, it would no longer be visible on MR images of surgically removes and fixed temporal lobe samples; however, we found that signal alterations could still be seen in our group 1 specimens.

Nevertheless, there were some differences between the presurgical 1.5 T MR images and the 7 T images of the surgical specimens. In group 1, the GWM border was clearly marked, but signal alterations were particularly pronounced in the deep WM; furthermore, the hyperintense signal was frequently dishomogeneous, and there were

patchy areas of different intensities. The differences between the 1.5 and 7 T images may be due to the higher resolution of the latter (which is also due to the number of repetitions allowing the use of thinner sections) or to the fixation procedures. However, the second hypothesis can be ruled out because we have previously shown that fixation procedures do not substantially alter 7 T images, which are comparable with those obtained *in vivo* using a 1.5 T machine (Garbelli *et al*., 2011).

The findings also rule out the hypothesis that the signal alterations have a vasculo-metabolic origin, and support the hypothesis of structural morphological alterations. Some authors have suggested that blurring might be caused by abnormalities in structural development (Hardiman *et al*., 1988; Thom *et al*., 2001), but our histopathological study revealed that patients with and without blurring may have similar neuropathological features, such as the presence of a cortical dysplasia and an excess of single WM neurons, thus excluding their potential involvement.

Other explanations of blurring are dilated perivascular spaces and inflammatory changes, but Mitchell *et al.* (1999) found that all of these minor changes are common regardless of the presence or absence of MRI blurring. Although we did not make a similarly precise analysis, our study did not reveal any difference in inflammatory changes or any significant alterations in blood vessels.

The presence of widespread gliosis has also been considered to explain the MRI abnormalities, but no differences have been found in the density of glial cell nuclei in the temporal WM between patients with and without blurring (Meiners *et al*., 1999; Mitchell *et al*., 1999) and, although our findings are in line with these reports as they also show considerable variability in the degree of gliosis detected by means of GFAP staining within and between the groups. However, dishomogeneous myelin staining indicated clear fibre alterations that correlated with the 7 T images, thus supporting a hypothesis that has

been previously proposed on the basis of the findings of neuropathological investigations (Meiners *et al*., 1999; Mitchell *et al*., 1999; Schijns *et al*., 2011) and modern imaging studies (Concha *et al*., 2009).

Meiners *et al.* (1999) found significantly reduced WM staining suggesting myelin loss in patients with MRI signal alterations, and therefore postulated that decreased myelin density in the temporal lobe of HS patients may be due to the trans-synaptic retrograde degeneration of collaterals of afferent axons in association bundles. Schijns *et al.* (2011) suggested that loss of the GM border may be a persistent immature appearance due to abnormal or delayed myelination during development.

Our morphological data demonstrate that the number of fibres in the subcortical WM of the patients in group 1 was significantly reduced and that the percentage of the area occupied by myelinated axons was smaller in comparison with group 2 patients. Consequently, the residual fibres are less circular, more elongated and wider presumably because of a spatial rearrangement.

Interestingly, the residual myelinated fibres did not show any substantial alteration in the myelin sheath, or any signs of inflammatory processes and remyelination. As demyelination is characterised by the destruction of normally formed myelin, and is often followed by remyelination associated with signs of inflammation, our morphological data seem to argue against this type of pathological process and, in line with the suggestion of Schijns *et al.* (2011), we believe that the term "dysmyelination" (characterised by the defective biosynthesis and formation of myelin sheaths) would be more appropriate in such cases. However, whatever the mechanism may be, our data demonstrate massive axonal loss and a redistribution of the remaining fibres that is similar to that observed in chronic degeneration processes.

The light and EM neuropathological data agree with the MRI findings and show decreased FA values in group 1. Although volumetric MRI has demonstrated extensive WM abnormalities in TLE patients, it is considered a non-specific measure, and so new imaging techniques such as DTI have been increasingly used over the last few years to characterise WM architecture *in vivo* and have provided information about the integrity and organisation of fibre tracts. In particular, DTI has been extensively used on the basis of the assumption that *in vivo* DTI abnormalities reflect underlying changes in WM micro-structure. However, although data from animal models and post-mortem human brains have given insights into the histological correlates of DTI parameters, there are still considerable limitations when drawing conclusions regarding the underlying microstructural features associated with human *in vivo* DTI findings (D'Arceuil *et al*., 2007). Among the various proposed indices, FA is most frequently used to quantify the direction of diffusion and therefore the structural integrity of tissue. Decreased FA values indicating a loss of WM integrity have been found in the ipsilateral temporal lobe, the cingulum, the corpus callosum and the external capsule of TLE patients with HS (Arfanakis *et al*., 2002; Concha *et al*., 2007; Focke *et al*., 2008; Gross *et al*., 2006), but the cause of these changes is still debated, although tissue edema, blood/brain barrier disturbances, neuronal loss and axonal demyelination have all been postulated. (Bernasconi *et al*., 1999; Margerison and Corsellis 1966;Seidenberg *et al*., 2005; Sutula *et al*., 2003).

In a recent study, Concha *et al.* (2010) found a correlation between EM and *in vivo* DTI findings that validated DTI findings as an *in vivo* marker of WM pathology. Our results show that, even in surgical specimens, FA is altered in TLE patients with HS, thus further confirming the correlation between altered MRI signals and neuropathological WM alterations at light and ultrastructural level. Abnormalities in structures other than the WM bundles in the temporal

pole were not detected in the routine 1.5 MRI of our patients and so the alterations other fibre bundles reported by other authors might have been missed. However, it needs to be underlined that we only considered temporo-polar abnormalities and the histopathological correlations of pre- and post-surgical images. Our study confirmed that high-resolution MRI and DTI can also be performed on well preserved and fixed surgical specimens (Garbelli *et al*. 2011).

Clinical correlations

Although anamnestic records of epilepsy risk factors (particularly febrile seizures) have to be considered with caution, our data do not suggest any correlation between febrile seizures and the presence of WM abnormalities, in line with previous reports (Mitchell *et al*., 2003; Schijns *et al*., 2011). As FCD or heterotopic neurons in the WM were equally distributed in both groups, they are not responsible for the temporo-polar abnormalities, but also not associated with the type or frequency of the seizures.

Our data confirm that patients with WM abnormalities in the temporal pole are significantly younger at the time of seizure onset than those without abnormalities. Mitchell *et al.* (2003) found a significant relationship between anterior temporal changes and the epilepsy onset before the age of two years in their pediatric population, but studies of adult (or mixed) populations such as ours indicate a mean age at onset of 7-8 years, even though the population described by Schijns *et al.* (2011) showed that a significant percentage of patients had a mean age of onset of two years. The difference in age at seizure onset in the group with blurring may have been due to the fact that "details of the change early in the patients' history are often more vague when obtained in adulthood and early details not well remembered" (Mitchell *et al*., 2003).

All of the published studies report possible myelin alterations with an early age of epilepsy onset, but our data show massive axonal loss

with preserved myelin in the residual axons, which suggests an early degenerative process involving some but not all of the fibres within the temporal lobe WM. The disappearance of selected axonal tract(s) might be secondary to a dysmyelination process caused by repetitive abnormal firing within the temporal lobe, a hypothesis that is supported by findings showing that axonal myelination at least partially depends on signals of axon origin, and that factors inducing myelin formation are mediated by electrical activity (Lubetzki and Stankoff. 2000). It is well known that major events in myelination processes occur within the first two years of life, even if more subtle changes continue beyond this age (Brody *et al*., 1987; Gao *et al*., 2009; Kinney *et al*., 1988).

It also needs to be considered that clinically detectable seizures are the result of long-lasting epileptogenic processes. During the period preceding clinically detectable seizures, it is possible that abnormal subclinical repetitive electrical discharges through maturing axons may perturb normal myelin formation, thus leading to subsequent axonal damage and degeneration. This is in line with the possibility that anterior temporal WM changes may be a side effect of early onset epileptogenic discharges and subsequent persistent seizures (Schijns *et al*., 2011). However, our data do not allow any conclusion to be drawn about the type of fibre bundles that are compromised.

Although none of the clinical differences was statistically significant, our patients with blurring had lower memory and abstract reasoning scores than those without, and the presence of blurring proved to predict the preoperative abstract reasoning score. These results extend previous findings (Mitchell *et al*., 1999) and suggest that blurring might contribute towards enhancing cognitive impairment in TLE patients.

In line with the results of previous studies (Mitchell *et al*., 1999; Mitchell *et al*., 2003; Schijns *et al*., 2011), there were no significant differences in the electroclinical data or postoperative seizure

outcomes between the two patient groups. The lack of an association between blurring and clinical features may depend on the small size of our patient sample, and it may also be argued that the clinical consequences of blurring are surpassed by the widespread and long-lasting effects of HS, which has a well-known relationship with the age of epilepsy onset and seizure severity. Future studies of larger cohorts are needed to determine the ability of WM abnormalities to predict very long-term postoperative outcomes. In particular, it would be interesting to evaluate, in a long post surgical follow-up, if patients not seizures free belong to the group with WM blurring thus supporting the hypothesis of the organisation of a new epileptogenic zone outside the excised zone.

Funding: This study was funded by the Italian Ministry of Health; an EU Functional Genomics and Neurobiology of Epilepsy (EPICURE) grant, Contract No. LSHM-CT-2006-0373315, the Associazione P. Zorzi per le Neuroscienze, and the Fondazione Banca del Monte di Lombardia (FBML).

Acknowledgements: We would like to thank Dr C. Marras, neurosurgeon at the Fondazione IRCCS, Istituto Neurologico "C. Besta", for providing the surgical samples and prof A Vercelli and Dr M. Boido at the Department of Anatomy, Pharmacology and Forensic Medicine, Neuroscience Institute of the Cavalieri Ottolenghi,University of Turin, Orbassano, Italy for your help in stereological analysis. We are also grateful to Prof. M. Bentivoglio for critically reading the manuscript.

Table 1 Main clinical characteristics of the patients

History	Blurring	No blurring	Total
History			
Febrile seizure (%)	10 (56)	8 (57)	18 (56)
Mean age at epilepsy onset (SD)	8.6 (7.0)[a]	16.9 (7.9)[b]	12.2 (8.4)
Side of surgery (right-left)	9-9	7-7	16-16
Mean monthly seizure frequency at surgery (SD)	6 (6.4)	10.9 (9.6)	8.1 (8.2)
Mean age at surgery (SD)	41.4 (9.7)	38.0 (8.7)	39.9 (9.3)
Mean duration of epilepsy (SD)	35.1 (13.6)[a]	21.1 (11.2)[b]	29.0 (14.3)
Class I after surgery (%)	15 (83)	14 (100)	29 (91)
Seizure semiology and video-EEG			
Convulsive seizures (%)	4 (22)	7 (50)	11 (34)
Morpheic seizures (%)	7 (39)	9 (64)	16 (50)
Fallings (%)	3 (17)	4 (29)	7 (22)
Verbal alert (%)	15 (83)	12 (86)	27 (84)
Oroalimentary automatisms (%)	15 (83)	12 (86)	27 (84)
Manual automatisms (%)	16 (89)	10 (71)	26 (81)
Bipedal automatisms (%)	3 (17)	1 (7)	4 (13)
Contralateral dystonia (%)	16 (89)[c]	5 (36)[d]	21 (66)
Omolateral head turning (%)	9 (50)	5 (36)	14 (44)
Awareness of the seizure (%)	18 (100)	12 (86)	30 (94)
Localized interictal abnormalities (%)	17 (94)	12 (86)	27 (84)
Contralateral interictal abnormalities (%)	3 (17)	2 (14)	5 (16)
Localized ictal EEG (%)	15 (83)	10 (71)	25 (78)
Low-voltage fast activity (%)	8 (44)	7 (50)	15 (47)
Mesial temporal seizure pattern (%)	16 (89)	13 (93)	29 (91)
Neocortical temporal seizure pattern (%)	2 (11)	2 (14)	4 (13)
Contralateral diffusion of ictal activity (%)	8 (44)	6 (43)	14 (44)

a versus b = $P < 0.01$.
c versus d = $P < 0.05$.

Table 2 Preoperative neuropsychological test scores in patients and controls

Neuropsychological test	Blurring Mean (range)	No blurring Mean (range)	Controls Mean (range)	Blurring versus no blurring*	Blurring versus controls*	No blurring versus controls*
Raven coloured progressive matrices	28.82 (21–35)	32.31 (28–36)	32.79 (20–36)	U = 51, $P = 0.01$	U = 111, $P < 0.001$	NS
Word fluency on phonemic cue	26.35 (13–46)	25.92 (12–45)	39.45 (21–65)	NS	U = 113, $P = 0.001$	U = 94, $P = 0.003$
Word fluency on semantic cue	32.18 (19–45)	33.46 (19–46)	42.45 (14–57)	NS	U = 95.5, $P < 0.001$	U = 94, $P = 0.003$
Short story	9.29 (3–19.5)	10.92 (4.5–19)	15.61 (9–24.5)	NS	U = 82, $P < 0.001$	U = 94.5, $P = 0.003$
Selective reminding procedure	91.53 (13–169)	118.27 (0–163)	125.46 (28–166)	NS	U = 115, $P = 0.019$	NS
Rey complex figure delayed reproduction	15.44 (8–25)	18.98 (7–35)	20.81 (9–32)	NS	U = 164.5, $P = 0.008$	NS
Corsi blocks supraspan learning	16.73 (6.18–27.84)	20.45 (7.32–28.72)	25.70 (18.42–18.94)	NS	U = 47.5, $P < 0.001$	NS

NS = not significant; *Mann–Whitney tests.

Table 3 Quantitative analysis of the morphometric parameters performed on semi-thin and ultra-thin sections

Evaluated parameters	Blurring		No blurring
	Mean (SD)		Mean (SD)
	Light zone	Dark zone	
Number of axon (OM)	2174 (599)[a]	2234 (294)[b]	3506 (591)[c]
Axonal density (axons/μm^2) (OM)	0.117 (0.003)[a]	0.120 (0.015)[b]	0.189 (0.032)[c]
Circularity (EM)	0.64 (0.059)	0.64 (0.079)	0.70 (0.079)
Elongation (EM)	2.14 (0.26)	2.21 (0.24)	1.90 (0.18)
Circumference (EM)	3.93 (0.84)	4.15 (0.83)	3.11 (0.67)
Area occupied by axons (μm^2) (EM)	1055 (166)[d]	1319 (185)	1588 (83)[e]

a, b versus c = $P < 0.05$.
d versus e = $P < 0.01$.
EM = electron microscopy, ultra-thin sections; OM = light miscrosopy, semi-thin sections.

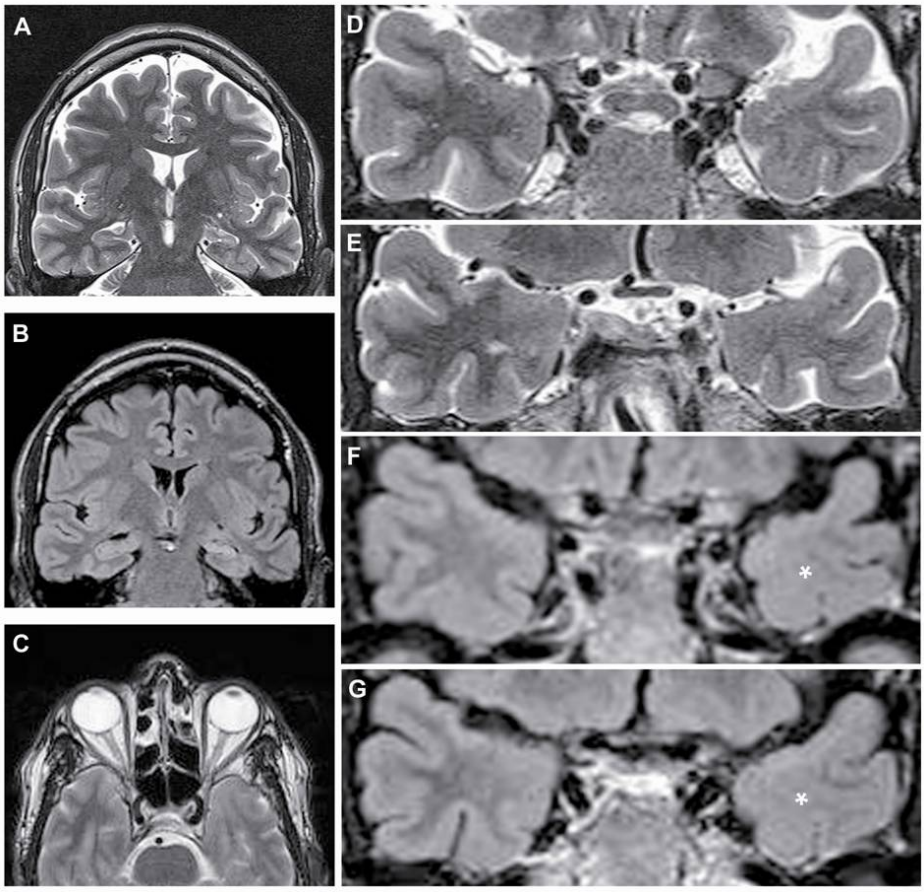

Fig. 1

Presurgical (1.5 T) MR images of a patient with left hippocampal sclerosis plus ipsilateral temporo-polar abnormalities.
The coronal T2-weighted (**A**) and FLAIR (**B**) images show atrophy and signal hyperintensity in the left hippocampal formation; the axial section (**C**) also shows atrophy of the temporal pole. Blurring of the ipsilateral temporal pole can be seen in contiguous T2-weighted (D, E) and FLAIR images (F, G); note the signal hyperintensity of the WM (asterisks) in the left temporal pole, with an ill-defined GWM junction.

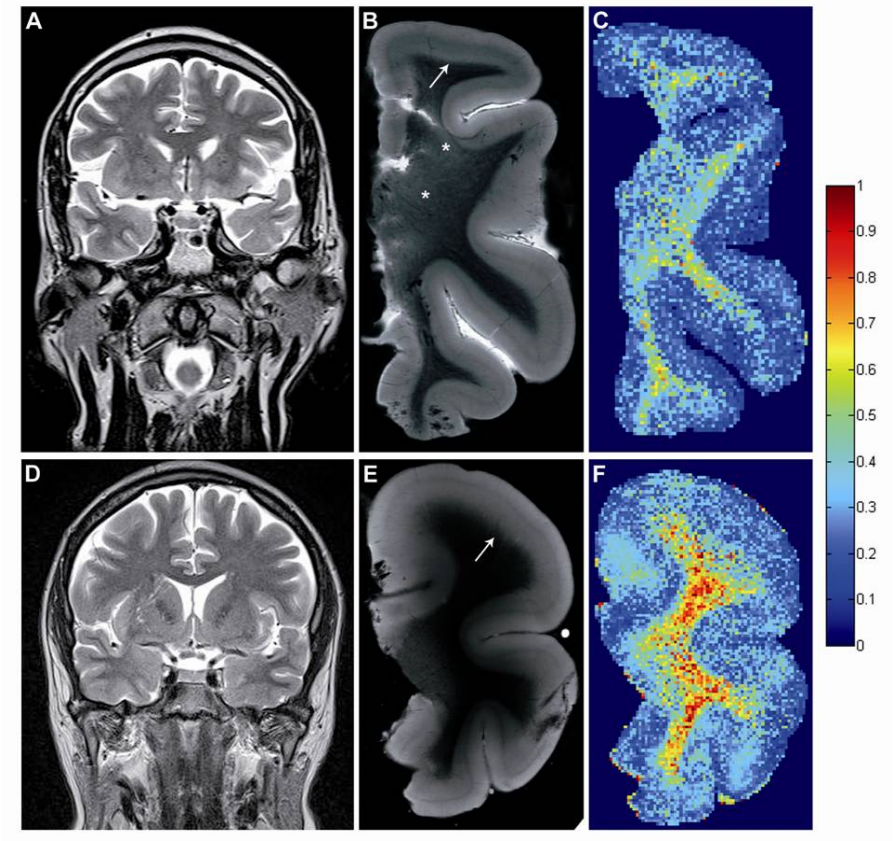

Fig. 2

Comparison of presurgical 1.5 (A, D) and *ex vivo* 7 T MR images (B,E) of patients with (A,B) and without blurring (D,E). In the T2-weighted images obtained from the surgical samples of both groups, the boundary between the GM and WM was always clear (B *vs* E, arrows), whereas signal intensity in the WM was dishomogeneous and showed patchy areas of hyperintensity (asterisks) only in the samples taken from patients with blurring. The FA maps show lower values in the WM of the patients (C *vs* F), thus suggesting the loss of WM integrity.

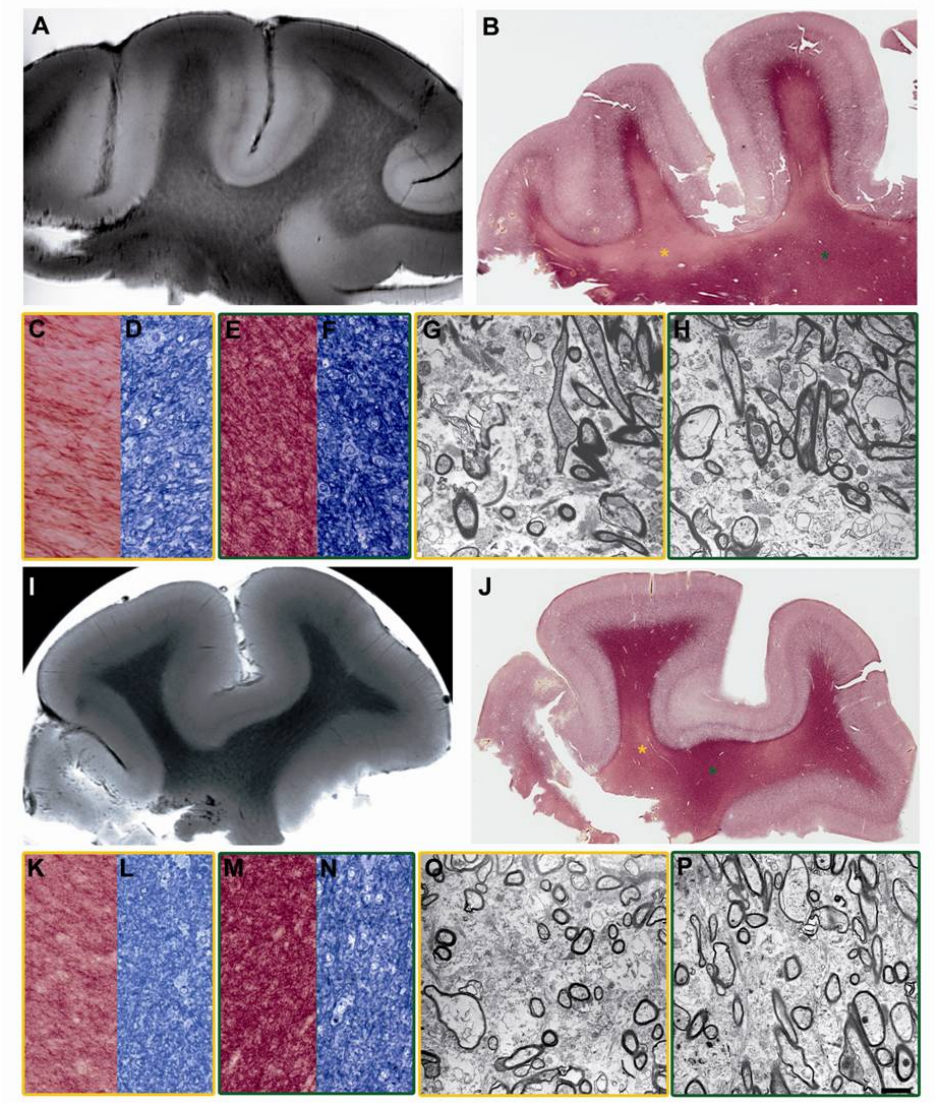

Fig. 3

Correlative data from the 7 T MR, histochemical and ultrastructural images of two patients with blurring.

The dishomogeneous signal intensity in the WM revealed by the T2-weighted images (A, I) correlates with the dishomogeneous staining of the myelinated fibres clearly visualised by means of Black Gold (B, J). The high-magnification images C, K and E, M respectively show the distribution of the myelinated fibres in a lightly stained zone (yellow asterisks) and an intensely stained zone (green asterisks). D, F, L and N show adjacent 0.5 µm semi-thin sections counterstained with Toluidine blue, and G, H, O and P are electron micrographs obtained from the lightly stained (yellow) and intensely stained zone (green).

The ultrastructural images clearly show a reduced number of axons in all of the sampled areas (compare with Fig. 4E and 4F) with a normal myelin sheath and increased extra-axonal spaces with vacuoles.
Bar: 45 µm (C, E, K, M); 25 µm (D, F, L, N); 0.6 µm (G, H, O, P).

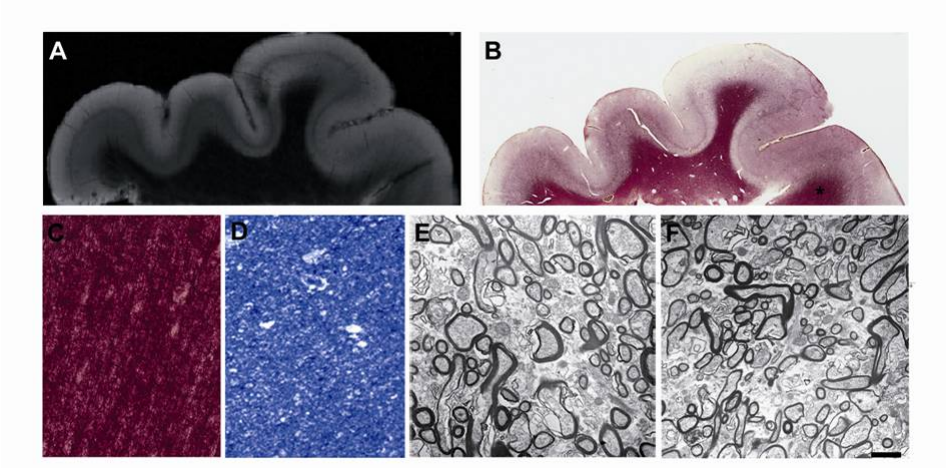

Fig. 4

Correlative 7 T MR, histochemical and ultrastructural images of one patient without blurring.
Note the homogeneous signal intensity in the WM revealed by the T2-weighted images (A), and the homogeneous staining of the myelinated fibres obtained from a section stained with Black Gold (B); the asterisk indicates the area shown at higher magnification in C. D, E and F show adjacent 0.5 µm semi-thin sections counterstained with Toluidine blue and electron micrographs: note the larger number of axons and fewer extra-axonal spaces in comparison with the patients with blurring (compare with Fig. 3G, 3H, 3O and 3P). Bar: 45 µm (C), 25 µm (D); 0.6 µm (E, F).

REFERENCES

Adachi Y, Yagishita A, Arai N. White matter abnormalities in the anterior temporal lobe suggest the side of the seizure foci in temporal lobe epilepsy. Neuroradiology 2006; 48: 460-4.

Arfanakis K, Hermann BP, Rogers BP, Carew JD, Seidenberg M, Meyerand ME. Diffusion tensor MRI in temporal lobe epilepsy. Magn Reson Imaging 2002; 20: 511-9.

Bernasconi A, Bernasconi N, Caramanos Z, Reutens DC, Andermann F, Dubeau F, et al. T2 relaxometry can lateralize mesial temporal lobe epilepsy in patients with normal MRI. Neuroimage 2000; 12: 739-46.

Bernasconi N, Natsume J, Bernasconi A. Progression in temporal lobe epilepsy: Differential atrophy in mesial temporal structures. Neurology 2005; 65: 223-8.

Bernasconi N, Bernasconi A, Andermann F, Dubeau F, Feindel W, Reutens DC. Entorhinal cortex in temporal lobe epilepsy: A quantitative MRI study. Neurology 1999; 52: 1870-6.

Blumcke I, Thom M, Wiestler OD. Ammon's horn sclerosis: A maldevelopmental disorder associated with temporal lobe epilepsy. Brain Pathol 2002; 12: 199-211.

Blumcke I, Thom M, Aronica E, Armstrong DD, Vinters HV, Palmini A, et al. The clinicopathologic spectrum of focal cortical dysplasias: A consensus classification proposed by an ad hoc task force of the ILAE diagnostic methods commission. Epilepsia 2011; 52: 158-74.

Brody BA, Kinney HC, Kloman AS, Gilles FH. Sequence of central nervous system myelination in human infancy. I. an autopsy study of myelination. J Neuropathol Exp Neurol 1987; 46: 283-301.

Chabardes S, Kahane P, Minotti L, Tassi L, Grand S, Hoffmann D, et al. The temporopolar cortex plays a pivotal role in temporal lobe seizures. Brain 2005; 128: 1818-31.

Chassoux F, Semah F, Bouilleret V, Landre E, Devaux B, Turak B, et al. Metabolic changes and electro-clinical patterns in mesio-temporal lobe epilepsy: A correlative study. Brain 2004; 127: 164-74.

Choi D, Na DG, Byun HS, Suh YL, Kim SE, Ro DW, et al. White-matter change in mesial temporal sclerosis: Correlation of MRI with PET, pathology, and clinical features. Epilepsia 1999; 40: 1634-41.

Concha L, Beaulieu C, Collins DL, Gross DW. White-matter diffusion abnormalities in temporal-lobe epilepsy with and without mesial temporal sclerosis. J Neurol Neurosurg Psychiatry 2009; 80: 312-9.

Concha L, Beaulieu C, Wheatley BM, Gross DW. Bilateral white matter diffusion changes persist after epilepsy surgery. Epilepsia 2007; 48: 931-40.

Coste S, Ryvlin P, Hermier M, Ostrowsky K, Adeleine P, Froment JC, et al. Temporopolar changes in temporal lobe epilepsy: A quantitative MRI-based study. Neurology 2002; 59: 855-61.

D'Arceuil HE, Westmoreland S, de Crespigny AJ. An approach to high resolution diffusion tensor imaging in fixed primate brain. Neuroimage 2007; 35: 553-65.

Engel Jr J. Outcome with respect to epileptic seizures. In Engel Jr J, editor. *Surgical treatment of the Epilepsies*. New York: Raven Press; 1987. p. 553-71.

Falconer MA, Serafetidinides EA, Corsellis JA. Etiology and pathogenesis of temporal lobe epilepsy. Arch Neurol 1964; 10: 233-48.

Focke NK, Yogarajah M, Bonelli SB, Bartlett PA, Symms MR, Duncan JS. Voxel-based diffusion tensor imaging in patients with mesial temporal lobe epilepsy and hippocampal sclerosis. Neuroimage 2008; 40: 728-37.

Gao W, Lin W, Chen Y, Gerig G, Smith JK, Jewells V, et al. Temporal and spatial development of axonal maturation and myelination of white matter in the developing brain. AJNR Am J Neuroradiol 2009; 30: 290-6.

Garbelli R, Munari C, De Biasi S, Vitellaro-Zuccarello L, Galli C, Bramerio M, et al. Taylor's cortical dysplasia: A confocal and ultrastructural immunohistochemical study. Brain Pathol 1999; 9: 445-61.

Garbelli R, Zucca I, Milesi G, Mastropietro A, D'Incerti L, Tassi L, et al. Combined 7-T MRI and histopathologic study of normal and dysplastic samples from patients with TLE. Neurology 2011; 76: 1177-85.

Giovagnoli AR, Franceschetti S, Reati F, Parente A, Maccagnano C, Villani F, et al. Theory of mind in frontal and temporal lobe epilepsy: Cognitive and neural aspects. Epilepsia 2011.

Gross DW, Concha L, Beaulieu C. Extratemporal white matter abnormalities in mesial temporal lobe epilepsy demonstrated with diffusion tensor imaging. Epilepsia 2006; 47: 1360-3.

Hardiman O, Burke T, Phillips J, Murphy S, O'Moore B, Staunton H, et al. Microdysgenesis in resected temporal neocortex: Incidence and clinical significance in focal epilepsy. Neurology 1988; 38: 1041-7.

Kahane P, Chabardes S, Minotti L, Hoffmann D, Benabid AL, Munari C. The role of the temporal pole in the genesis of temporal lobe seizures. Epileptic Disord 2002; 4 Suppl 1: S51-8.

Kinney HC, Brody BA, Kloman AS, Gilles FH. Sequence of central nervous system myelination in human infancy. II. patterns of myelination in autopsied infants. J Neuropathol Exp Neurol 1988; 47: 217-34.

Lubetzki C, Stankoff B. Role of axonal signals in myelination of the central nervous system. Pathol Biol (Paris) 2000; 48: 63-9.

Margerison JH, Corsellis JA. Epilepsy and the temporal lobes. A clinical, electroencephalographic and neuropathological study of the brain in epilepsy, with particular reference to the temporal lobes. Brain 1966; 89: 499-530.

Meiners LC, Witkamp TD, de Kort GA, van Huffelen AC, van der Graaf Y, Jansen GH, et al. Relevance of temporal lobe white matter changes in hippocampal sclerosis. magnetic resonance imaging and histology. Invest Radiol 1999; 34: 38-45.

Meiners LC, van Gils A, Jansen GH, de Kort G, Witkamp TD, Ramos LM, et al. Temporal lobe epilepsy: The various MR appearances of histologically proven mesial temporal sclerosis. AJNR Am J Neuroradiol 1994; 15: 1547-55.

Mitchell LA, Harvey AS, Coleman LT, Mandelstam SA, Jackson GD. Anterior temporal changes on MR images of children with hippocampal sclerosis: An effect of seizures on the immature brain? AJNR Am J Neuroradiol 2003; 24: 1670-7.

Mitchell LA, Jackson GD, Kalnins RM, Saling MM, Fitt GJ, Ashpole RD, et al. Anterior temporal abnormality in temporal lobe epilepsy: A

quantitative MRI and histopathologic study. Neurology 1999; 52: 327-36.

Moran NF, Lemieux L, Kitchen ND, Fish DR, Shorvon SD. Extrahippocampal temporal lobe atrophy in temporal lobe epilepsy and mesial temporal sclerosis. Brain 2001; 124: 167-75.

Ryvlin P, Coste S, Hermier M, Mauguiere F. Temporal pole MRI abnormalities in temporal lobe epilepsy. Epileptic Disord 2002; 4 Suppl 1: S33-9.

Ryvlin P, Bouvard S, Le Bars D, De Lamerie G, Gregoire MC, Kahane P, et al. Clinical utility of flumazenil-PET versus [18F]fluorodeoxyglucose-PET and MRI in refractory partial epilepsy. A prospective study in 100 patients. Brain 1998; 121 (Pt 11): 2067-81.

Sankar T, Bernasconi N, Kim H, Bernasconi A. Temporal lobe epilepsy: Differential pattern of damage in temporopolar cortex and white matter. Hum Brain Mapp 2008; 29: 931-44.

Schijns OE, Bien CG, Majores M, von Lehe M, Urbach H, Becker A, et al. Presence of temporal gray-white matter abnormalities does not influence epilepsy surgery outcome in temporal lobe epilepsy with hippocampal sclerosis. Neurosurgery 2011; 68: 98,106; discussion 107.

Seidenberg M, Kelly KG, Parrish J, Geary E, Dow C, Rutecki P, et al. Ipsilateral and contralateral MRI volumetric abnormalities in chronic unilateral temporal lobe epilepsy and their clinical correlates. Epilepsia 2005; 46: 420-30.

Sutula TP, Hagen J, Pitkanen A. Do epileptic seizures damage the brain? Curr Opin Neurol 2003; 16: 189-95.

Tassi L, Meroni A, Deleo F, Villani F, Mai R, Russo GL, et al. Temporal lobe epilepsy: Neuropathological and clinical correlations in 243 surgically treated patients. Epileptic Disord 2009; 11: 281-92.

Thom M, Sisodiya S, Harkness W, Scaravilli F. Microdysgenesis in temporal lobe epilepsy. A quantitative and immunohistochemical study of white matter neurones. Brain 2001; 124: 2299-309.

Thom M, Eriksson S, Martinian L, Caboclo LO, McEvoy AW, Duncan JS, et al. Temporal lobe sclerosis associated with hippocampal sclerosis in temporal lobe epilepsy: Neuropathological features. J Neuropathol Exp Neurol 2009; 68: 928-38.

Weder BJ, Schindler K, Loher TJ, Wiest R, Wissmeyer M, Ritter P, et al. Brain areas involved in medial temporal lobe seizures: A principal component analysis of ictal SPECT data. Hum Brain Mapp 2006; 27: 520-34.

West MJ, Slomianka L, Gundersen HJ.. Unbiased stereological estimation of the total number of neurons in the subdivisions of the rat hippocampus using the optical fractionator. Anat Rec 1991; 231: 482–97.

Wiebe S, Blume WT, Girvin JP, Eliasziw M, Effectiveness and Efficiency of Surgery for Temporal Lobe Epilepsy Study Group. A randomized, controlled trial of surgery for temporal-lobe epilepsy. N Engl J Med 2001; 345: 311-8.

Chapter 4

High-resolution 7T *ex vivo* MRI and histopathology in human hippocampus in normal condition and hippocampal sclerosis

Manuscript in preparation

Roland Coras[1,2], **Gloria Milesi[1]**, Ileana Zucca[3], Alfonso Mastropietro[3,4], Alessandro Scotti[3], Matteo Figini[3], Carolina Frassoni[1], Angelika Mühlebner[2], Andreas Hess[5], Giovanni Tringali[6], Ingmar Blümcke[2], Roberto Spreafico[1] and Rita Garbelli[1]

[1]Clinical Epileptology and Experimental Neurophysiology Unit, Fondazione I.R.C.C.S. IstitutoNeurologico "C. Besta", 20133 Milano, Italy

[2]Department of Neuropathology, UniversityHospitalErlangen, 91054 Erlangen, Germany

[3]Scientific Department, Fondazione I.R.C.C.S. IstitutoNeurologico "C. Besta", 20133 Milano, Italy

[4]Department of Bioengineering, Politecnico di Milano, 20133, Italy

[5]Department of Experimental and Clinical Pharmacology and Toxicology, University of Erlangen-Nuremberg, Fahrstraße 17, 91054 Erlangen, Germany

[6]Department of Neurosurgery, Fondazione I.R.C.C.S. Istituto Neurologico "C. Besta", 20133 Milano, Italy

Running title: 7T MRI and histology in human hippocampi

Key Words: high resolution 7T-MRI, hippocampus, hippocampal sclerosis, neuropathology, DTI, fibre tracking

Abstract

Objective Hippocampal sclerosis (HS) is the major structural brain lesion in patients with temporal lobe epilepsy (TLE). However, the internal anatomical structure of the human hippocampus remains difficult to recognize at 1.5 or 3 Tesla (T) magnetic resonance imaging (MRI), which does not allow to identify specific pathology patterns nor their proposed value to predict postsurgical outcome, cognitive impairment or underlying etiologies. We aimed to identify specific patterns of HS subtypes in resected surgical TLE samples on 7T MRI by juxtaposition with corresponding histological sections.

Methods Fifteen normal and 18 sclerotic hippocampi were studied *ex vivo* using an experimental 7T MRI scanner. T2-weighted images (T2wi) and diffusion tensor imaging (DTI) data were acquired and validated using a systematic histological analysis of same specimens along the anterior-posterior axis of the hippocampus.

Results In normal hippocampus, differences in MR-intensity could be assigned to seven clearly recognizable layers and anatomical boundaries as confirmed by histology. All hippocampal subfields could be visualized also in the hippocampal head with three-dimensional imaging and angulated coronal planes. Only four discernible layers were identified when applying the same technique to TLE specimens with histopathologically confirmed HS. All sclerotic hippocampi showed a significant atrophy and increased signal intensity along the pyramidal cell layer. Diffusion tensor change such as an increased mean diffusivity, allowed to distinguish ILAE HS Type 1 and Type 2 from no HS specimens. Whereas the increase in T2weighted signal intensities could not be attributed to a specific histopathological substrate, i.e. decreased neuronal or increased glial cell densities, intrahippocampal projections and fibre tracts were distorted in HS specimens suggesting a complex disorganization of the cellular composition, fiber networks as well as its extracellular matrix.

Significance Our data further advocates high-resolution MRI as helpful and promising diagnostic tool for the investigation of hippocampal pathology along the anterior-posterior extent in TLE, as well as in other neurological and neurodegenerative disorders.

Introduction

Magnetic Resonance Imaging (MRI) is a well-recognized diagnostic tool in most brain disorders. Indeed, technical advances as well as post-processing methods have significantly improved sensitivity of structural brain imaging (Duncan et al., 2009)and permanent increase of static magnetic field strength will further enhance spatial resolution and tissue contrast(Weigele et al., 2010). High-field and ultra-high-field MRI (≥4T) will allow to study also complex anatomical brain regions in detail, such as the hippocampal formation (Wieshman et al., 1999; Fatterpekar et al., 2002; Augustinack et al., 2005).The human hippocampus is histologically characterized by the cornu ammonis (CA) and the dentate gyrus (DG), each consisting of distinct sublayers(Duvernoy, 2005), and plays a pivotal role in mesial temporal lobe epilepsy (MTLE) (Blumcke et al., 2002).The major histopathological hallmark of MTLE is hippocampal sclerosis (HS), a condition characterized by segmental loss of pyramidal neurons and reactive gliosis as well as structural alterations within the DG, i.e. granule cell dispersion and/or granule cell loss (Blumcke et al., 2002; Blumcke et al., 2009). Different patterns of hippocampal neuronal cell loss have been frequently described leading to different types of classification schemes and, clinico-pathological examinations have suggested a correlation between HS subtype with post-surgical seizure control, cognitive impairment or underlying etiologies (de Lanerolle et al., 2003; Blumcke et al., 2007; Thom et al., 2010). Recently, a new

classification system, that identifies three HS subtypes (Types 1,2,and 3),has been proposed by the ILAE Commission (Blumcke et al., 2013). HS can readily be identified on clinical MRI as characterised by marked atrophy, hyperintensity on T2-weighted (T2wi) and FLAIR images and partial loss of the internal architecture. To date, the different patterns of HS have not been identified on *in vivo* MRI but the advent of presurgical high-field MRI opens the possibility that subtle variability in imaging allows us to identify HS variants and to predict postsurgical outcome. Despite promising studies on TLE patients using structural MRI (Eriksson et al., 2008; Mueller et al., 2009; Breyer et al., 2010; Henry et al., 2011; Mitsueda-Ono et al., 2013), a precise delineation of hippocampal subregions and layers remains difficult both *in vivo* and *ex vivo*, and manual segmentation protocols based on anatomic atlases, rather than differences in signal intensities, are often used to validate anatomical borders also in normal conditions (Winterburn et al., 2013; Yushkevich et al., 2009). The only exception is a recent paper by Adler et al. (2013) that proposed an histology-derived MRI atlas of the normal hippocampal formation.

Diffusion tensor imaging (DTI), a technique sensitive to the characteristics of water diffusion reflecting the bio-physical structure of the examined tissue, has been recently applied to improve imaging of the hippocampus. An increase of the mean diffusivity (MD), which quantifies water mobility, and a reduction of fractional anisotropy (FA), related to the presence of ordered structures such as fibers, have been reported in patients with HS (Thivard et al., 2005; Salmenpera et al., 2006; Liacu et al., 2010). Moreover, *ex vivo* high resolution DTI has been used to study diffusion characteristics of the different lamina of human hippocampus (Shepherd et al., 2007). However, in most of the cases correlation with histopathology was not sufficient or even missing.

On these premises, we present a case series in which *ex vivo* 7T MRI and accurate histopathologic correlation were performed in normal

and sclerotic hippocampi. Our aims were:i) to achieve a highly reliable anatomical delineation of normal hippocampus and its inner structures on structural MRI; ii) to identify distinct MRI patterns, corresponding to histopathologic subtypes of HS, based on structural and diffusion-weighted MR data; iii) to track major intrahippocampal pathways in normal and sclerotic hippocampi by DTI. Our results will be helpful to further advance preclinical and clinical imaging in patients suffering from brain diseases affecting the hippocampus such as MTLE.

Material and Methods

Hippocampal specimens

Human hippocampi were collected from the University Hospital Erlangen, Germany and the C. Besta Neurological Institute in Milan, Italy and divided in two groups: no HS (4 post-mortem and 11 surgical samples) and HS (18 surgical samples, Table 1). The post-mortem cases were from patients with no clinical history of neurological disorders and no significant histopathological changes in the hippocampus. The hippocampi were dissected from the temporal lobe preserving the head, body and tail with the fimbria and the adjacent parahippocampal gyrus (Fig. 1A). The specimens were fixed in 4% formalin, subsequently embedded into 6% agaroseand then submitted to MRI. For post-mortem studies informed written consent was given from the patients' next of kin. Surgical hippocampi (11 no HS and 18 HS) were obtained from patients with medically intractable TLE who underwent surgery for the relief of seizure after written consent. The resection was performed for strictly therapeutic reason on the basis of the electroclinical and/or imaging presurgical work-up. In patients without MRI signs of HS, the hippocampus was resected based on the electroclinical evidence of its involvement in seizures generation. Neuropathological confirmation was obtained for all cases.

Immediately after surgery, the hippocampi were fixed in 4% paraformaldehyde buffered solution, embedded into agarose and submitted to *ex vivo* MRI studies. All procedures have been approved by the local ethical commissions.

High-field 7T-MRI

MRI was performed using a 7T scanner (BioSpec 70/30 USR, Bruker, Ettlingen, Germany) and high-resolution two dimensional (2D) T2wi were acquired in coronal plane. In order tovisualize all hippocampal subregions in the head of hippocampus, a subgroup of samples were submitted to a different protocol (see Table 1). First, three dimensional T2wi were used to estimate the best fitting angles that restore all the hippocampal subregions in the head and in the very anterior mid-body. Then, 2DT2wi were acquired according to these angles,ranging from 30°-50° for the mid-anterior level and 70°-90° in the head, with respect to the tilt angle for the slices in the body region (Fig. 2H). Alignment of the histological sections to the oblique MR datasets was performed with Amira 5.3.3 software (Visage Imaging, Berlin, Germany). DTI were acquired by an EPI sequence in a subgroup of samples (see Table 1). The images were corrected for motion and eddy current distortions with FMRIB's Linear Image Registration Tool (FLIRT, Jenkinson, 2002) in FSL (http://www.fmrib.ox.ac.uk/fsl/). The Diffusion Tensor in each voxel was estimated from the DTI raw data and FA and MD maps (Basser-Pierpaoli, 1996) were computed using Diffusion Toolkit (http://www.trackvis.org). Fibre tracking was performed with the interpolated streamline algorithm, with an FA threshold of 0.15 and an angle threshold of 35°. MRI acquisition parameters are summarized in detail in supplementary table 1.

Histological preparations

Following MRI acquisition, the hippocampal specimens were cut into 0.5cm thick slabs according to image-acquisition geometries. Subsequently, the slabs were alternately embedded in paraffin or cut by a vibratome (VT1000S, Leica, Heidelberg, Germany). For cytoarchitectural analyses, sections were stained for Cresyl Violet and Thionin. Kluver-Barrera and Black Gold II (0.3% dissolved in 0.9% saline, Histo-Chem) were applied for the illustration of the myeloarchitecture. NeuN (neuronal nuclear antigen, Chemicon International, Tamecula, CA, U.S.A.), GFAP (glial fibrillary acid protein, Chemicon) and MBP (myelin basic protein, Dako, Denmark) immunohistochemistry were performed in all samples according to standard immunoperoxidase procedures to visualized selective neuronal loss, gliosis and myelin distribution. Each stained section was digitized with a slice scanner (ScanScope, Aperiotechnologies, CA, U.S.A.). The same histological procedures were applied in a group of control hippocampi (ID 7-15, Table 1), not admitted to MRI investigation, and used as reference values for quantitative field fraction.

Comparison between MRI findings and histopathology

To enable correlations between MRI and neuropathological data, the MRI slices were visually compared with digitized histological sections by two experienced observers (GR and CR) and the best fitting slices were chosen (Eriksson et al., 2005). Anatomical landmarks (i.e., blood vessels, hippocampal curvature or ependymal lining) served as reference. Then, quantitative evaluations were performed on these selected slices (one MRI and one histological section per case).

7T-MRI measurements in the stratum pyramidale/radiatum of the hippocampal subfields. Focal measurements of signal intensity, area and MD-FA values were performed in the different hippocampal subregions guided by the corresponding histological NeuN-stained

sections. Because the different neuropathological patterns of hippocampal damage are mainly due to alterations of the stratum (sr) pyramidale/radiatum, the measurements were performed in these layers. Signal intensity was measured on T2wi by manually drawing two regions of interest (ROIs) using, as anatomic landmarks, the hypointense bands corresponding to the myelinated fibres in the sr lacunosum/moleculare and oriens/alveus which can be reliably visualized on these high-resolution images both in normal and sclerotic hippocampi. On the same slice, the area of the hippocampal subfields was delineated and measured. FA and MD values were measured in each subfield drawing a single ROI on the corresponding maps; the identification of the sr pyramidale was performed on FA map where the resolution was excellent. Because FA is more related to fiber organization, a ROI on the sr lacunosum-moleculare was added. An example of images used for these measures is shown in Supplementary Figure 1A-C.

*Histologic measurements in the stratum pyramidale/radiatum of the hippocampal subfields.*Quantitative field fraction estimates of NeuN, GFAP and MBP immunostaining were evaluated in each hippocampal subfield using the image analysis system Image Pro-Plus 7.0 software (Media Cybernetics, Bethesda, MD, U.S.A). Field fraction is a method which gives an accurate estimation of the percentage of immunostaining within an area of interest (Eriksson et al., 2007) and, with NeuN immunohistochemistry, can be considered a reliable method to estimate neuronal loss. We measured field fraction in two ROIs (each representing 0,1 mm^2) outlined at x20 magnification in the sr pyramidale of each subregion. An example of images used for field fraction analyses is shown in Supplementary Figure 1D-F. According to the value of neuronal loss patterns proposed in the new classification system (Blumcke et al., 2013), only two HS subtypes were identified in our specimens: Type 1 (13 samples) and Type 2 (5 samples).

Line profiles. Signal intensity profiles for both MR and histological images were generated for CA1 subfield, along a vector perpendicular to the cortex, using ImageJ software.

Data analysis

Differences in mean values of the signal intensity, areas and histological measures among the groups (no HS, Type 1 and Type 2 HS) were evaluated by Kruskal-Wallis test followed by *post hoc* comparisons using Mann-Whitney test. The significance limit was set at $p<0.01$, considering Bonferroni's correction. Signal intensities and areas were correlated with quantitative histological measures using the Pearson product-moment correlation coefficient. Statistical analyses were performed using SPSS version 17.0 (SPSS, Chicago, III, U.S.A.).

Results

Structural MRI and histology in normal specimens

Differences in MR intensity on high resolution T2wi revealed the distinct anatomical organization of the hippocampal formation. In particular, seven hippocampal layers (i.e. alveus, sr pyramidale, sr radiatum, sr lacunosum, sr moleculare as well as the sr moleculare and granule cell layer of the DG) were clearly visible on 7T MRI (Fig. 1C, G, J) with the exception of the hippocampal sroriens, and confirmed on histological sections (Fig. 1D, H, K). Furthermore, parahippocampal structures as the subiculum, the presubiculum as well as the entorhinal, transentorhinal and temporal cortex were distinguished by their unique cyto- and myelo-architecture (Fig. 1C, D, G, H) (Duvernoy, 2005). Signal intensity profiles of 7T images and histology (Fig. 1I, L) proved consistency between both methods. Anatomical subregions and layers with high neuronal cell densities

and/or high myelin content showed low signal intensities on MR images, whereas less cellular or myelinated regions were characterized by increased MR signal. Based on these findings, even more subtle regions within the hippocampal formation were recognized such as the terminal zone of the perforant path extending to the srradiatum of CA2 (arrow in Fig. 1G) or the srlucidum. The cell dense granule layer of the DG was characterized by a low MR signal (arrowheads in Fig. 1G). However, even at the high resolution and contrast of the present study, the boundaries between subfields were not visually discernible (Figs. 1G and 3A) and quantification of the MRI signal intensity confirmed this observation (Fig. 4C).

Because the inclined/olique orientation of the hippocampal head renders any anatomical identification of different subfields difficult when evaluating coronal planes, either in histology or imaging (Fig.2B-F), we assessed this anatomical region by choosing different angulations along the arch of the hippocampal head. Using this procedure, the hippocampal head was clearly visible in both MRI and histological sectionswith the possibility to discriminate different layers and CA subfields as identified in the hippocampal body (Fig. 2G-O).

Structural MRI and histopathology in HS specimens

Visual analysis of the T2wi acquired in surgically resected hippocampi from patients with HS revealed a marked atrophy in all subregions, more pronounced in CA1, and signal hyperintensity in all subfields, except CA4 and subiculum, particularly evident in the sr pyramidale and radiatum, in comparison to normal hippocampi (Fig. 3Cvs 3A). The granule cell layer of the DG was almost undetectable presumably due to the wide inhomogeneous signal intensity or the presence of granular cell dispersion. The boundaries between subfields were not identifiable except the border between CA1 and subiculum (Fig. 3C). Only four discernible layers (i.e. alveus, sr pyramidale-radiatum, sr lacunosum-moleculare of CA and sr moleculare of DG) were clearly

visible both on MRI and histological sections (Fig. 3Cvs 3A and 3D vs 3B) and signal intensity line profiles supported this observation (Fig. 3C' vs 3A' and 3D' vs 3B').

To evaluate whether the structural MRI changes were be related to histological alterations such as cell loss, myelinated fibre reorganization, gliosis and thus potentially predict the different histological HS patterns, a subset of histological and radiological parameters were quantitatively evaluated in the different hippocampal subfields in control and HS specimens.

Field fraction analysis in NeuN-stained sections was used to classify the individual specimens according to the new ILAE HS classification scheme. We observed in all sclerotic cases a significant reduction in NeuN staining in each CA sector in comparison to control hippocampi. Differences between Type 1 and 2 HS were due tomore pronounced cell loss in CA 3-4 in Type 1 HS with respect to Type 2 (Fig. 4A). Gliosis, evaluated using GFAP-stained sections, was significantly present in all subfields and apparently not related with neuronal loss, in fact its extent was similar both in Type 1 and 2 HS (Fig. 4B). Myelinated fibres, evaluated with MBP immunohistochemistry didn't show quantitative differences between control and sclerotic hippocampi (data not shown). Concerning MRI parameters, signal intensity and area were significantly different in sclerotic hippocampi in comparison to control, although unable to discriminate between the two HS subtypes (Fig. 4C, D). Moreover, no significant correlation was observed between NeuN, GFAP, MBP field fraction and MRI parameters (data not shown).

Our experimental approach to visualize the hippocampal head, based on oblique slicing of the anterior level confirmed that sclerosis was present both in the head and midbody in all pathological samples with a MRI pattern similar to those observed in the body region. Notably, the histological grading of sclerosis could be different along the longitudinal axis (Supplementary Fig. 2A-Cvs 2D-F).

DTI parameters and tracking of hippocampal fibres

Since structural MRI data did not allowed to discriminate between HS Type 1and Type 2, others parameters (i.e. MD, FA and fibre tracking) were evaluated.

Despite an intrinsic range of variability, thevalues of MD, calculated in 4 HS specimens, were always higher in comparison to normal hippocampi (Fig. 5A). However, when two typical histological samples of HS Type 1 and Type 2 (Fig. 5B,E) with highest degree of neuronal loss in their respective sectors according to field fraction analysis (Fig. 5C, D) were chosen, the MD values were able to discriminate between the two HS subtypes.

FA values, calculated on sr pyramidale-radiatum and lacunosum-moleculare, were uninformative with no clear difference between control and HS and HS subtypes while qualitative differences in FA maps were observed. In control sample, FA maps demonstrated a spatial resolution sufficient to distinguish the hippocampal sublayers with fine anatomical detail (Fig. 5F). Diffusion anisotropy was higher in region of white matter or densely packed axonal projection such as fimbria and alveus. By contrast, lower FA was observed in the DG and hilus. Intermediate values were found in sr lacunosum-moleculare, moleculare of DG, pyramidale and subiculum. Regions with high FA values clearly correlated with areas of closely packed myelinated axons in MPB-stained sections (inset in Fig. 5F), whereas low and intermediate values occurred where prevalent neuronal soma or a complex mixture of soma and neuropil, not visualized by myelin staining, were present. In sclerotic hippocampi, no evident changes (Fig. 5G) were observed in the regions with high content of fibres (alveus, fimbria, and white matter) in comparison to control samples but the laminar division in the sr lacunosum-moleculare and moleculare of the DG was less evident and MBP immunohistochemistry revealed a different organization of the fibres (inset in Fig. 5G).

Fibre tracking was performed to reconstruct the trajectory of the main projections. The main afferent is the perforant path, originating from the entorinal cortex. It is important to note that the entorhinal cortex is restricted to the uncal segment, therefore, perforant path fibers aiming at the hippocampal body must follow a longitudinal route along the anterior-posterior axis (Hjorth-Simonsen, 1972). Fibre tracking (Fig.5H) was able to visualize this anatomical feature showing fibres travelling through the plane of the image (from the entorhinal cortex in the angular bundles, blue colour) and vertical fibers crossing the subiculum towards the molecular layer (green colour). The alvear path, also rising from the entorhinal cortex and continuing towards the alveus, was visible as fibres running around the surface of hippocampus (mixed colour). The radial fibres observed in the stratum pyramidale and radiatum might be due at least in part to the large and regularly arranged apical dendrites of CA pyramidal neurons.The main efferent of the hippocampus, the fimbria, was clearly recognized as fibres running through the plane of the image (blue colour) whereas, the fibers of the sr lacunosum-moleculare within the hippocampal formation (terminal part of the perforant path and Shaffer collateral), were less evident. In sclerotic hippocampus, fibre tracking clearly showed a general disorganization of the reconstructed fibers(Fig. 5I).

Discussion

The human hippocampus is anatomically characterized by distinct compartments, which are differentially involved in memory and learning (van Strien NM et al., 2009, Coras R. et al., 2010) and selectively compromisedin neurological disorders such as Alzheimer's disease or MTLE (Braak H, Braak E. 1991, Blumcke I. et al., 2002). *In vivo* imaging of disease specific pathology patterns will thus be important to achieve early reliable diagnosis and to monitor disease

progression or modifying therapies. However, subtle changes in the internal hippocampal anatomy can be yet detected only at histopathological level in postmortem or surgical brain specimens. Rapidly evolving high-field and ultra-high-field MRI may offers the unique opportunity to specifically study and to repetitively monitor hippocampal anatomy along its anterior-posterior axis. Previous work using *in vitro* as well as *in vivo* MRI significantly increased spatial resolution and signal to noise ratio, thereby uncovering almost all hippocampal subfields and layers (Wieshmann UC et al., 1999, Fatterpekar GM et al., 2002, Duvernoy HM 2005, Theysohn JM et al., 2009, Chakeres DW 2005 et al., Thomas BP et al., 2008, Yushkevich PA et al., 2009). However, validation of anatomical compartments and boundaries by congruent comparison between high-field MRI and histology is mandatory for preclinical or clinical use. In the present study, we approached this issue by comparing high-resolution imaging with fully digitized microscopy slides and assessing also the difficult anatomical orientation of the hippocampus head as well as major hippocampal fibre tracks to achieve a comprehensive high-resolution MRI survey of the human hippocampus. Moreover, a comparison between high resolution imaging and histopathology was also performed in surgical specimens from patients operated on for intractable MTLE with HS.

Structural MRI and histology in normal specimens

Despite the improvement of the anatomical resolution obtained with progressive high-resolution structural MRI, imaging protocols failed to separate all the intra-hippocampal layers and the parcellation of the hippocampal subregions was often conventionally-defined and not histologically-proved (Wieshmann et al., 1999; Chakeres DW et al., 2005; Yushkevich et al., 2009; Winterburn et al., 2013). In our MRI study we were able to identify seven distinct layers within the hippocampal formation, which was confirmed by reference histology

from same specimens and same plane of sections. Whether a similar resolution can be obtained in a clinical 7T *in vivo* scanner remains to be shown. However, despite the high static magnetic field coupled with high performing magnetic gradient and long acquisition time used in the present study it was not possible to discriminatethe boundaries among the different subfields using discernible MRI signature. Since the hippocampus head is affected in many neurological disorders (Bouchard TP et al., 2008, Wood SJ et al., 2010, Bernasconi N et al., 2003 TLE, Bonilha L. et al., 2011, Yasuda CL et al., 2010), in a set of experiments, we applied 3D and 2D T2wi of the hippocampus head to discriminate different subfields like in the midbody. These protocols may offer more insights into hippocampal MRI anatomy and will provide a basis for precise segmentation techniques of this complex anatomical region.

Structural MRI and histopathology in HS specimens

In pathologic HS specimens several findings were observed in comparison to the normal specimens. It is well-known that marked volume loss is a cardinal sign of HS, and our data revealed that atrophy involved all subfields with an increased signal intensity particularly evident in the sr pyramidale-radiatum. Both atrophy and signal hyperintensity were present in all samples regardless the two histologically defined subtypes of HS. This observation pose a question of the histopathological basis for the MRI signal. Few studies have investigated correlations between neuropathology and MRI findings in human hippocampus. While some authors suggest that hippocampal volumes reflect neuron cell density (Cascino et al., 1991, Lee et al 1995), a significant correlation between neuron cell counts in CA1 sector and volume loss was not found by others (Briellmann et al 2002). Signal increase in HS has been suggested to reflect gliosis (Kuzniecky et al., 1987). In the present work NeuN, GFAP and MBP field fraction analysis did not correlate with the hyperintensity and

atrophy calculated on T2wi. These data suggest that the gliosis and neuronal loss per se do not significantly influence MRI parameters and that alterations in MRI signal are presumably due to a combination of pathological processes including an increased extracellular space and water content in the affected areas as demonstrated by EM investigations (Witcher et al. 2010).

The layering observed in normal specimens was completely disrupted in HS specimens and a good correspondence between MRI and histopathology was found and corroborated by the line profiles. These data suggest that during the sclerotic process along with the neuronal loss, a profound rearrangement and disorganization of the internal fibre bundles is occurring.

DTI parameters and tracking of hippocampal fibres

The most commonly used diffusion tensor indices are the mean diffusivity and fractional anisotropy. Both are DTI-derived parameters sensitive to the water diffusion and are indirect indices of tissue microstructure able to detect subtle changes induced by pathological states. Although MD has been reported to increase in HS with respect to control (Thivard et al., 2005; Salmenpera et al., 2006; Liacu et al., 2010), only one work is dealing with the evaluation of the diffusion properties in different areas of postmortem hippocampi (Shepherd et al., 2007). In the present study, albeit in a limited number of cases, we evaluated MD changes in different subfields of normal and sclerotic hippocampi. Measurements performed in sr pyramidale showed higher MD values in all HS with respect to controls thus reflecting presumably neuronal loss. When two histopatologically-representative cases of Type 1 and Type 2 HS were chosen, characterized by the almost total cells loss in the respective sectors, MD values were able to differentiate between the two subtypes. Based on these data we can argue that the increased diffusivity in the affected tissue may be an indirect consequence of neuronal cell death followed by an expansion

of the extracellular space in which water molecules move. However, due to the high variability of neuronal loss within each hippocampal subfield it was not possible with this modality to discriminate HS grading in all the other tested cases. FA values, more linked to the microstructural organization of the white matter, were not useful to differentiate either HS from no HS or different HS grading.

In summary, our high-resolution MR-microscopy study will provide a valuable resource for clinical and preclinical investigations of physiological and pathophysiological conditions in patients suffering from diseases affecting the hippocampus and adjacent brain regions such as MTLE and Alzheimer's disease. In particular, the possibility to discriminate HS pattern based on diffusion data, although will require further validation in *in vivo* studies, may lead to novel imaging biomarkers with improved diagnostic and prognostic value.

		Sample ID	Side/Size	T2wi (7T MRI)	DTI (7T MRI)	MRI measures	Histologic measures
no HS	autoptic samples	1	R/head+body	3D-2D with different angulations	yes	yes	yes (MBP only)
		2 + 3	R-L/head+body	3D-2D with different angulations	yes/yes	yes	yes (MBP only)
		4	L/head+body	3D-2D with different angulations	no	yes	yes (MBP only)
	surgical samples	5	L/head+body	3D-2D with different angulations	yes	yes	yes
		6	R/head+body	3D-2D with different angulations	yes	yes	yes
		7	R/body	no	no	no	yes
		8	R/body	no	no	no	yes
		9	L/body	no	no	no	yes
		10	R/body	no	no	no	yes
		11	R/body	no	no	no	yes
		12	L/body	no	no	no	yes
		13	R/body	no	no	no	yes
		14	R/body	no	no	no	yes
		15	R/body	no	no	no	yes
HS	surgical samples	1	R/head+body	3D-2D with different angulations	Yes	yes	yes
		2	R/head+body	3D-2D with different angulations	Yes	yes	yes
		3	R/head+body	3D-2D with different angulations	yes	yes	yes
		4	L/head+body	3D-2D with different angulations	no	yes	yes
		5	R/head+body	3D-2D with different angulations	no	yes	yes
		6	R/body	2D	no	yes	yes
		7	R/body	2D	no	yes	yes
		8	L/body	2D	no	yes	yes
		9	L/body	2D	no	yes	yes
		10	R/body	2D	no	yes	yes
		11	L/body	2D	no	yes	yes
		12	R/body	2D	no	yes	yes
		13	L/body	2D	no	yes	yes
		14	L/body	2D	no	yes	yes
		15	R/body	2D	no	yes	yes
		16	R/body	2D	no	yes	yes
		17	R/body	2D	no	yes	yes
		18	R/body	2D	yes	yes	yes

Table 1

Analysed specimens / patients and experimental protocols.

Legend to Table 1: DTI= diffusion tensor imaging; HS= hippocampal sclerosis; L= left; MBP= myelin basic protein; R= right; T2wi= T2 weighted MR images; 3D-2D= three and two dimensional MR images.

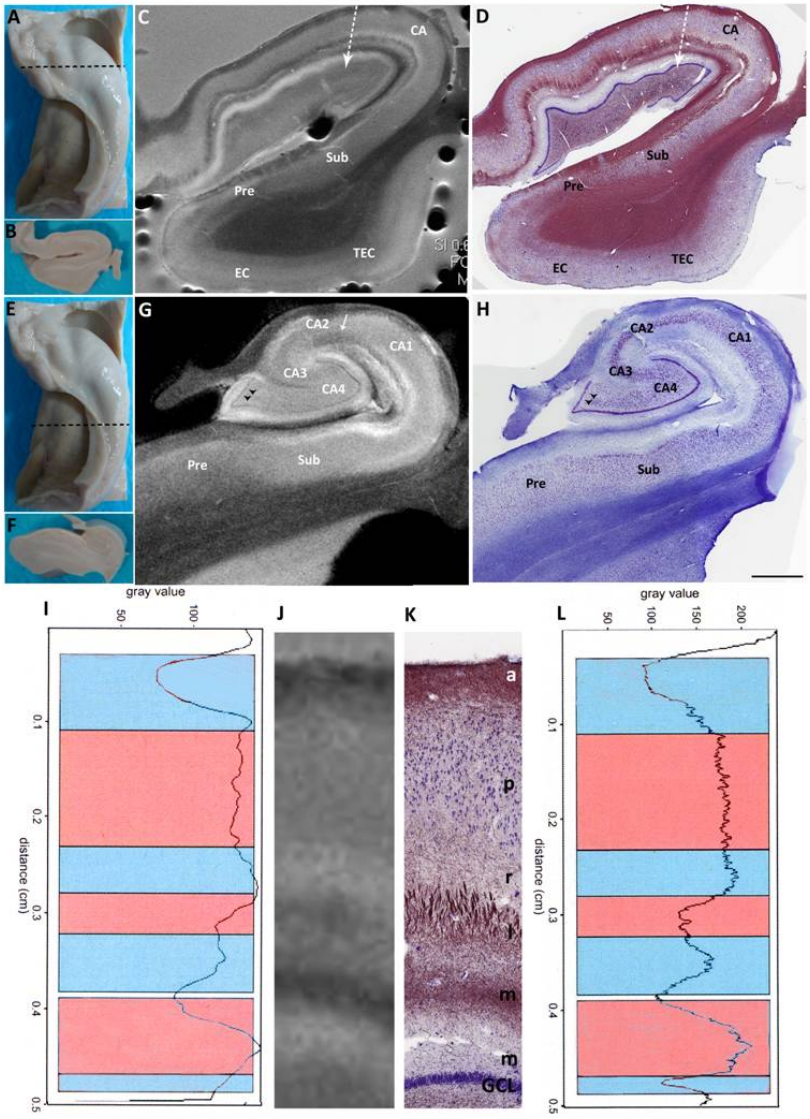

Fig. 1

Anatomical specification of hippocampal subregionsand layers along the anterior-posterior axis in normal hippocampus.

A-D: Coronal sections through the hippocampal head. **A**: Macroscopic view of the entire hippocampus and (**B**) slab obtained after coronal slicing through the hippocampal head using the cutting plane indicated in A. Based on discernible intensity change in MR images, hippocampal subregions and layers were clearly identify (**C**) and proved on corresponding histological section with Cresyl violet-Black Gold staining (**D**).**E-H**:Coronal sections through the hippocampal body. **E**: Macroscopic

view of the entire hippocampus and (**F**) slab obtained after coronal slicing through the hippocampal body using the cutting plane indicated in E. Arrow in **G** indicated the terminal zone of the perforant path in the stratum radiatum of CA2 while arrowheads pointed the granule cell layer as confirmed in the corresponding cresil violet-stained section (**H**).**J**, **K**: Enlargements of the area indicated by the dotted arrow in C and D respectively clearly showed the layered anatomic features of the hippocampus. Seven hippocampal layers both in MR image (**J**) and corresponding histological section stained with Cresyl violet-Black Gold (**K**) were visible and signal intensity profiles overlapped between 7T MRI (**I**) and histology (**L**).
Scale bars: D= 2800um; H=1850um

a:alveus, CA: cornu ammonis CA1-CA4: subfields of CA, EC: entorhinal cortex, GCL: granule cell layer of the dentate gyrus, l: stratum lacunosum, m: stratum moleculare of the CA and moleculare of the dentate gyrus, p: stratum pyramidale of CA, Pre: presubiculum, Sub: subiculum, TEC: transentorhinal cortex.

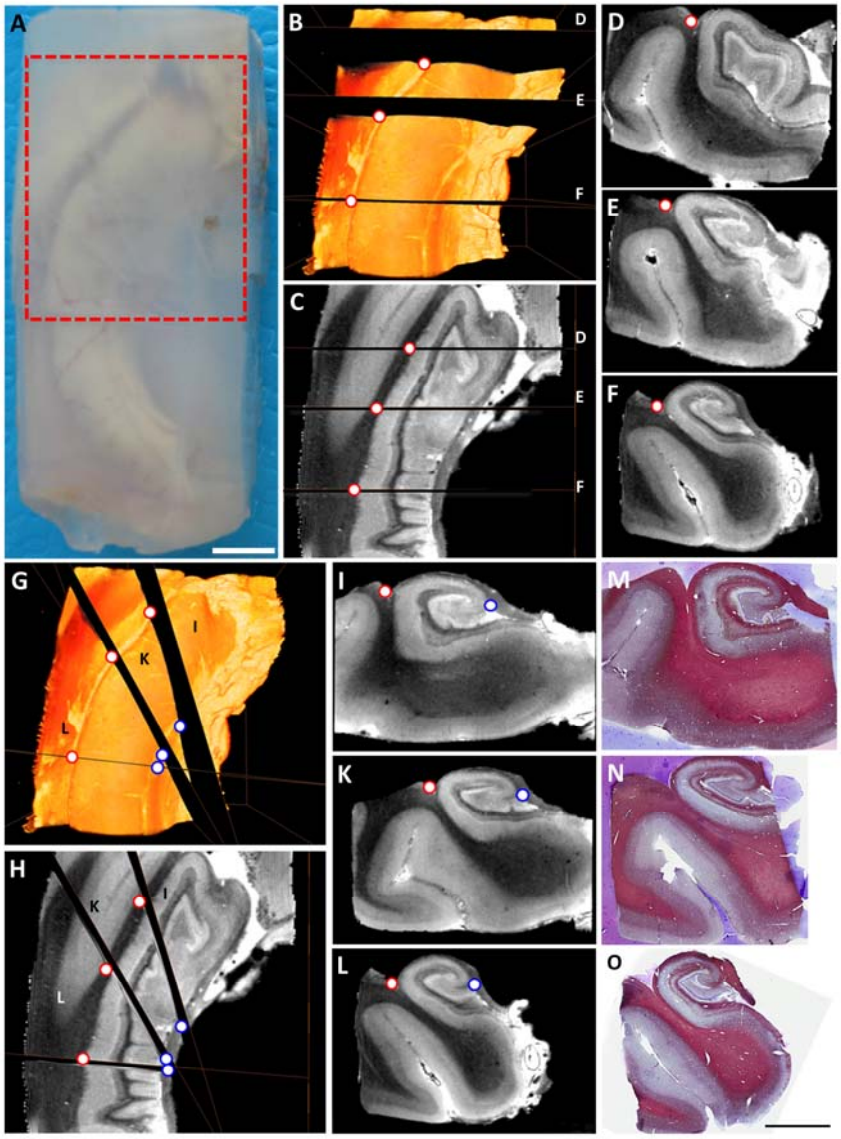

Fig. 2

Three-dimensional anatomical specification of the hippocampus head in normal hippocampus

A: Macroscopic view of the entire hippocampus embedded in agar. Red dotted rectangle indicated the area of the three-dimensional MRI scan. **B** and **G**: Volume rendering displayed the analyzed three-dimensional field with labelling of coronal (B) and inclined (G) planes. **C** and **H**: Horizontal geometry with labelling (black planes and bars) of coronal (C) and inclined (H) planes. White dots with red margins in B-L: collateral eminence as

landmark. **D**, **E**, **F**: Coronal planes along the anterior-posterior axis of scanned sample. Here, the delineation of hippocampal subregions is difficult to read, particularly in the hippocampal head (D) and the very anterior hippocampal midbody (E) compared to a plane through the hippocampal body (F). **I**, **K**, **L**: Inclined coronal planes restored all hippocampal subregions also in the hippocampal head (I) and the very anterior hippocampal midbody (K). **M**, **N**, **O**: Corresponding histological sections with Cresyl Violet-Black Gold staining to I, K, L. White dots with blue margins in G-L: fimbrio-dentate sulcus as landmark point for inclinations (white dots with red margins in B-L).
Scale bars: M=6400um; N=6200um; O=6650um

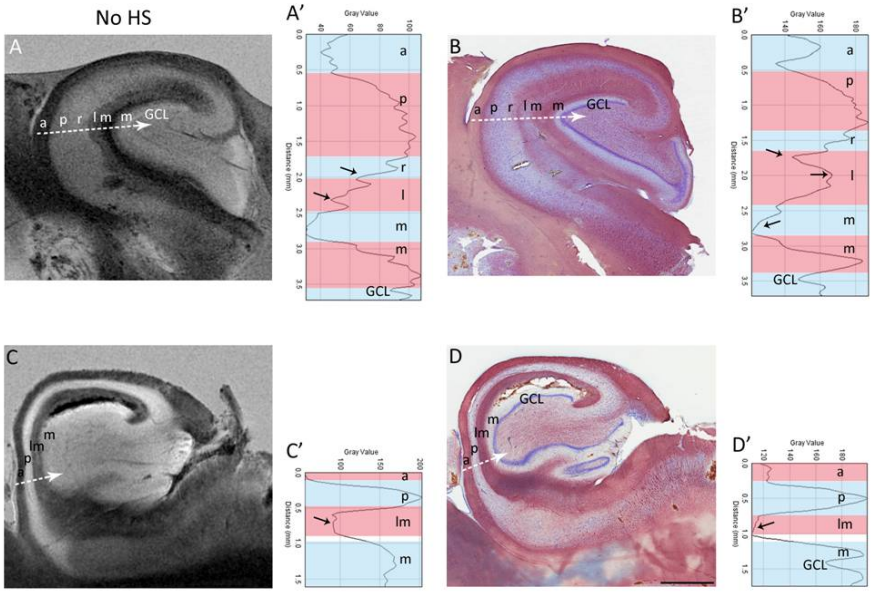

Fig. 3
Qualitative MRI features and histopathology in sclerotic human hippocampus (example of Type 2 HS)
A, C: High-resolution MR imaging revealed in sclerotic hippocampus (C) higher signal intensity in all subfields, except in CA4 and subiculum, and atrophy in comparison to normal hippocampus (A). The sr pyramidale and radiatum were particularly affected. Corresponding histological sections, obtained from the same specimens, revealed in Cresyl Violet-Black Gold staining segmental neuronal loss, more prominent in CA1 sector in this specimen, and rearrangement of the fibre bundles in the sr lacunosum-moleculare (**D** vs **B**). Signal intensity profiles, calculated along the track of the dotted arrows, confirmed loss of distinct layers in the sclerotic hippocampus both in MR images (**C',**with only 4 discernible layersvs **A'**with well evident 7 layers) and Cresyl Violet-Black Gold staining sections (**D'**vs**B'**);

a:alveus, GCL: granule cell layer of the dentate gyrus, l: stratum lacunosum, m: stratum moleculare of the CA and moleculare of the dentate gyrus, p: stratum pyramidale. Scale bars: B=1980um; D=1860um

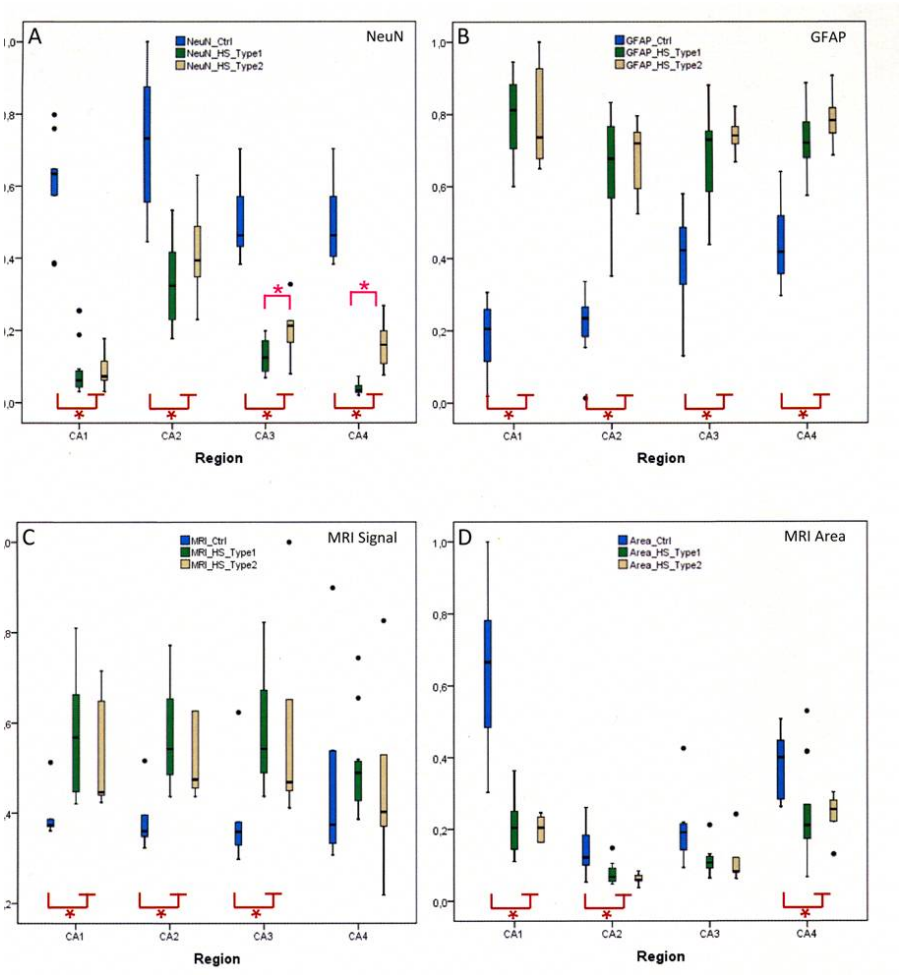

Fig. 4

Quantitative analysis of the histological and radiological parameters in normal and sclerotic hippocampus

A, B: Box plots showing NeuN and GFAP field fraction measures performed in histological slices from normal and sclerotic hippocampi. **A**: NeuN field fraction revealed three different patterns: control hippocampi with no evident cell loss (blu bars), Type 1 HS with prominent cell loss in CA1, 3, 4 sectors (green bars) and Type 2 HS with prominent cell loss in CA1 (yellow bars). **B**: GFAP field fraction revealed in sclerotic hippocampi a significant increased of GFAP in all subfields in comparison to control cases. No differences were observed between Type 1 and 2 HS. **C**, **D**: Box

plots showing MRI measures performed in T2wi from hippocampi grouped according to histological patterns. **C**: Signal intensity, measured in the srpyramidale-radiatum, was significantly higher in CA1-2-3 subfields in all sclerotic hippocampi in comparison to control cases. **D**: The areas of CA1, 2 and 4 were significantly reduced in sclerotic compared to the control samples. Nevertheless, both signal intensity and atrophy not revealed difference between Type 1 and 2 HS. Statistical significance is indicated by asterisks.

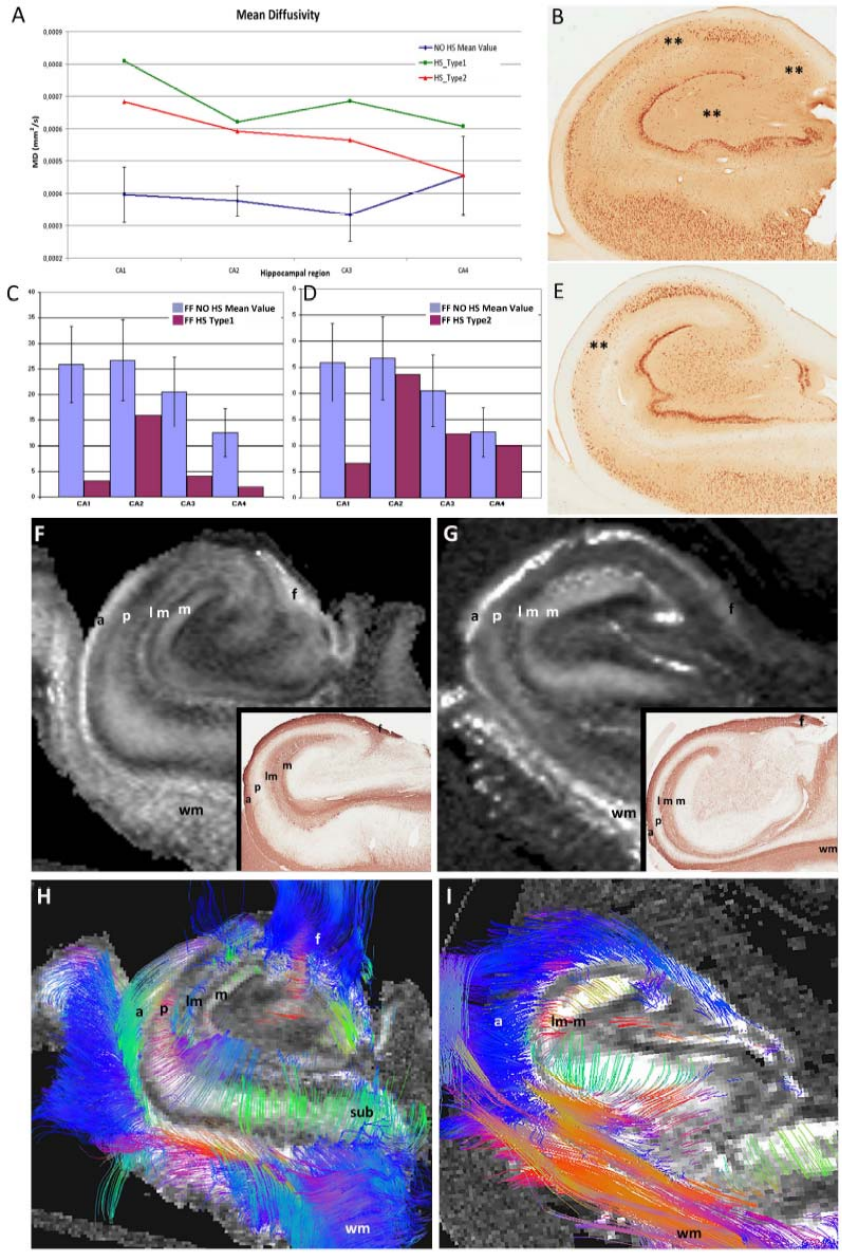

Fig. 5

DTI-derived parameters andfiber tracking in normal and sclerotic hippocampus

A: MD values obtained from no HS specimens (5 samples) and from a typical histopathological example of Type 1 HS (**B**, NeuN-stained section) and Type 2 HS (**E**, NeuN-stained section). Higher values of MD were obtained in both HS specimens in comparison to no HS group. Note that Type 1 HS, characterized by more severe neuronal loss affecting multiple subfields (**C**, field fraction), had higher MD values than Type 2 HS characterized instead by neuronal loss affecting only CA1 sector (**D**, field fraction). **F:** Fractional anisotropy maps in normal hippocampus (F) revealed excellent resolution of the hippocampal regions and sublayers. Areas with highest diffusion anisotropy (white) were: white matter, fimbria, alveus. Lower FA (black) was observed in the granular cell layer and hilus. Intermediate values (grey) were found in sr lacunosum-moleculare, moleculare of the dentate gyrus, subiculum and pyramidal cell layer. In sclerotic hippocampi (**G**), no evident changes of FA values were observed in alveus, fimbria, and white matter but, differently from controls, FA map did not reveal a laminar division in the regions of the stratum lacunosum-moleculare and moleculare of the dentate gyrus. Inset in F and G, examples of corresponding MPB-stained sections, showed that highest diffusion anisotropy was observed in regions of densely packed myelinated axons whereas low and intermediate values occurred where neuronal soma or a complex mixture of soma and neuropil, not visualized by myelin staining, were present.**H, I:** Examples of tractography showed the trajectory of the main projections obtained from the same specimens depicted in F, G. Note in sclerotic hippocampus (**F**) a different organization of the fibres in comparison to a control case (**E**).
Scale bars: B=1410um; E=1410um; insert in F=2080um; insert in G= 2060um

A: alveus, f: fimbria, lm: stratum lacunosum-moleculare of CA, m: stratum moleculare of the dentate gyrus, p: stratum pyramidale; sub: subiculum, wm: white matter.

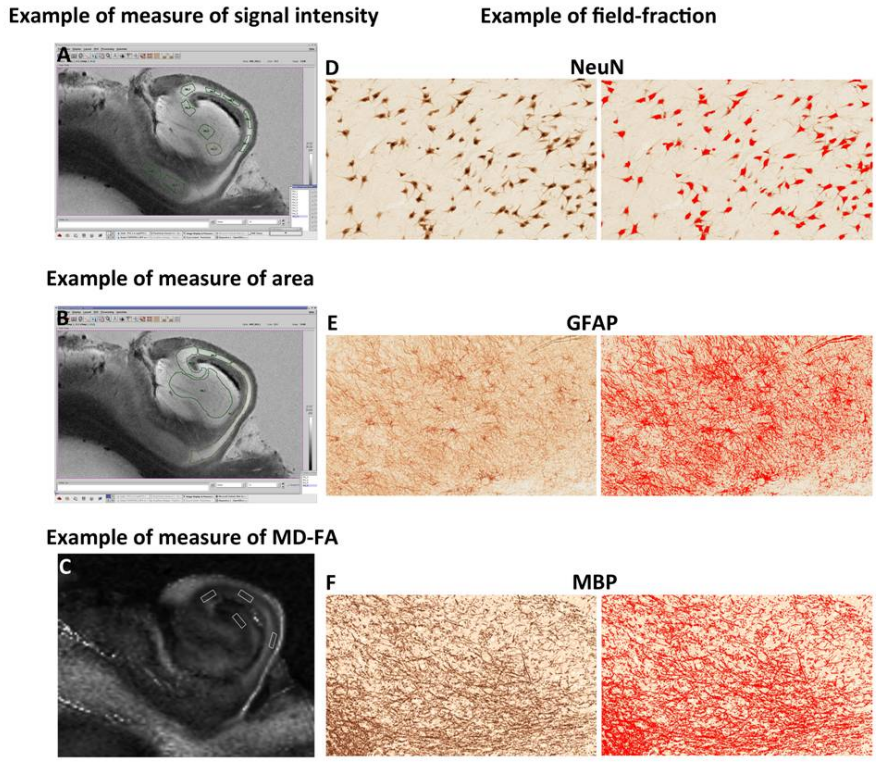

Supplementary Fig. 1

Examples of MRI and histological measures

A-C: Examples of ROIs manually drawn on T2wi(A, B) and on FA map (C) obtained from a sclerotic hippocampus to measures signal intensity (A), area (B) and FA value (C). To calculate MD values, the same ROIs in the same position were translatefrom FA map to MD map. **D-F**: Examples of field fraction analysis performed on NeuN-, GFAP-, and MBP-immunostained sections used to classify hippocampal specimens according to new HS variants, and to evaluate gliosis and myelin staining.

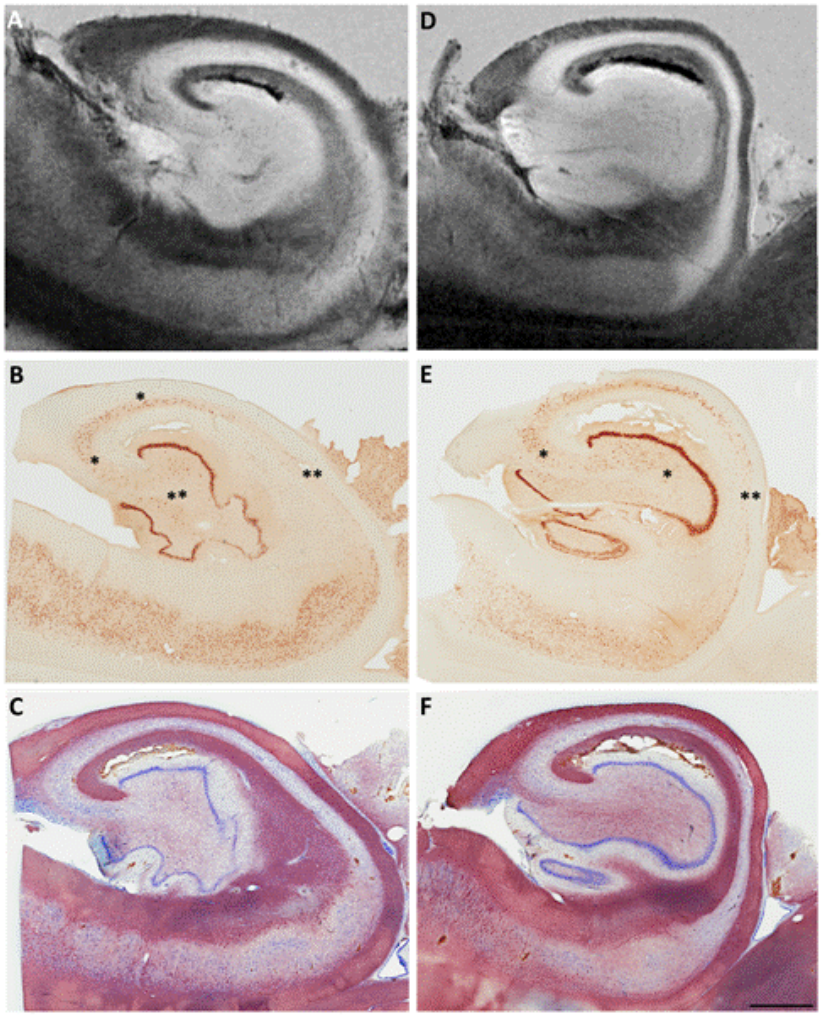

Supplementary Fig. 2

High resolution anatomical specificationof the head in sclerotic hippocampus

Comparison between MR and corresponding histological images obtained in the head of hippocampus (**A-C**), according to angulated coronal plane, and in the body of the same specimen (**D-F**). T2wi showed signal hyperintensity and atrophy, well evident in sr pyramidale and radiatum, as observed in the body region (A vs B). Corresponding histological sections with NeuN immohistochemistry (B) and Cresyl Violet-Black Gold staining (C) confirmed the presence of sclerosis also in the very anterior head. Notably, the pattern of neuronal loss was more severe in the head in comparison to the body. Asterisks indicated subfields affected by neuronal loss.

Scale bars: B=1570um; E=1450; C=1500; F=1480um

References

Adler DH et al Histology-derived volumetric annotation of the human hippocampal subfileds in post-mortem MRI Neuroimage 2013

Augustinack JC, van der Kouwe AJ, Blackwell ML, et al. (2005) Detection of entorhinal layer II using 7Tesla [corrected] magnetic resonance imaging. Ann Neurol57:489-494

Basser PJ, PierpaoliC. Microstructural and physiological features of tissues elucidated by quantitative-diffusion-tensor MRI.J MagnReson B. 1996 111(3):209-219.

Bernasconi N, Bernasconi A, Caramanos Z, Antel SB, Andermann F, Arnold DL. Mesial temporal damage in temporal lobe epilepsy: a volumetric MRI study of the hippocampus, amygdala and parahippocampal region. Brain 2003;126:462-469

Blumcke I, Thom M, Wiestler OD. Ammon's horn sclerosis: a maldevelopmental disorder associated with temporal lobe epilepsy. Brain Pathol 2002;12:199-211

Blumcke I, Pauli E, Clusmann H, et al. A new clinico-pathological classification system for mesial temporal sclerosis.ActaNeuropathol 2007;113:235-244

Blumcke I, Kistner I, Clusmann H, et al. Towards a clinico-pathological classification of granule cell dispersion in human mesial temporal lobe epilepsies. ActaNeuropathol 2009;117:535-544

Blümcke I, Thom M, Aronica E, Armstrong DD, Bartolomei F, Bernasconi A, Bernasconi N, Bien CG, Cendes F, Coras R, Cross JH, Jacques TS, Kahane P, Mathern GW, Miyata H, Moshé SL, Oz B, Ozkara C, Perucca E, Sisodiya S, Wiebe S, Spreafico R. International consensus classification of hippocampal sclerosis in temporal lobe epilepsy: A Task Force report from the ILAE Commission on Diagnostic Methods. Epilepsia 2013 54:1315:1329

Bonilha L, Halford JJ, Morgan PS, Edwards JC (2012) Hippocampal atrophy in temporal lobe epilepsy: the 'generator' and 'receiver'. ActaNeurol Scand 125(2):2011

Bouchard TP, Malykhin N, Martin WR, et al. Age and dementia-associated atrophy predominates in the hippocampal head and amygdala in Parkinson's disease. Neurobiol Aging 2008;29:1027-1039

Braak H, Braak E. Neuropathological stageing of Alzheimer-related changes. ActaNeuropathol 1991;82:239-259

Breyer T, Wanke I, Maderwald S, Woermann FG, Kraff O, Theysohn JM, Ebner A, Forsting M, Ladd ME, Schlamann M.Imaging of patients with hippocampal sclerosis at 7 Tesla: initial results. AcadRadiol 2010 17:421-426

Briellmann RS, Kalnins RM, Berkovic SF, Jackson GD. Hippocampal pathology in refractory temporal lobe epilepsy: T2-weighted signal change reflects dentate gliosis.Neurology. 2002 Jan 22;58(2):265-71.dacontrollare

Cascino GD, Jack CR Jr, Parisi JE, Sharbrough FW, Hirschorn KA, Meyer FB, Marsh WR, O'Brien PC. Magnetic resonance imaging-based volume studies in temporal lobe epilepsy: pathologicalcorrelations.Ann Neurol. 1991 Jul;30(1):31-6

Chakeres DW, Whitaker CD, Dashner RA, et al. High-resolution 8 Tesla imaging of the formalin-fixed normal human hippocampus.ClinAnat 2005;18:88-91

Coras R, Siebzehnrubl FA, Pauli E, et al (2010) Low proliferation and differentiation capacities of adult hippocampal stem cells correlate with memory dysfunction in humans. Brain 133:3359-3372

de Lanerolle NC, Kim JH, Williamson A, Spencer SS, Zaveri HP, Eid T, Spencer DD. (2003) A retrospective analysis of hippocampal pathology in human temporal lobe epilepsy: evidence for distinctive patient subcategories. Epilepsia 44:677-687.

Duncan J. The current status of neuroimaging for epilepsy.CurrOpinNeurol 2009;22:179-184

Duvernoy HM. The Human Hippocampus.Functional Anatomy, Vascularization and Serial Sections with MRI.Heidelberg: Springer; 2005

Eriksson SH, Free SL, Thom M, Harkness W, Sisodiya SM, Duncan JS (2005) Reliable registration of preoperative MRI with histopathology after temporal lobe resections Epilepsia 46 (10):1646-1653

Eriksson SH, Free SL, Thom M, Martinian L, Symms MR, Salmenpera TM, McEvoy AW, Harkness W, Duncan JS, Sisodiya SM (2007) Correlation of quantitative MRI and neuropathology in epilepsy surgical resection specimens-T2 correlates with neuronal tissue in gray matter. Neuroimage 37(1):48-55

Eriksson SH, Thom M, BartlettPA, et al. PROPELLER MRI visualizes detailed pathology of hippocampal sclerosis. Epilepsia 2008;49:33-39

Fatterpekar GM, Naidich TP, Delman BN, et al. Cytoarchitecture of the human cerebral cortex: MR microscopy of excised specimens at 9.4 Tesla. AJNR Am J Neuroradiol 2002;23:1313-1321

Henry TR et al Hippocampal sclerosis in temporal lobe epilesy: findings at 7T Radiology 2011

Hjorth-Simonsen A. Projection of the lateral part of the entorhinal area to the hippocampus and fascia dentata. J Comp Neurol 1972;146:219-232

Kuzniecky R, de la Sayette V, Ethier R, Melanson D, Andermann F, Berkovic S, Robitaille Y, Olivier A, Peters T, Feindel W. Magnetic resonance imaging in temporal lobe epilepsy: pathological correlations. Ann Neurol. 1987 Sep;22 (3):341-7.

Liacu D, de Marco G, Ducreux D, Bouilleret V, Masnou P, Idy-Peretti I. Diffusion tensor changes in epileptogenic hippocampus of TLE patients.Neurophysiol Clin. 2010 Jun;40(3):151-7. doi: 10.1016/j.neucli.2010.01.003. Epub 2010 Feb 7.

Mitsueda-Ono T et al.,Structural changes in the hippocampus observed on 3-Tesla MRI in patients with Mesial temporal lobe epilpsy Internal medicine 2013)

Mueller SG, Laxer KD, Barakos J, Cheong I, Garcia P, Weiner MW. Subfield atrophy pattern in temporal lobe epilepsy with and without mesial sclerosis detected by high-resolution MRI at 4 Tesla: preliminary results. Epilepsia 2009;50:1474-1483

Salmenpera TM, Simister RJ, Bartlett P, Symms MR, Boulby PA, Free SL, Barker GJ, Duncan JS. High-resolution diffusion tensor imaging of the hippocampus in temporal lobe epilepsy.
Epilepsy Res. 2006 Oct;71(2-3):102-6. Epub 2006 Jul 25.

Shepherd TM, Ozarslan E, Yachnis AT, King MA, Blackband SJ. Diffusion tensor microscopy indicates the cytoarchitectural basis for diffusion anisotropy in the human hippocampus. AJNR Am J Neuroradiol 2007;28:958-964

Theysohn JM, Kraff O, Maderwald S, et al. The human hippocampus at 7 T--in vivo MRI.Hippocampus 2009;19:1-7

Thivard L, Lehéricy S, Krainik A, Adam C, Dormont D, Chiras J, Baulac M, Dupont S. Diffusion tensor imaging in medial temporal lobe epilepsy with hippocampal sclerosis.
Neuroimage. 2005 Nov 15;28(3):682-90. Epub 2005 Aug 9.

Thom M Liagkouras I, Elliot KJ, Martinian L, Harkness W, McEvoy A, Caboclo LO, Sisodiya SM. 2010 Reliability of patterns of hippocampal sclerosis as predictors of postsurgical outcome Epilepsia 2010 51:1801-1808
Thomas BP, Welch EB, Niederhauser BD, et al. High-resolution 7T MRI of the human hippocampus in vivo.J MagnReson Imaging 2008;28:1266-1272

vanStrienNM, Cappaert NL, Witter MP. The anatomy of memory: an interactive overview of the parahippocampal-hippocampal network. Nat Rev Neurosci 2009;10:272-282

Weigele JB. 7.0 Tesla MRI: the "field of dreams"? AcadRadiol 2010;17:407-409

Wieshmann UC, Symms MR, Mottershead JP, et al. Hippocampal layers on high resolution magnetic resonance images: real or imaginary? J Anat 1999;195 (Pt 1):131-135

Winterburn et al., A novel in vivo atlas of human hippocampal subfileds using high resolution 3T magnetic resonance imaging 2013

Witcher MR, Park YD, Lee MR, Sharma S, Harris KM, Kirov SA. Three-dimensional relationships between perisynapticastroglia and human hippocampal synapses. Glia. 2010 Apr;58(5):572-87. doi: 10.1002/glia.20946

Wood SJ, Kennedy D, Phillips LJ, et al. Hippocampal pathology in individuals at ultra-high risk for psychosis: a multi-modal magnetic resonance study. Neuroimage 2010;52:62-68

Yasuda CL, Morita ME, Alessio A, et al. Relationship between environmental factors and gray matter atrophy in refractory MTLE. Neurology 2010;74:1062-1068

Yushkevich PA, Avants BB, Pluta J, et al. A high-resolution computational atlas of the human hippocampus from postmortem magnetic resonance imaging at 9.4 T. Neuroimage 2009;44:385-398

Chapter 5

Assessment of human hippocampal developmental neuroanatomy by *ex-vivo* 7T magnetic resonance imaging approaches

International Journal of developmental Neuroscience, *submitted*

Gloria Milesi[1], Rita Garbelli[1], Ileana Zucca[2], Eleonora Aronica[3,4], Roberto Spreafico[1] and Carolina Frassoni[1]

[1]Clinical Epileptology and Experimental Neurophysiology Unit and [2]Scientific Department, Fondazione I.R.C.C.S. Istituto Neurologico "C. Besta", Milan, Italy: [3a]Department of (Neuro)Pathology, Academic Medical Center and [3b]Swammerdam Institute for Life Sciences, Center for Neuroscience, University of Amsterdam; [4]SEIN – Stichting Epilepsie Instellingen Nederland, Heemstede, The Netherlands.

Key words: high resolution MRI, hippocampus, fetal and postnatal development, immunohistochemistry, histology

Abstract

During development the hippocampus undergoes numerous changes, concerning the cytoarchitecture, the cellular morphology and the myeloarchitecture which begin in the fetal period and continues after birth. In this study, we investigated the developmental changes occurring in human healthy fetal (from 20 to 32 gestational weeks) and postnatal (from 1 day to adulthood) hippocampus by combining high-resolution 7 Tesla Magnetic Resonance Imaging (MRI) and histological and immunohistochemical analysis to compare variations in signal intensity with cito- and myeloarchitectural organization. During fetal period the intensity of the T2-weighted images was related to the cellular density. In fact, the subregions of Ammon's horn and dentate gyrus, characterized by densely packed neurons, were recognizable as hypointense areas. The inverse correlation between MRI signal intensity and cellular density was visualized by line profile results. At the age of two postnatal weeks, the low MRI signal was still linked to the cell density even if thin myelinated fibers were observed in the hypointense MRI regions like the alveus and the stratum lacunosum-moleculare. The myelin content increases with advancing development till to get the complete hippocampal myeloarchitecture in the adulthood. From 7 years until the adulthood, comparison between MRI and corresponding histological sections indicated that the differences in T2-weighted images reflected the increased density of myelinated fibers.

The present results provide useful information to evaluate *in vivo* MRI performed at lower field strengths and might be used as reference in the perspective that high spatial resolution MRI will be used in clinical practice.

Introduction

The human hippocampal development consists of a series of events at cito and architectural level strictly regulated and distinct within its different anatomical compartments which begin in the fetal period and continues after birth. The cytoarchitectural and myeloarchitectural appearances of the human hippocampus from early fetal age into adulthood have been extensively characterized (Humphery et al., 1987; Bayer and Altman, 2004; Arnold and Trojanowski, 1996a) and the time course of myelination were examined (Abraham et al., 2010). Notably, abnormalities in hippocampal formation have been described in several brain developmental disorders including lissencephaly, tuberous sclerosis, polymicrogyria, heterotopia and agenesis of the corpus callosum (Baker and Barkovic 1992; Kappeler et al., 2007; Fallet-Bianco et al., 2008; Kuchukhidze et al., 2010; Friocourt et al., 2011).

Magnetic Resonance Imaging (MRI) represents an important tool in prenatal diagnosis to perform *in vivo* examination of developmental changes during fetal life and few studies have examined morphological development of the human hippocampus (Righini et al., 2006; Cho et al., 2010; Jacob et al., 2011) without obtain fine anatomical details.

In the last years, comparative studies of normal fetal cerebrum using *ex-vivo* MRI and histology were addressed to analyze the age-specific changes occurring during brain development (Kostovic et al., 2002; Rados et al., 2006; Zhang et al., 2011; Kostovic et al., 2012). The changes found in the MRI lamination pattern of the human fetal cerebral wall are important in evaluating the health status of the whole brain and can serve as a marker for dating developmental disorders. Transformations in fetal human hippocampal formation have been documented in a comparative study using 1.5T MRI scan and provided a developmental basis for understanding hippocampal anatomy but the precise delineation of hippocampal subfields was

lacking (Kier et al., 1997). Recently, high-field MRI scanners (≥4T) equipped with high performing magnetic field gradients are emerging tools which offer images with a greatly increased spatial resolution and tissue contrast compared with the 1.5T and 3T MRI instruments usually employed in the clinical practice, so they allow to obtain more detailed radiological images which can be supported by the histological findings. Structural high resolution MRI approach has already been applied to *ex-vivo* study of adult hippocampal morphology and it has proven able to visualize fine anatomical details (Wiesmann et al. 1999; Chakeres et al. 2005; Shepherd et al., 2007; Adler et al., 2013). Here we performed anatomical MRI sequence on 7T MRI in human fetal and postnatal hippocampus in order to compare variations in signal intensity with cito- and myeloarchitectural organization matching 7T MRI with histological and immunohistochemical findings. We aimed to provide normal developmental basis for the high spatial resolution study of hippocampal abnormalities *in vivo* in the perspective of future clinical applications in prenatal diagnosis.

Materials and Methods

Human specimens and tissue preparation

Ten human fetal (from 20 to 32 gestational weeks, GW) and six post natal (from 1 day to adulthood) hippocampal specimens were included in this study (Table 1). The hippocampal slabs originated from hippocampal midbody with the exception of the case of three months that originated from hippocampal head.

The subjects were selected from the databases of the Departments of Neuropathology of the Academic Medical Center (AMC), University of Amsterdam. Tissue was obtained and used in a manner compliant with the Declaration of Helsinki and the Academic Medical Center (AMC) Research Code provided by the Medical Ethics Committee of the AMC

(Amsterdam, The Netherlands). Fetal brain was obtained from spontaneous or medically induced abortions with appropriate maternal written consent for brain autopsy. Gestational ages were based on obstetric data, fetal and brain weights and standard fetal anthropometric measurements. We perform a careful histological and immunohistochemical analysis and evaluation of clinical data (including genetic data, when available). We excluded cases with other chromosomopathies, major central nervous system (CNS) malformations, brains with postmortem autolysis, severe hypoxic/ischemic encephalopathy, intraventricular hemorrhages, severe hydrocephalus and meningitis or ventriculitis. We only included as control cases, specimens displaying a normal hippocampal and cortical structure for the corresponding age and without any significant brain pathology. All autopsies were performed within 24 h after death.

Hippocampal slabs (about 5 millimeters thick) were fixed in 4% formalin for approximately 4-5 weeks and subsequently embedded in 6% agarose to limit the motion of samples and resulting artifacts during 7T MRI acquisition. After the MRI study the specimens were processed for neuroanatomical evaluation and subsequent comparison between matching sections obtained with the two methodologies.

7T MRI

MRI was performed using 7T scanner (Bruker BioSpec 70/30 USR, Ettlingen, Germany) equipped with a gradient system reaching the maximum amplitude of 400 mT/m. A 35mm quadrature volume coil was used for radio frequency excitation and signal reception. For anatomical references, T2-weighted images (T2-wi) were acquired in three orthogonal planes: axial, sagittal, and coronal. In order to improve the contrast in the T2-wi between tissues with different water content and cellular and fibers density, the TE and TR parameters were optimized for each sample because such contrast depends on

specimen age. For this purpose, the acquisition protocol included a Multi Slice Multi Echo (MSME) sequence with twenty echo times and echo spacing 11 msec and a Saturation Recovery sequence with TR=10-8-6-4-2 sec and TE=23-70-116-160-210-260msec. High-resolution T2-wi were acquired by Spin Echo sequence with Slice Thickness (ST) 0.25 mm for fetal samples and 0.5 for postnatal samples, in plane resolution 0.08x0.08 mm^2 for fetal samples and 0.04x0.04 mm^2 for postnatal samples, Echo Time (TE) was of 160 ms for fetal samples, 140 ms for 2 weeks old sample, 100 ms for 3 months old sample, 60 ms for 7 years old and adult samples.

Histological and immunohistochemical study

After 7T MRI scans, the specimens were embedded in paraffin and cut in to 7 μm thick coronal sections by means of a microtome RM2245 (Leica, Hiedelberg, Germany) taking care to maintain the same orientation of MRI slices. The cito- and the myeloarchitecture were evaluated by using Cresyl violet and Kluver-Barrera staining. Adjacent sections were processed for immunohistochemical analysis according to standard immunoperoxidase procedure and then counterstained with Cresyl violet. To detect axons we used mouse anti-SNAP25, mouse anti-α internexin and mouse anti-SMI312 antibodies. To investigate the appearance and distribution of oligodendrocytes and myelinated fibers we used mouse anti-CNPase and rabbit anti-MBP antibodies. The antibodies used in this study were listed in Table 2. To test the specificity of the immunohistochemical procedure, control sections were processed without the primary and secondary antibodies and no immunostaining was detected under these conditions. Each stained section was digitized with a slide scanner (ScanScope, Aperio technologies, CA, USA) and compared with the corresponding radiological slice.

Signal intensity profiles in MRI and histological preparations were carried out on 23 GW and adult samples along a selection line starting

from the alveus in the CA1 field till the dentate gyrus by means of ImageJ software 1.46r (National Institutes of Health, USA).

Results

During development the hippocampus undergoes numerous changes, with respect to its cytoarchitecture, cellular morphology and myeloarchitecture, leading to a gradual increase of the complexity and of the degree of maturation of this structure. Some of these changes were visible at the 7T MRI as variations in signal intensity that can be interpreted by correlating high resolution imaging with the corresponding histological and immunohistochemical sections.

Human fetal hippocampus

At 20 GW the cytoarchitectural organization of hippocampus was already well defined and it was clearly visible on both MRI images (Fig. 1A) and histological preparations (Fig. 1B). Distinct differences in signal intensity can be clearly recognized on T2-wi (Fig. 1A,C,E,G,I) matching with histology of the corresponding Cresyl violet stained sections (Fig. 1B,D,F,H,L). The pyramidal cell layer of Ammon's horn (CA) and the granular cell layer of dentate gyrus (DG), characterized by high cellular density in histological sections (Fig. 1B,D) appeared as defined bands of low MRI signal intensity (Fig. 1A,C). At high magnification these hypointense bands corresponded to the stratum (str) pyramidale and to granular cell layer while signal hyperintensity was detectable in correspondence to the intermediate zone (IZ) and str. radiatum (compare Fig. 1E with F). Confirming what it has been observed in hippocampus, variation of MRI signal intensity, mainly related to difference cellular density was also clearly observed in the cerebral fetal mantle (Fig. 1G-L). Five fetal zones from the ventricle to the pial surface (ventricular zone, VZ; subventricular zone, SVZ;

intermediate zone, IZ; subplate, SP; cortical plate, CP) can be delineated in both MRI and histological sections. Very low-intense MR signal intensity corresponded to the high cell-packing density in the VZ and CP while a high and moderate MR signal intensity was depicted in the SP and IZ respectively (Fig. 1G,H). A sharp decline in MRI signal intensity was also evident at the transition from the neocortex and periallocortex (Fig. 1I) which was characterized by a decrease of cellular density (Fig. 1L). Immunohistochemistry for axonal markers, SNAP25, α-internexin and SMI312 revealed the presence of bundles of fibers in the alveus and thin fibers in the str. lacunosum-moleculare (Fig. 2A,B,C and at high magnification in F and G). In accordance with previous studies (Abraham et al., 2010), at this developmental stage MBP-immunoreactivity was only detected in scattered oligodendroglial cells prevalently located in the alveus and the str. oriens (Fig. 2H) but not in myelinated fibers (Fig. 2D) which appear later during development. A comparable pattern of immunoreactivity revealed by MBP was detected using CNPase as myelin marker (Fig. 2E) that identified earliest oligodendrocytes characterized by relatively large somata and short processes (Fig. 2I).

At the subsequent developmental stages examined (22, 23, 25 and 32 GW), MR signal intensity was always associated with high cell density as demonstrated by comparison with the corresponding Cresyl violet stained sections (Fig. 3). Low MR signal intensity clearly correlated with CA and granular cells layer of DG (Fig. 3, asterisks in A-F).

The analysis of the intensity profiles confirmed this correspondence in figure 6: a fetal representative case shows how the variation of the signal intensity profile follows the cell density distribution (compare Fig. 6B with D), when the same selection area was considered for both MR images (Fig. 6A) and matched histological slice (Fig. 6C).

An increase of immunolabelled axonal fibers was detected starting from 25 GW and it was particularly noticeable in alveus by α-internexin antibody (insert in Fig. 3D). Conversely, at this

developmental stage, myelinated fibers were not present and MBP and CNPase immunoreactivity only revealed oligodendrocytes cells (data not shown).

Human post-natal hippocampus

At the age of two postnatal weeks the low MR signal was still mainly related to the cell density (Fig. 4A,B, asterisks). MBP-immunoreactive thin fibers, not detected at 32 GW, were observed in the alveus and in the str. lacunosum-moleculare (Fig. 4C,D).

At the age of three months, no clear differences in MR signal intensity were appreciable although a moderately lowest MR signal corresponded to the areas rich of fibers as revealed by Kluver-Barrera staining and MBP immunoreactivity (Fig. 4F-G). An increase of myelinated fibers was observed in the alveus (Fig. 4H), in the str. lacunosum-moleculare (Fig. 4I) and in the subiculum.

At the age of 7 years differences in MR signal intensity were mainly related to the increase of myelinated fibers. Anatomical subregions and layers with high myelin content or moderate cellular density showed low signal intensity on MR images, whereas regions with lower cellular and myelin fibers density were characterized by increased MR signal (Fig. 5A,B,C). At high magnification, the hypointense bands (Fig. 5E) corresponded to the alveus, str. oriens and str. lacunosum-moleculare as revealed by histological comparison (Fig. 5F) and they reflected the highest density of myelinated fibers (Fig. 5G). This higher myelin fibers content was also proven by an increase, even if modest, of CNPase immunoreactivity, especially in the alveus (Fig. 5D,H). The correlation between high myelin content and low MR signal was also proven by the trend of intensity profiles as shown in Fig.6F and H derived from on the MRI section (Fig. 6E) and the corresponding MBP histology (Fig. 6G) from the adult hippocampus.

Discussion

In this study we showed the major underlying histological substrates of MR signal in ultra high field imaging of the human developing hippocampus by comparing MRI with histological and immunohistochemical findings. The principal findings of this study are 1) that high spatial resolution *ex-vivo* MRI allows to study intrahippocampal organization during fetal and postnatal development, 2) that from 20 GW to early postnatal life the signal intensity on the T2-wi signal is mainly related to cellular density, and 3) that at the age of 7 years until adulthood the comparison between MRI and MBP immunoreactivity indicate that the differences in T2-wi signal mainly reflect the increased density of myelinated fibers. To the best of our knowledge, this is the first study that correlates cytoarchitectonic developmental changes and high resolution MRI in human fetal and postnatal hippocampus.

Previous MRI and histological correlations study on *ex-vivo* fetal hippocampus have been realized (Kier et al., 1997). This study documented the transformations of fetal human hippocampal formation from 12 to 24 GW but the images obtained from the whole brain by 1.5T scanner, not allowed a reliable visualization of anatomical subcompartments.

Recently 7T MRI findings have highlighted the potential of high magnetic field strength in providing supplementary information compared to lower fields both on *ex-vivo* fetal brain (Lin et al.,2011) and in adult hippocampus (Wiesmann et al. 1999; Chakeres et al. 2005; Adler et al., 2013). In this study we performed anatomical sequence on a 7T MRI in order to visualize and delineate the layered structure and changes occurring during hippocampal development. The reduced thickness of the hippocampal slabs allowed us to obtain images with high spatial resolution and to distinguish hippocampal structural layers. Comparison of T2-wi and histological slices obtained

from the same tissues specimens allowed us to make a careful analyses of variations in signal intensity respect to the cito- and myeloarchitectural organization.

During fetal period the hippocampal structure undergoes a maturation process involving many changes related with cytoarchitecture, neuronal morphology and fibers development. The hippocampus displays individual subfields already at 20th week of gestation when CA and DG layers were well arranged and distinctly recognizable on the histology (Arnold and Trojanowski, 1996a). We revealed that these sectors, characterized by densely packed neurons, were easily recognizable on *ex vivo* MRI as hypointense areas. The inverse correlation between MR signal intensity and cellular density was visualized by line profile and it was confirmed in fetal cerebral mantle. These results were in agreement with previous comparative studies correlating *ex-vivo* MRI with histology realized on human fetal brain (Kostovic et al., 2002; Rados et al., 2006; Kostovic and Vasung, 2009). With the advance of the gestation and until two post-natal weeks despite clear differences in terms of relative cytoarchitectural maturation, the low MR signal was still influenced by the cell density. At birth the hippocampus reaches its mature cytoarchitectural appearance; however many postnatal events occur to achieve full maturity (Arnold and Trojanowski, 1996a,b) especially regarding myelination process that starts at midgestation (Abraham et al., 2010) but it continues until the adolescence. Using Snap25, α-internexin and SMI312 markers, we revealed the appearance of axonal fibers more precociously than Abraham and co-workers (2010). At the first postnatal week, the low MR signal was still linked to the cell density and only few thin myelinated fibers can be detected. When the MRI data from the post-natal cases were compared with those obtained at histological and immunohistochemical level, the correlation between cell density and low MR signal found in preterm samples becomes less obvious and from 7 years of age until the adulthood, the differences in

T2-wi signal appeared strongly related to the increase of density of myelinated fibers. In line with our results, previous *ex-vivo* studies have been reported in adult human visual and temporal cortex (Barbier et al., 2002; Garbelli et al., 2011) the reduced MR signal intensity in regions (i.e. the stripe of Gennari, infra-granular layers of temporal cortex) characterized by higher density of myelinated fibers.

Development of the hippocampal formation occurs via the progressive infolding of the fetal dentate gyrus, cornus Ammonis, subiculum and parahippocampal fissure (Kier et al., 1997). Abnormalities of the hippocampus have been described in important neurologic and neuropsychiatric disorders (Sala et al., 2004; Boyer et al., 2007; Sanchez et al., 2011) as well as in several congenital malformations (Baker and Barkovich, 1992; Kuchukidze et al., 2010). Hippocampal abnormalities seen with MR imaging included infolding malrotation, abnormal shape and volume of the hippocampus. Although in the last years *in vivo* fetal MRI has provided important new insights into fetal brain maturation (Clouchoux et al., 2012; Huang and Vasung, 2013) and it has confirmed its importance in prenatal diagnosis (Righini et al., 2012; Righini et al., 2013), some structures such as hippocampus, cannot be delineate in detail due to poor spatial resolution and short acquisition times. There have been few MRI studies on the hippocampaus in fetal population (Righini et al., 2006; Jacob et al., 2011) and they have performed using 1.5 scanner. No long-term MR fetal studies are currently available regarding higher strength magnets thus long-term safety has not yet demonstrated (Bulas and Egloff, 2013).

Thus our postmortem study by taking advantage of ultra-high field strength, long acquisition times, and focused fields of view, realize enormous gains in image quality respect to the previous studies providing a good anatomic definition of the healthy immature hippocampus and allows to identify histological substrates of MR signal. Although the present results cannot be used directly in a

clinical setting, they provide useful information that can be beneficial to evaluate *in vivo* MRI performed at lower field strengths. In addition, these data might be valuable as a reference in the perspective that high field and high spatial resolution MRI will be used in clinical practice for advanced diagnosis of hippocampal developmental disorders.

Conflicts of interest

The authors have no conflicts of interest to declare regarding the study described in this article and its preparation.

Acknowledgments

The authors thank C. Regondi for technical support and Dr. A. Righini for critical reading of manuscript. This work was supported by funding from the Italian Health Ministry Young Investigator Grants: RF 141 (to CF) and RF114 (to RG); Fondazione Banca del Monte di Lombardia, FBML (to RS); EU FP7 project DEVELAGE, Grant Agreement N 278486 (to EA).

TABLE 1

Age range	Number of cases	Cause of death
20 GW	2	spontaneous abortions
22 GW	2	medically induced abortions
23 GW	3	medically induced abortions
25 GW	2	medically induced abortions
32 GW	1	medically induced abortions
1 day	1	heart defect/ heart failure
2 weeks	1	bronchopneumonia
3 months	1	heart defect/ heart failure
7 years	2	plexus arteriovenous malformation
32 years	1	Heart failure

Analyzed specimens

TABLE 2

Primary antibody	Immunogen	Host	Code/clone	Dilution	Manufacturer
SNAP25	Whole, unaltered SNAP-25 protein, the critical epitope lies amino-terminal of the C-terminal peptide	Mouse	SMI81	1:250	Sternberger Monoclonals, BA
α internexin	Full length recombinant rat α internexin, specificity is localized to the C-terminal 164 amino acids	Mouse	MAB522	1:400	Chemicon, Temecula, CA
SMI312	Pan axonal neurofilament marker	Mouse	SMI312 SMI312R	1:500	Sternberger Monoclonals, BA; Covance, BA
CNPase	Human brain 2' 3'-cyclin nucleotide 3' phosphodiesterase	Mouse	MAB326,	1:200	Millipore, Temecula, CA
MBP	Myelin basic protein from human brain	Rabbit	A0623,	1:500	Dako, Carpinteria, CA

List of Primary Antibody

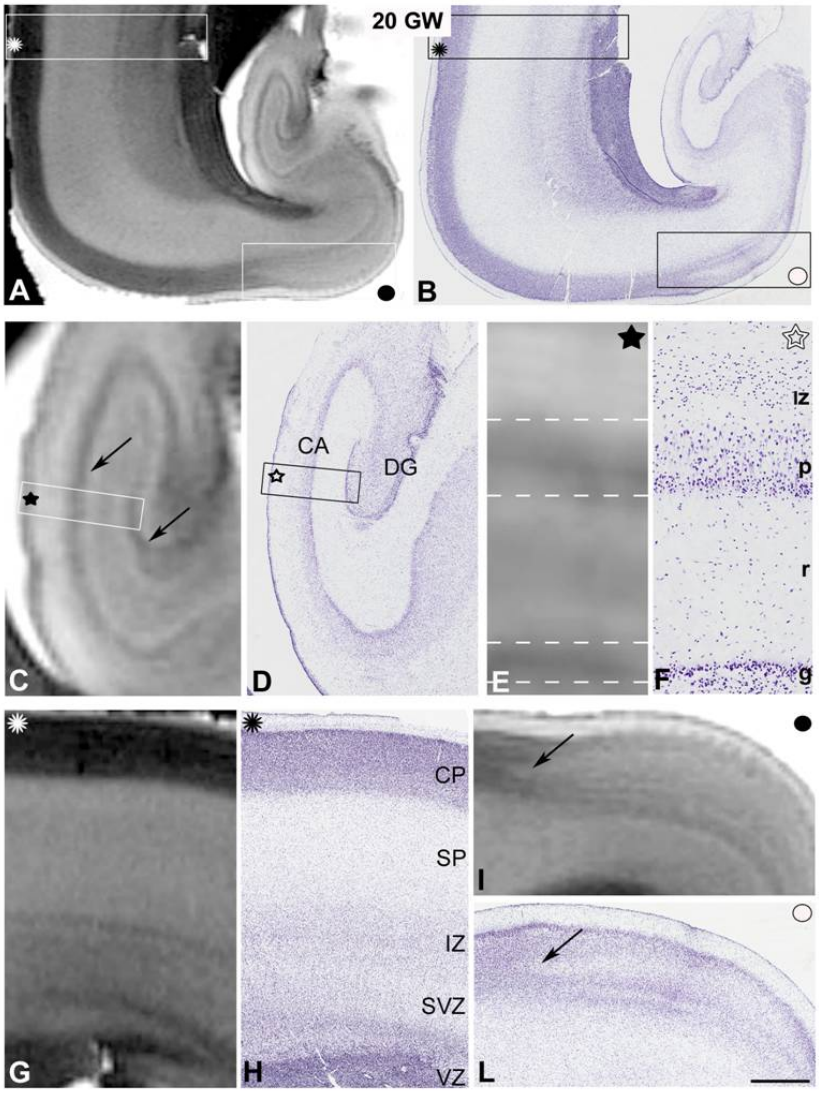

Fig. 1

Comparison of magnetic resonance and histologic images in a sample at 20 GW.

High-resolution T2-weighted images (A,C,E,G,I) and corresponding histological coronal sections with Cresyl violet-staining (B,D,F,H,L) of fetal human hippocampus and adjacent cerebral cortex at the 20th gestational week. A,B: High resolution MRI reveals differences in signal intensity (A) matching with histology (B) that shows a pattern of lamination in the hippocampus and cerebral wall. C-F: Bands of low MRI signal intensity (C, arrows) are visible in subregions of Ammon's horn (CA) and the dentate gyrus (DG). At high magnification (E, boxed areas in C) the hypointense bands correspond to the areas characterized by high cellular density such

as the stratum pyramidale (p) and to the granular cell layer (g) (F, boxed area in D). G-L: High resolution MRI of the fetal cerebral wall (G, high magnification of boxed area in A) reveals different signal intensity corresponding to the variable cellular density of the five transient layers (H, high magnification of boxed area in B). Note very low MRI intensity in correspondence of densely packed neurons in cortical plate (CP) and ventricular zone (VZ). A decline on MRI signal intensity (I, arrowhead) and decrease in cellular density (L, arrow) are evident at the transition from the neocortex and periallocortex. r, stratum radiatum; IZ, intermediate zone; SP, subplate.
Scale bars = 1950 μm in B; 950 μm in D, H and L; 160 μm in F.

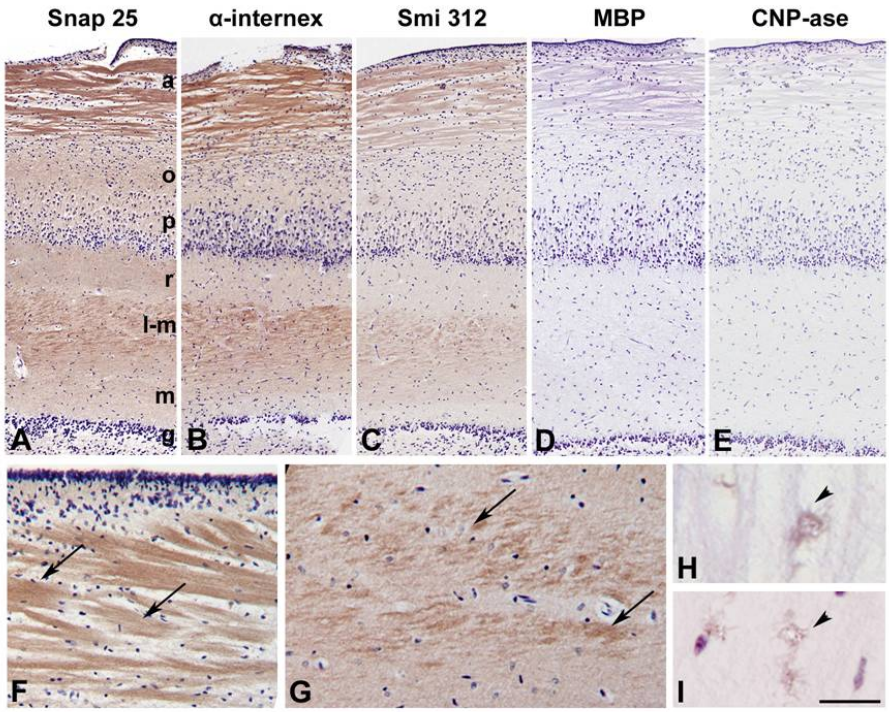

Fig. 2
Immunohistochemstry for axonal markers in a sample at 20 GW.
Immunohistochemstry for axonal markers and oligodendroglial cells in hippocampal layers at the 20th gestational week. Bundles of fibers in the alveus (a) and thin fibers in the stratum lacunosum-moleculare (l-m) (arrows) are labeled with Snap25 (A,F,G), α-internexin (B) and SMI312 (C) but not with MBP (D) and CNPase (E), markers of myelinated fibers and oligodendroglial cells. Scattered MBP and CNPase immunopositive oligodendrocytes are shown at high magnification in H and I

(arrowheads). a, alveus; o, stratum oriens; p, stratum pyramidale; r, stratum radiatum; m, stratum moleculare; g, granular cell layer.
Scale bars = 175 μm in A-E; 55 μm in F and G; 18 μm in H and I.

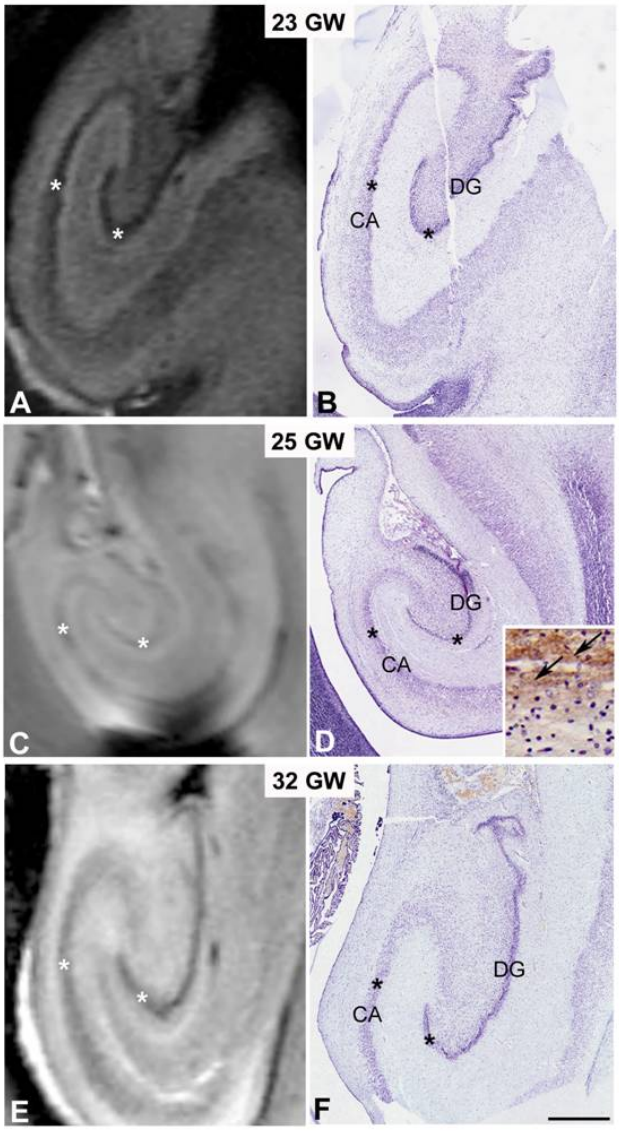

Fig. 3
Comparison of magnetic resonance and histologic images in samples at 23, 25 and 32 GW.
Comparison between T2-weighted images (A,C,F) and corresponding histological coronal sections with Cresyl violet-staining (B,D,G) of fetal hippocampi at different gestational weeks (23 GW, 25 GW, 32 GW). Note

that MRI low signal intensity correspond to the regions with densely packaged cells (see asterisks in subregions of Ammon's horn (CA) and dentate gyrus (DG)). Inset in D show an increase of α-internexin immunolabelled axons (arrows) in the alveus respect to earliest developmental stages.
Scale bars = 840 μm in B, D and F; 65 μm in inset in D.

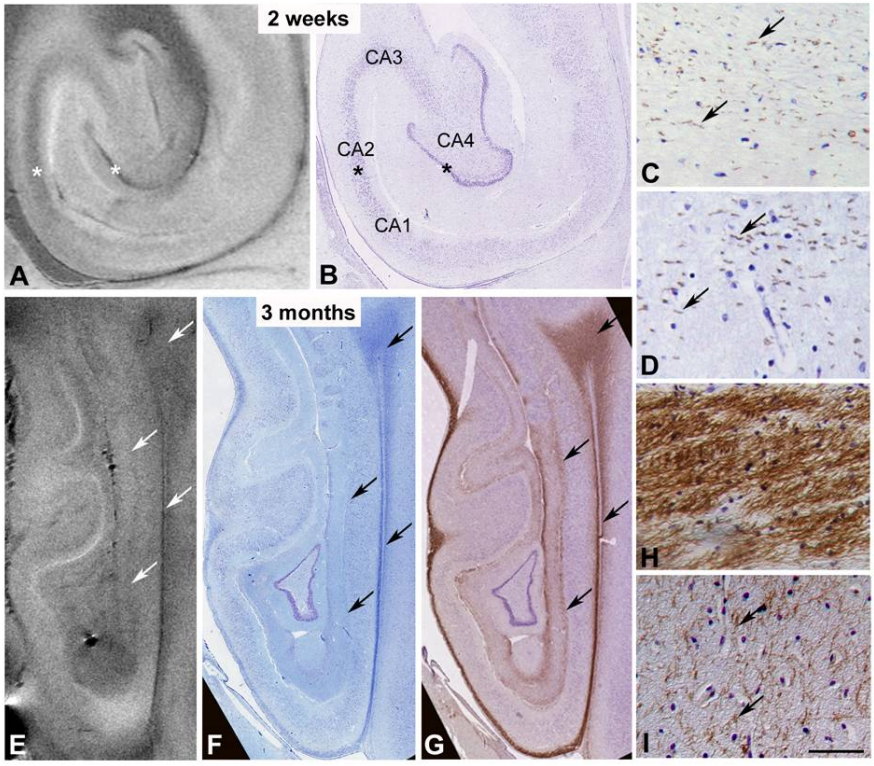

Fig. 4
Comparison of magnetic resonance and histologic images in samples at 2 weeks and 3 month.
T2-weighted images (A,E) and corresponding histological coronal sections (Cresyl violet in B, Kluver-Barrera staining in F, MBP-immunostaining in G) of post-natal hippocampi at the age of two weeks (A-D) and three months (E-I). At two postnatal weeks, the low MRI signal is still linked to cellular density (asterisks in A and B) while at three months no clear differences in MRI signal intensity is appreciable even if a lowest MRI signal (E, arrows) correspond to the areas rich of fibers (F,G arrows). MPB-immunostaining reveals the appearance of thin myelinated axons in the alveus and in the lacunosum-moleculare layer at the second post-natal week (C,D arrows)

and their increase at the age of three months (H,I). CA, pyramidal cell layer of Ammon's horn. Scale bars = 1105 μm in B; 45 μm in C and D; 1800 μm in F and G; 60 μm in H and I.

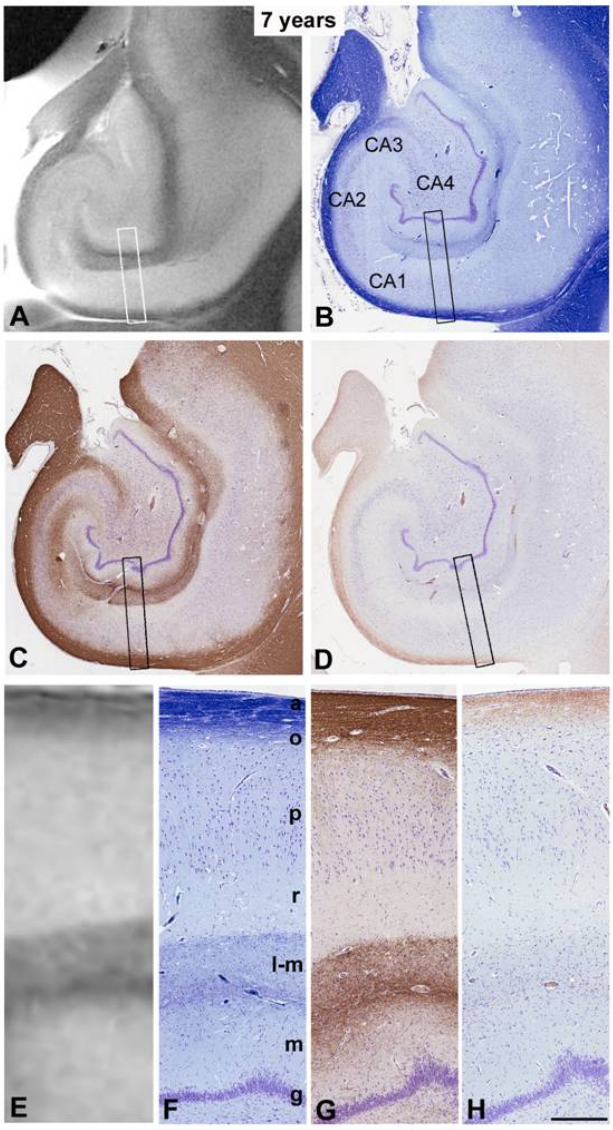

Fig. 5

Comparison of magnetic resonance and histologic images in a sample at 7 years.

Comparison between T2-weighted images (A,E) and the myelin distribution (B-D; F-H) in a 7 years old hippocampus. At lower magnification, low signal intensity on MRI (A) is clearly related to the

increase of myelin fibers as revealed by Kluver-Barrera staining (B), MBP (C) and CNPase (D) immunostaining. At high magnification note that the hypointense bands (E, boxed area in A) correspond to the region with high myelin content such as alveus, str. oriens and. str. lacunosum-moleculare (F-H, boxed areas in B-D). CA, pyramidal cell layer of Ammon's horn; a, alveus; o, stratum oriens; p, stratum pyramidale; r, stratum radiatum; l-m, stratum lacunosum-moleculare; m, stratum moleculare; g, granular cell layer. Scale bars = 1700 μm in B-D; 395 μm in F-H.

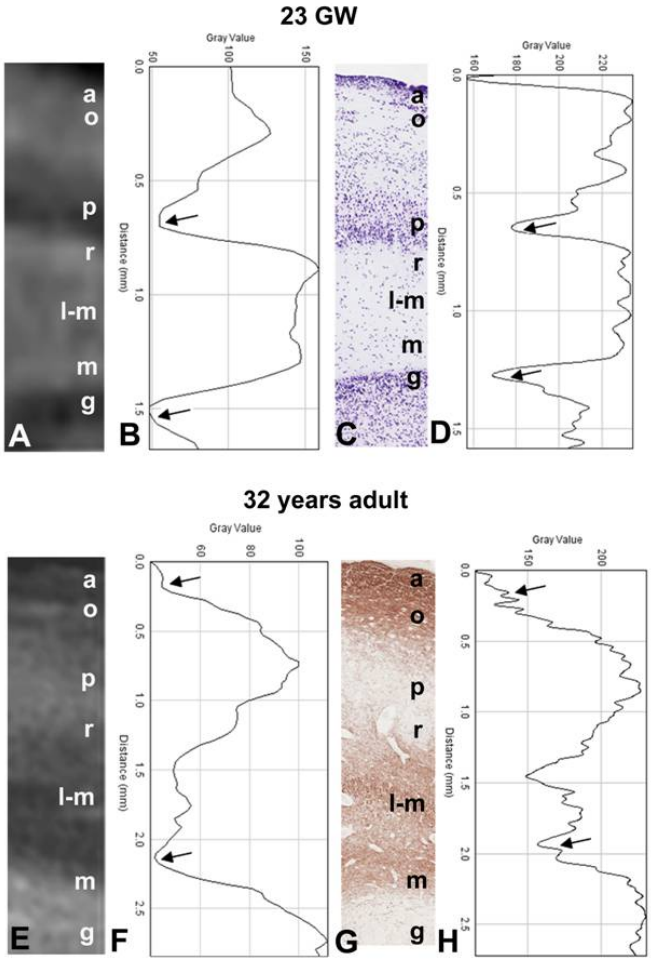

Fig. 6
Line profiles analysis in samples at 23 GW and 32 years.
Signal intensity profiles calculated on MR images and histological sections along a selection line starting from the alveus in the CA1 field till the dentate gyrus in a fetal hippocampus at the 23 GW and in a adulthood. In fetal sample the MRI contrast (A) is linked to cell distribution (C): marked

dips of hypointense signal (arrows in B) correspond to dips of highly cellular regions on histological line profile (arrows in B and D). In mature hippocampus the drops of signal intensity correspond to areas with high myelin density (compare E and F with G and H). a, alveus; o, stratum oriens; p, stratum pyramidale; r, stratum radiatum; l-m, stratum lacunosum-moleculare; m, stratum moleculare; g, granular cell layer.

References

Abraham, H., Vincze, A., Jewgenow, I., Veszpremi, B., Kravjak, A., Gomori, E., Seress, L., 2010. Myelination in the human hippocampal formation from midgestation to adulthood. Int J Dev Neurosci 28,401-410.

Adler, DH., Pluta, J., Kadivar, S., Craige, C., Gee, J.C., Avants, B.B., Yushkevich, P.A., 2013. Histology-derived volumetric annotation of the human hippocampal subfields in postmortem MRI. Neuroimage Sep 12;84C,505-523. doi 10.1016/j.neuroimage. 2013.08.067. [Epub ahead of print]

Arnold, S.E., Trojanowski, J.Q., 1996a. Human fetal hippocampal development: I. Cytoarchitecture, myeloarchitecture, and neuronal morphologic features. J Comp Neurol 367,274-292.

Arnold, S.E., Trojanowski, J.Q., 1996b. Human fetal hippocampal development: II. The neuronal cytoskeleton. J Comp Neurol 367,293-307.

Bayer, S.A., Altman, J., 2004. Atlas of human central nervous system development. Volume 2-5, CRC Press.

Baker, L.L., Barkovich, A.J., 1992. The large temporal horn: MR analysis in developmental brain anomalies versus hydrocephalus. Am. J. Neuroradiol. 13,115-122.

Barbier, E.L., Marrett, S., Danek, A., Vortmeyer, A., van Gelderen, P., Duyn, J., Bandettini, P., Grafman, J., Koretsky, A.P., 2002. Imaging cortical anatomy by high-resolution MR at 3.0T: detection of the stripe of Gennari in visual area 17. Magn Reson Med 48,735-738.

Boyer, P., Phillips, J.L., Rousseau, F.L., Ilivitsky, S., 2007. Hippocampal abnormalities and memory deficits: new evidence of a strong pathophysiological link in schizophrenia. Brain Res Rev 54,92-112.

Chakeres, D.W., Whitaker, C.D., Dashner, R.A., Scharre, D.W., Beversdorf, D.Q., Raychaudhury, A., Schmalbrock, P., 2005. High-resolution 8 Tesla imaging of the formalin-fixed normal human hippocampus. Clin Anat 18,88-91.

Cho, Z.H., Han, J.Y., Hwang, S.I., Kim, D.S., Kim, K.N., Kim, N.B., Kim, S.J., Chi, J.G., Park, C.W., Kim, Y.B., 2010 Quantitative analysis of the hippocampus using images obtained from 7.0 T MRI. Neuroimage 49,2134-40.

Clouchoux, C., Kudelski, D., Gholipour, A., Warfield, S.K., Viseur, S., Bouyssi-Kobar, M., Mari, J.L., Evans, A.C., du Plessis, A.J., Limperopoulos, C., 2012. Quantitative in vivo MRI measurement of cortical development in the fetus. Brain Struct Funct 217,127-139.

Fallet-Bianco, C., Loeuillet, L., Poirier, K., Loget, P., Chapon, F., Pasquier, L., Saillour, Y., Beldjord, C., Chelly, J., Francis, F., 2008. Neuropathological phenotype of a distinct form of lissencephaly associated with mutations in TUBA1A. Brain 131,2304-2320.

Friocourt, G., Marcorelles, P., Saugier-Veber, P., Quille, M.L., Marret, S., Laquerriere, A., 2011. Role of cytoskeletal abnormalities in the neuropathology and pathophysiology of type I lissencephaly. Acta Neuropathol 121,149-170.

Garbelli, R., Zucca, I., Milesi, G., Mastropietro, A., D'Incerti, L., Tassi, L., Colombo, N., Marras, C., Villani, F., Minati, L., Spreafico, R., 2011. Combined 7-T MRI and histopathologic study of normal and dysplastic samples from patients with TLE. Neurology 76,1177-1185.

Huang, H., Vasung, L., 2013. Gaining insight of fetal brain development with diffusion MRI and histology. Int J Dev Neurosci http://dx.doi.org/10.1016/j.ijdevneu.2013.06.005.

Humphrey, T., 1967. The development of the human hippocampal fissure. J Anat 101,655-676.

Jacob, F.D., Habas, P.A., Kim, K., Corbett-Detig, J., Xu, D., Studholme, C., Glenn, O.A., 2011. Fetal hippocampal development: analysis by magnetic resonance imaging volumetry. Pediatr Res. 69,425-429.

Kappeler, C., Dhenain, M., Phan Dinh Tuy, F., Saillour, Y., Marty, S., Fallet-Bianco, C., Souville, I., Souil, E., Pinard, J.M., Meyer, G., Encha-Razavi, F., Volk, A., Beldjord, C., Chelly, J., Francis, F., 2007. Magnetic resonance imaging and histological studies of corpus callosal and hippocampal abnormalities linked to doublecortin deficiency. J Comp Neurol 500,239-254.

Kier, E.L., Kim, J.H., Fulbright, R.K., Bronen, R.A., 1997. Embryology of the human fetal hippocampus: MR imaging, anatomy, and histology. Am J Neuroradiol 18,525-532.

Kostovic, I., Judas, M., Rados, M., Hrabac, P., 2002. Laminar organization of the human fetal cerebrum revealed by histochemical markers and magnetic resonance imaging. Cereb Cortex 12,536-544.

Kostovic, I., Vasung, L., 2009. Insights from in vitro fetal magnetic resonance imaging of cerebral development. Semin Perinatol 33,220-233.

Kostovic, I., Jovanov-Milosevic, N., Rados, M., Sedmak, G., Benjak, V., Kostovic-Srzentic, M., Vasung, L., Culjat, M., Rados, M., Huppi, P., Judas, M., 2012. Perinatal and early postnatal reorganization of the subplate and related cellular compartments in the human cerebral wall as revealed by histological and MRI approaches. Brain Struct Funct DOI 10.1007/s00429-012-0496-0.

Kuchukhidze, G., Koppelstaetter, F., Unterberger, I., Dobesberger, J., Walser, G., Zamarian, L., Haberlandt, E., Maier, H., Ortle, M., Gotwald, T., Gelpi, E., Czech, T., Feucht, M., Bauer, G., Delazer, M., Felber, S., Trinka, E., 2010. Hippocampal abnormalities in malformations of cortical development: MRI study. Neurology 74,1575-1582.

Lin, X., Zhang, Z., Teng, G., Meng, H., Yu, T., Hou, Z., Fang, F., Zang, F., Liu, S., 2011.
Measurements using 7.0 T post-mortem magnetic resonance imaging of the scalar dimensions of the fetal brain between 12 and 20 weeks gestational age. Int J Dev Neurosci 29,885-889.

Rados, M., Judas, M., Kostovic, I., 2006. In vitro MRI of brain development. Eur J Radiol 57,187-198.

Righini, A., Zirpoli, S., Parazzini, C., Bianchini, E., Scifo, P., Sala, C., Triulzi, F., 2006. Hippocampal infolding angle changes during brain development assessed by prenatal MR imaging. Am J Neuroradiol 27,2093-2097.

Righini, A., Parazzini, C., Doneda, C., Avagliano, L., Arrigoni, F., Rustico, M., Consonni, D., Re, T.J., Bulfamante, G., Triulzi, F., 2012. Early formative stage of human focal cortical gyration anomalies: fetal MRI. Am J Roentgenol 198,439-447.

Righini, A., Frassoni, C., Inverardi, F., Parazzini, C., Mei, D., Doneda, C., Re, T.J., Zucca, I., Guerrini, R., Spreafico, R., Triulzi, F., 2013.

Bilateral Cavitations of Ganglionic Eminence: A Fetal MR Imaging Sign of Halted Brain Development. Am J Neuroradiol 34,1841–1845.

Sala, M., Perez, J., Soloff, P., Ucelli di Nemi, S., Caverzasi, E., Soares, J.C., Brambilla, P., 2004. Stress and hippocampal abnormalities in psychiatric disorders. Eur Neuropsychopharmacol 14,393-405.

Sanchez, M.M., Moghadam, S., Naik, P., Martin, K.J., Saleh, A., 2011. Hippocampal network alterations in Alzheimer's disease and Down syndrome: from structure to therapy. J Alzheimers Dis 26,29-47.

Sato, N., Hatakeyama, S., Shimizu, N., Hikima, A., Aoki, J., Endo, K., 2001. MR evaluation of the hippocampus in patients with congenital malformations of the brain. Am J Neuroradiol 22,389-393.

Shepherd, T.M., Ozarslan, E., Yachnis, A.T., King, M.A., Blackband, S.J., 2007. Diffusion tensor microscopy indicates the cytoarchitectural basis for diffusion anisotropy in the human hippocampus. Am J Neuroradiol 28,958-964.

Wieshmann, U.C., Symm, M.R., Mottershead, J.P., MacManus, D.G., Barker, G.J., Tofts, P.S., Revesz, T., Stevens, J.M., Shorvon, S.D., 1999. Hippocampal layers on high resolution magnetic resonance images: real or imaginary? J Anat 195,131-135.

Zhang, Z., Liu, S., Lin, X,. Teng, G., Yu, T., Fang, F., Zang, F., 2011. Development of laminar organization of the fetal cerebrum at 3.0T and 7.0T: a postmortem MRI study. Neuroradiology 53,177-184.

Chapter 6

Summary

This study demonstrates the 7T MRI ability to detect the developmental or pathological changes in human temporal cortex and in the hippocampus not still characterized or ill visualized by clinical MRI.

Conclusions

In this project some abnormalities in the temporal lobe in TLE patients have been characterized by high field MRI and neuropathological analysis.

In the first part of the project we demonstrated the ability of *ex-vivo* 7T MRI of studying the intracortical organization in normal and pathological areas and of visualizing possible subtle cortical alterations in FCD samples. In fact, increasing the resolution of MR images by using a 7T instrument the architecture and some lamination abnormalities in cortical thickness of fixed human specimens, not seen on conventional scan, can be revealed. This is demonstrated by the fact that the MRI findings correlate well enough with histopathology: the differences in MRI signal intensity mainly reflect the myelin fibers distribution and the neuronal density (Garbelli et al., 2011, Neurology).

In the second part of the project, we clarified the significance of the temporo-polar blurring frequently reported in the temporal pole of TLE patients. It is visible as a poorly demarcation beetween gray and white matter on clinical 1.5T MRI and corrisponds to patchy anomalous signal intensity in deep white matter at the 7T MRI. In fact, at morphological level we provided robust evidence that it is caused by massive axonal loss in the white matter associated with a redistribution of the remaining fibers with preserved myelin sheath. Since the analysis of the clinical data revealed that these patients

present an earlier age at epilepsy onset in comparison to those without blurring, and longer epilepsy duration, we can suggest that the continuous and prolonged epileptic discharges might determine a progressive and chronic degeneration of fibres in these patients (Garbelli et al., 2012, Brain).

Finally, we have investigated the hippocampal structures in adult normal and sclerotic hippocampus and at different stages of development.

7T MRI can identify the main anatomical structures and the sublayers of the healty adult hippocampus along its anterior-posterior axis thanks to their differences in MRI signal intensities depending on different density and distribution of cells and myelin fibers.

In sclerotic hippocampi, the major finding in patients with TLE, high resolution MRI show areas of anomalous hyperintensity of signal associated to marked loss of neurons and intense gliosis as reveal by histological analysis for neuronal and glial cells. Moreover, using DTI technique, we were able to identify different HS subtype and to demonstrate a disorganization of fiber bundles in sclerotic samples in comparison to normal hippocampi. Whether a similar resolution can be obtained in a clinical 7T *in vivo* scanner remains to be shown, however these results will be helpful to further advance preclinical and clinical imaging in patients suffering from brain diseases affecting the hippocampus such as MTLE (manuscript in preparation).

During development, the hippocampus undergoes numerous changes concerning the cytoarchitecture, the cellular morphology and the myeloarchitecture which begin in the fetal period and continues after birth. We investigated these changes by comparing variations in 7T MRI signal intensity with corresponding histological and immunohistochemical data. During fetal period, the intensity of the T2 weighted images is related to the cellular density. In post-natal specimens, the MRI signal is still linked to the cell density but with the

appearance and the progressive increase of the myelin fibers content, this correlation becomes less obvious and the myelin represent the histological component which mainly contributes on MRI signal intensity.

These results shows the potential utility of high resolution MRI for detection of developmental changes in human hippocampus and will be useful in the understanding of hippocampal abnormalities occurring in developmental disorders when in the future high-field MRI might be used in clinical practice (Milesi et al., *International Journal of developmental Neuroscience, submitted*).

Future perspectives

This study demonstrates the high-resolution ex vivo MRI microscopy, which occupies a space between the histological modalities used by professional neuroanatomists and the in vivo MRI used by neuroimagers, has excellent potential to provide reference datasets. By taking advantage of ultra-high field strengths (7 T and above), long acquisition times, and focused fields of view, ex vivo studies realize enormous gains in image quality over in vivo MRI. Whether a similar resolution can be obtained in a clinical 7T in vivo scanner remains to be shown.

However, the last decade has been characterized by a steady shift from 1.5 T to 3 T scanners at the majority of epilepsy surgery centers, and 4 T and 7 T systems are already rapidly diffusing. It appears reasonable to speculate that increasing field strength, coupled with the development of new coils, pulse sequences, and software, may make it possible to replicate our findings in vivo in the near future in a setup transferable to clinical practice.

References

Milesi et al., *International Journal of developmental Neuroscience, submitted*
Garbelli et al., 2012, Brain
Garbelli et al., 2011, Neurology

Publications

Milesi G., Garbelli R., Zucca I., Aronica E., Spreafico R., Frassoni C.
Assessment of human hippocampal developmental neuroanatomy by ex-vivo 7T magnetic resonance imaging approaches
International Journal of developmental Neuroscience, *submitted*

Garbelli R., **Milesi G.**, Medici V., Villani F., Didato G., Deleo F., D'Incerti L., Morbin M., Mazzoleni G., Giovagnoli AR., Parente A., Zucca I., Mastropietro A.,Spreafico R.
Blurring in temporal lobe epilepsy patients: clinical, high-field imaging and ultrastructural study. Brain 2012, 135(P8):2337-49

Garbelli R., Zucca I., **Milesi G.**, Mastropietro A., D'Incerti L., Tassi L., Colombo N., Marras C., Villani F., Minati L., Spreafico R.
Combined 7-T MRI and histopathologic study of normal and dysplastic samples from patients with TLE. Neurology 2011;76(13):1177-85

Tassi L., Garbelli R., Colombo N., Bramerio M., Lo Russo G., Deleo F., **Milesi G**., Spreafico R.
Type I focal cortical dysplasia: surgical outcome is related to histopathology. Epileptic Disorders 2010,12(3):181-91

Spreafico R., Medici V., Rossini L., **Milesi G.**
Maturation and migration determinants of corticogenesis. Genetics of epilepsy and genetic epilepsies. Avanzini G. and Noebels J. 2009 John Libbey Eurotext, pp 161-166

Acknowledgments

Thanks to all people who have collaborated on this project.